

THE PROCESSING OF Mg-Ti POWDER FOR HYDROGEN STORAGE

A THESIS SUBMITTED TO
THE GRADUATE SCHOOL OF NATURAL AND APPLIED SCIENCES
OF
MIDDLE EAST TECHNICAL UNIVERSITY

BY

GÜLHAN ÇAKMAK

IN PARTIAL FULFILLMENT OF THE REQUIREMENTS
FOR
THE DEGREE OF DOCTOR OF PHILOSOPHY
IN
METALLURGICAL AND MATERIALS ENGINEERING

FEBRUARY 2011

Approval of the thesis

THE PROCESSING OF MAGNESIUM-TITANIUM POWDER FOR HYDROGEN STORAGE

submitted by **GÜLHAN ÇAKMAK** in partial fulfillment of the requirements for the degree of **Doctor of Philosophy in Metallurgical and Materials Engineering, Middle East Technical University** by

Prof. Dr. Canan Özgen _____
Dean, Graduate School of **Natural and Applied Sciences**

Prof. Dr. Tayfur Öztürk _____
Head of Department, **Metallurgical and Materials Engineering**

Prof. Dr. Tayfur Öztürk _____
Supervisor, **Metallurgical and Materials Engineering, METU**

Examining Committee Members:

Prof. Dr. Vedat Akdeniz _____
Metallurgical and Materials Engineering, METU

Prof. Dr. Tayfur Öztürk _____
Metallurgical and Materials Engineering, METU

Assoc. Prof. Caner Durucan _____
Metallurgical and Materials Engineering, METU

Assoc. Prof. Figen Kaya _____
Metallurgical Engineering, Zonguldak Karaelmas University

Assist. Prof. Dr. Emrah Ünal _____
Metallurgical and Materials Engineering, METU

Date: 24. 02. 2011

I hereby declare that all information in this document has been obtained and presented in accordance with academic rules and ethical conduct. I also declare that, as required by these rules and conduct, I have fully cited and referenced all material and results that are not original to this work.

Name, Last name: GÜLHAN ÇAKMAK

Signature:

ABSTRACT

THE PROCESSING OF Mg-Ti POWDER FOR HYDROGEN STORAGE

Çakmak, Gülhan

Ph.D., Department of Metallurgical and Materials Engineering

Supervisor: Prof. Dr. Tayfur Öztürk

February 2011, 100 pages

A study was carried out on the selection of processing condition that would yield Mg-Ti with most favourable hydrogenation properties. Processing routes under consideration were; mechanical milling under inert atmosphere, reactive milling i.e. milling under hydrogen atmosphere, ECAP (equal channel angular pressing) and thermal plasma synthesis. Structure resulting from each of these processing routes was characterized with respect to size reduction, coherently diffracting volume and the distribution of Ti catalyst.

Mechanical milling yielded a particulate structure made up of large Mg agglomerates with embedded Ti fragments with a uniform distribution. Mg agglomerates have sizes larger than 100 μm which arises as a result of a balance between cold welding process and ductile fracture. Repeated folding of Mg particles entraps Ti fragments inside the Mg agglomerates resulting in a very uniform distribution. Coherently diffracting volumes measured by X-ray Rietveld analysis have small sizes ca. 26 nm which implies that the agglomerates typically comprise 10^{11} crystallites. Mechanical milling under hydrogen, i.e. reactive milling, led to drastic reduction in particle size. Mg and Ti convert to MgH_2 and TiH_2 which are milled efficiently due to their brittleness resulting in particle sizes of sub-micron range. Hydrogenation

experiments carried out on Mg-10 vol % Ti milled under argon yields enthalpy and entropy values of $-76.74 \text{ kJ/mol-H}_2$ and $-138.64 \text{ J/K.mol-H}_2$ for absorption and 66.54 kJ/mol H_2 and $120.12 \text{ J/K.mol H}_2$ for desorption, respectively. For 1 bar of hydrogen pressure, this corresponds to a hydrogen release temperature of $280 \text{ }^\circ\text{C}$. This value is not far off the lowest desorption temperature reported for powder processed Mg based alloys.

ECAP processing is a bulk process where the powders, consolidated in the first pass, have limited contact with atmosphere. This process which can be repeated many times lead to structural evolution similar to that of milling, but for efficient mixing of phases it was necessary to employ multi-pass deformation. An advantage of ECAP deformation is strain hardening of the consolidated powders which has improved milling ability. Based on this, a new route was proposed for the processing of ductile hydrogen storage alloys. This involves several passes of ECAP deformation carried out in open atmosphere and a final milling operation of short duration under inert atmosphere.

The plasma processing yields Mg particles of extremely small size. Evaporation of Mg-Ti powder mixture and the subsequent condensation process yield Mg particles which are less than 100 nm . Ti particles, under the current experimental condition used, have irregular size distribution but some could be quite small, i.e. in the order of a few tens of nanometers.

Of the four processing routes, it was concluded that both reactive milling and thermal plasma processing are well suited for the production of hydrogen storage alloys. Reactive milling yield particles in submicron range and plasma processing seems to be capable of yielding nanosize Mg particles which, potentially, could be decorated with even smaller Ti particles.

Keywords: Magnesium, hydrogen storage, mechanical milling, severe plastic deformation, thermal plasma synthesis, structural characterization

ÖZ

Mg-Ti ALAŞIMLARININ HİDROJEN DEPOLAMA AMACIYLA ÜRETİLMESİ

Çakmak, Gülhan

Doktora, Metalurji ve Malzeme Mühendisliği Bölümü

Tez Yöneticisi: Prof. Dr. Tayfur Öztürk

Şubat 2011, 100 sayfa

Çalışma, Mg-Ti esaslı hidrojen depolama alaşımlarının üretimi için uygun üretim yöntemlerinin seçimini hedef almıştır. Bu amaçla seçilen yöntemler; argon altında öğütme, hidrojen altında öğütme, eş kanallı açısız pres (EKAP) ve ısıl plazma yöntemleridir. Elde edilen yapılar, tane büyüklüğü, kristal/hücre boyutu ve Ti dağılımı bakımından incelenmiş ve karşılaştırılmıştır.

Öğütme yöntemi ile elde edilen yapı, büyük Mg taneler üzerinde homojen dağılmış küçük Ti parçacıkları şeklindedir. Mg parçacıklar genellikle 100 μm 'dan büyüktür. Bu başlangıç tozlarından daha büyük olan parçacık boyutu, topların çarpma etkisi ile birbirine yapışması ve sünek kırılma etkisi ile oluşmuştur. Mg tanelerin katlanarak tekrar yapışması Ti taneciklerinin yapı içinde homojen dağılmasına olanak sağlamıştır. X ışınları yöntemi ile elde edilen kristal boyutu 26 nm'dir. Bu değer Mg tanelerinin genellikle 10^{11} hücreden oluştuğunu göstermektedir. Hidrojen altında öğütme tane boyutunda belirgin bir düşüşe neden olmuştur. Bu yöntemde Mg ve Ti tozlarının öğütme esnasında kırılğan MgH_2 ve TiH_2 tozlarına dönüşmesi sonucunda mikron altı tane boyutlarına ulaşılmıştır. Argon altında öğütülmüş Mg-10 hacim % Ti sırasıyla hidrojen emme ve geri verme için 76.74 kJ/mol- H_2 and -138.64 J/K.mol- H_2 , 66.54 kJ/mol H_2 and 120.12 J/K.mol H_2 entalpi ve entropi değerleri vermiştir. Bu değerler Mg esaslı malzemeler için literatürde bulunan en düşük değerlerden çok da uzaktır.

EKAP'ın ktle halinde bir yntem olması nedeniyle tozların ortamla etkileşimi en az dzeydedir. Yntem aynı numuneye tekrar tekrar uygulanabilmekte ve bu sayede ğtme yntemi ile elde edilen hcre/kristal boyutuna ulaşılabilmektedir. Fakat bu yntemde fazların birbiri iinde karışabilmeleri iin ok yksek miktarlarda deformasyona ihtiya vardır. ECAP yntemi gerinim sertleşmesine neden olarak daha hızlı ğtmeye olanak sağlamaktadır. Yntem bu nedenle snek hidrojen depolama alaşımlarının ğtlebilmesi iin zellikle uygundur. Bu amala nerilen yntem hidrojen depolama alaşımının nce hava ortamında ECAP yntemi ile deforme edilmesi ve takiben inert ortamda ğtlmesidir.

Plazma yntemi ok kk tane boyutunda Mg tozlarının retimine olanak saėlar. Mg-Ti toz karışımının buharlaştırılması ve ktrlmesi yntemi ile 100 nm'den daha kk Mg taneleri retilebilmiştir. Ti boyutları nanometre mertebesinden mikron mertebesine geniř bir daėılım gstermekle birlikte tanelerin nemli bir kısmı 10-20 nm aralıėındadır.

Bu alıřma kullanılan yntemler arasında hidrojen altında ğtme ve ısıl plazma yntemlerinin hidrojen depolama alaşımlarının retimi iin uygun olduėunu gstermektedir. Hidrojen altında ğtme yntemi mikron altı, ısıl plazma yntemi ise nano boyutta tozların retimine olanak saėlamıştır. Plazma yntemi kullanılarak ok kk Ti paracıklarla kaplanmış Mg tozlarının oluřturulabilmesi mmkn gzkmektedir.

Anahtar Kelimeler: Magnezyum, hidrojen depolama, ğtme, aşırı plastik deformasyon, ısıl plazma yntemi, yapısal karakterizasyon

*To my family
with love*

ACKNOWLEDGEMENTS

I wish to express my deepest gratitude to my supervisor Prof. Dr. Tayfur Öztürk for his guidance, advice, criticism, encouragements and insight throughout the research.

I would like to thank to Prof Dr. Vedat Akdeniz, Prof. Dr. Hakan Gür, Assoc. Prof. Dr. Figen Kaya, Assoc. Prof. Dr. Caner Durucan, Assist. Prof. Dr. Emrah Ünalın, for their precious helps, advice and encouragement during the development of the study.

I would like to also mention that the period of PhD affect my understanding of life, and my inner world. I would also like to thank all who initiate, encourage and help this journey into my inner world.

I am indepted to the members of metal hydrogen research group and; Assoc. Prof Dr. Mehmet Şimşir, Rabia Ölmez Günay, Çağla Özgıt, Taylan Örs, Serdar Tan, Semra Tan, Hasan Akyıldız, Mustafa Yılmaz, Zeynep Öztürk, Ayshe Gharavi, Aslı Boran, Fatih Pişkin, Burak Aktekin for their help and patience.

I would also like to thank my colleagues and friends: Betül Akköprü Akgün, Onur R. Bingöl, Arda Çetin, Ali Erdem Eken, Metehan Erdoğan, Emre Ergül, Ziya Esen, Tufan Güngören, Volkan Kalem, Serdar Karakaş, Şerif Kaya, Deniz Keçik, Alper Kınacı, Güher Kotan, B. Pelin Maradit, Fatih G. Şen, Evren Tan, and Serkan Yılmaz.

Help of the technical and administrative staff of Metallurgical and Materials Engineering Department especially Necmi Avcı, Cengiz Tan and Cemal Yanardağ are gratefully acknowledged.

Special thanks to my family, Osman, Hürriyet, Hakan, Pınar Çakmak and especially to Nisan Duru for the continuous support and the joy they bring into my life.

I thank all who have loved me in their hearts, with thanks and love from mine.

TABLE OF CONTENT

| | |
|---|-------------|
| ABSTRACT | iv |
| ÖZ | vi |
| ACKNOWLEDGEMENT | ix |
| TABLE OF CONTENT | x |
| LIST OF TABLES | xii |
| LIST OF FIGURES | xiii |
| 1.INTRODUCTION | 1 |
| 2.LITERATURE REVIEW | 5 |
| 2.1. Introduction | 5 |
| 2.2. Processing of hydrogen storage alloys..... | 9 |
| 2.2.1. Solid State Processing..... | 9 |
| 2.2.1.1. Direct Synthesis of hydrogen storage alloys from their oxides..... | 9 |
| 2.2.1.2. Mechanical Milling | 10 |
| 2.2.1.3. Equal Channel Angular Pressing..... | 15 |
| 2.2.2. Melt Processing | 17 |
| 2.2.3. Vapour Phase Processing..... | 18 |
| 2.2.3.1. Thin Film Processing..... | 18 |
| 2.2.3.2. Thermal Plasma Processing..... | 19 |
| 2.3. Summary..... | 22 |
| 3.THE PROCESSING OF Mg-Ti FOR HYDROGEN STORAGE WITH MECHANICAL MILLING | 23 |
| 3.1. Introduction | 23 |
| 3.1.1. Hydrogen Storage in Mg-Ti system | 28 |

| | |
|--|-----------|
| 3.2. Experimental Procedure | 31 |
| 3.3. Results and Discussion | 34 |
| 3.3.1. Structural Observations:..... | 34 |
| 3.3.2. Hydrogenation Experiments:..... | 40 |
| 3.4. Discussion | 43 |
| 3.5. Conclusions | 44 |
| 4.THE PROCESSING OF Mg AND Mg-Ti WITH SEVERE PLASTIC DEFORMATION..... | 45 |
| 4.1. Introduction | 45 |
| 4.2. Material and Method..... | 46 |
| 4.3. Results..... | 49 |
| 4.3.1. ECAP Processing of Mg and Mg-Ti..... | 49 |
| 4.3.2. Milling after ECAP deformation..... | 61 |
| 4.4. Discussion | 62 |
| 4.5. Conclusions | 63 |
| 5.THE PROCESSING OF Mg-Ti FOR HYDROGEN STORAGE; PLASMA SYNTHESIS..... | 64 |
| 5.1. Introduction | 64 |
| 5.2. Experimental Procedure | 65 |
| 5.3. Results..... | 68 |
| 5.3.1. Mechanical Milling | 68 |
| 5.3.2. Thermal Plasma Processing..... | 73 |
| 5.4. Discussion | 79 |
| 5.5. Conclusions | 80 |
| 6.CONCLUSIONS | 82 |
| REFERENCES | 85 |
| CURRICULUM VITAE..... | 99 |

LIST OF TABLES

TABLES

| | |
|---|----|
| Table 3.1. Some examples of hydrogen storage systems produced by mechanical alloying. | 26 |
| Table 3.2. Reactively milled Mg based systems and their storage results. | 27 |
| Table 3.3. Structural characteristics of Mg-10 vol%Ti powders processed via mechanical milling under argon and hydrogen atmosphere..... | 38 |
| Table 4.1. Structural characteristics of Mg powder compacts ECAP deformed to true strains of $\epsilon=1, 2, 3$ and 4. The same mixture milled for 5 hours are also included | 50 |
| Table 4.2. Structural characteristics of Mg-10 vol%Ti powder compacts ECAP deformed to true strains of $\epsilon=1, 2, 3,$ and 4.The same mixture milled for 5 hours are also included for comparison. | 51 |
| Table 5.1. Experimental conditions for thermal plasma synthesis..... | 67 |
| Table 5.2. Structural Characteristics of Mg-10 vol%Ti powders processed via mechanical milling | 70 |
| Table 5.3. Structural characteristics of mg-10 vol % Ti obtained with plasma processing ... | 74 |
| Table 6.1. Structural parameters in Mg-Ti following different processing routes. | 82 |

LIST OF FIGURES

FIGURES

| | |
|---|----|
| Figure 2.1. Phase diagram of Mg-H system (Manchester et al. ,1988). | 6 |
| Figure 2.2. Pressure composition isotherm of Mg-MgH ₂ system (Milonas,2009). | 7 |
| Figure 2.3. Pressure-composition-temperature diagram of Mg-H system (Manchester et al.1988)..... | 8 |
| Figure 2.4. Die used for equal channel angular pressing. Φ refers to channel angle, Ψ refers to the angle of curvature..... | 15 |
| Figure 2.5. Schematic diagram of an RF plasma torch..... | 20 |
| Figure 3.1. Van't Hoff plot of Mg based storage materials. (Liang 2004)..... | 23 |
| Figure 3.2. Binary Phase Diagram of Mg-Ti, Nayeb-Hashemi et.al.(1998)..... | 29 |
| Figure 3.3. SEM images of starting powders a) Ti ($\leq 44\mu\text{m}$) and b) Mg ($\leq 44\mu\text{m}$). | 31 |
| Figure 3.4. Schematic representation of processing routes in mechanical milling and reactive milling used in the study..... | 32 |
| Figure 3.5. Vials used for mechanical milling and reactive milling. | 32 |
| Figure 3.6. (a) General view of the apparatus used for experiment. (b) Schematic diagram of the sample reactor..... | 34 |
| Figure 3.7. X-ray diffractogram of milled sample before (a) and after hydrogenation (b).... | 35 |
| Figure 3.8. X-ray diffractogram of reactively milled sample(a). Figure also shows the diffractogram of dehydrided(b) and rehydrided (c) samples..... | 36 |
| Figure 3.9. X-ray diffractograms of mechanically milled samples (a) argon (b) hydrogen.... | 37 |
| Figure 3.10. The microstructure of Mg-10 vol%Ti samples (a)unmilled (b) milled under argon (c) milled under hydrogen (10 bar)..... | 38 |
| Figure 3.11. PCT diagram of Mg-10 vol % Ti milled under argon..... | 40 |
| Figure 3.12. Van't Hoff plot of the mechanically milled samples; milled under argon, milled under hydrogen. | 41 |
| Figure 3.13. (a)Pressure change (hydrogen) as a function of temperature in Mg-10 vol. % Ti milled under hydrogen, (b) PCT diagram of Mg-10 vol % Ti milled under hydrogen. | 42 |

| | |
|--|----|
| Figure 4.1. Dies used for equal channel angular pressing of compacted powder samples. Φ refers to channel angle, Ψ refers to the angle of curvature. (a) Single zone die with $\Phi = 90^\circ$, (b) Two-zone parallel die with $\Phi = 120^\circ$. The sample (white) is shown in a partially deformed state..... | 48 |
| Figure 4.2. X-ray diffractogram of Mg ECAP deformed to a true strain of $\epsilon=4.0$ | 50 |
| Figure 4.3. Structural characteristics of Mg-10 vol%Ti powder compacts ECAP deformed to true strains of $\epsilon=1, 2,3$, and 4. The same mixture milled for 5 hours are also included for comparison. | 52 |
| Figure 4.4. The variation of density in Mg-10 vol.%Ti with ECAP deformation. Note that the density increase in the first pass is quite high..... | 53 |
| Figure 4.5. Microstructures in Mg powder compact a) Initial structure(transverse section), b) after ECAP deformation (longitudinal section), c) after ECAP deformation (transverse section) | 55 |
| Figure 4.6 Microstructures in Mg-10 vol % Ti powder compact a) Initial structure (transverse section), b) after ECAP deformation $\epsilon=4$ (transverse section). and c) after ECAP deformation $\epsilon=4$ (longitudinal section)..... | 56 |
| Figure 4.7. SEM micrographs of Mg powder after milling for (b)0.5 h (c) 1 h (d) 2 h (e) 5 h.(a) refers to the starting powder. | 58 |
| Figure 4.8. Particle size distribution of Mg powders obtained after direct milling (dotted lines) and milling after ECAP deformation ($\epsilon=4$) (continuous lines). Note that ECAP deformed Mg yields finer particles with milling..... | 59 |
| Figure 4.9. SEM micrograph of Mg-10 vol % Ti milled for 1 hour. Bright phase is Ti. | 59 |
| Figure 4.10. Microstructure of Mg-Ti deformed to $\epsilon= 24$ using the parallel die | 61 |
| Figure 4.11. SEM micrographs of Mg powder compacts ECAP deformed to $\epsilon=4$ and milled for (a)0.5 h (b) 1 h (c) 2 h (d) 5 h..... | 62 |
| Figure 5.1. Schematic representation of RF plasma system. | 66 |
| Figure 5.2. SEM micrographs of Mg-10 vol% Ti a) the initial mixture and (b) after 30 hours of milling..... | 68 |
| Figure 5.3. Particle size distribution of Mg-10vol% Ti powders milled for 1,5 and 30 hours. The initial distribution is also shown. | 69 |
| Figure 5.4. SEM micrographs of Mg-10%vol Ti after milling for a) 1 hour (b) 5 hours (c) 30 hours recorded in back-scattered image mode. Ti appear bright in a dark background of Mg agglomerates. | 71 |
| Figure 5.5. X-ray diffractograms of Mg-10vol%Ti (Rietveld refined). (a) the initial powder mixture (b) after 30 hours of milling..... | 72 |
| Figure 5.6. SEM micrographs of pure powders after plasma processing. (a), (b) Ti powders and c) Mg powders. | 75 |

Figure 5.7. SEM micrographs of Mg-10 vol%Ti powder mixture after plasma processing. a) A spheroidized Ti particle. b) Mg nanopowders. c) Mg nanopowders synthesized with quenching. 77

CHAPTER 1

INTRODUCTION

Due to the problem of gas emission leading to greenhouse effect as well as future outlook for remaining reserves for oil resources, it become highly desirable to develop alternative and abundant sources of a new energy.

Among all possible candidates, hydrogen appears to be best suited energy carrier for that purpose. In fact, the combustion of hydrogen i) produces nothing else then water, ii) produces three times more energy than the usual fuels (Hydrogen 130 kJ/g as compared to 48 kJ/g for natural gas or 40 kJ/g for gasoline). The major issue with hydrogen remains the problem of storing hydrogen economically and conveniently. Conventional techniques such as gas storage do not fulfill the requirement due to weight and volume issues. Storage in the liquid form is an energy intensive process and unpractical due to "boil-off" problem.

An alternative method is to store hydrogen within a solid material. There are various candidates which could store hydrogen in solid form. Metallic hydrides (MgH_2 , LaNi_5 , TiFe , CeNi_3) and complex hydrides ($\text{Al}(\text{BH}_4)_3$, LiBH_4) are candidates that are actively being developed (Sakintuna et al. 2007).

Among the various alternatives, storing hydrogen in the form of metal hydrides has two advantages. One is related to safety and the other is the high volumetric capacity. In fact with hydrides, volumetric capacity is much higher than that achieved when storing hydrogen in liquid form (85 g/L- MgH_2 compared to 70 g/L).

Among all possible hydrides, magnesium is an attractive candidate due to its low density, low toxicity and great abundance. The production of Magnesium (Mg) is a well established process and therefore the cost of Magnesium is quite reasonable.

It is well known that MgH_2 has high stability with an enthalpy value of $\Delta H = 74.7$ kJ/mol- H_2 which means that temperatures in excess of 350 °C would be required for dehydrogenation. This high stability is a major problem that needs to be solved so that Mg can be used as a hydrogen storage medium.

This thermodynamic barrier can be overcome by changing the bond strength between Mg and H. This change usually requires modifications in the local arrangements of the atoms. The strategy is to find out right combinations of atoms, i.e. additives that sufficiently weaken Mg-H bond strength. An alternative method is to modify the bulk material by the formation of nanocrystalline structure, which results in a large fraction of grain boundary volumes. Similarly, the processing that can lead to the formation of amorphous structure can alter Mg-H bond strength producing the same effect.

To this end over the years, various additives; rare earths (e.g. Ce, La), transition metals (Ni, Co, Fe, Cu, Y, Ti), non transition elements (Al, Li) have been alloyed with Mg. Efforts are concentrated on systems such as Mg-Ni, Mg-Fe, Mg-Cu, Mg-Si. In these systems, some improvements in the enthalpy values were observed. Ni addition in Mg, for instance, results in Mg_2Ni phase formation which has an hydrogenation enthalpy of -65 kJ/mol- H_2 instead of -75 kJ/mol- H_2 for Mg. The associated effect on capacity was, however, always negative, i.e. the capacity was lowered (Reilly et al. 1968).

In order to overcome the thermodynamical limitations, the formation of metastable phases was also considered. An example for this is the formation of metastable γ - MgH_2 (Augey-Zinsou and Ares-Fernández, 2010). This phase is known to have lower stability compared to β - MgH_2 . But the problem is that the phase is unstable at dehydrogenation temperatures. Metastable phases in binary and ternary Mg hydrides are currently being investigated (Hong et al. 2000, Bouodina and Guo 2002).

Another major problem in Mg is the slow kinetics in hydrogenation and dehydrogenation reactions. Addition of catalytic elements as well as the production of nanocrystalline or amorphous structures has been the main strategy in accelerating the reaction rates.

Catalytic additions to Mg cover pure elements, oxides, nitrides, carbides. But the most impressive improvements were obtained with the transition elements such as Pd, Ti, V (Sakintuna et al. 2007). Elements such as Ti and V have no solubility in Mg; therefore, heavy milling is usually employed so as to finely distribute these elements over the particulate structure.

Nanocrystallisation is another strategy to improve the sorption rates (Augey-Zinsou and Ares-Fernández, 2010). High energy ball milling is a common method to refine the powders to small sizes. By carefully controlling the milling conditions, it is possible to obtain nanocrystalline Mg with this method. The accelerated kinetics is usually explained by small particle size as well as a large fraction of grain boundary volumes within the particles that have amorphous structure. The process is facilitated if the milled material is brittle. For this reason, often MgH_2 is the preferred form as a starting material which has better milling ability than Mg (Bobet et al., 2000). Milling of Mg under hydrogen atmosphere produces the same result with in situ conversion of Mg to MgH_2 . For both techniques, due to brittleness of hydrides, milling leads to very rapid fragmentation resulting in a large increase in the surface area.

A drawback in the synthesis of hydrogen storage alloys with mechanical milling is the necessity to process the material under a protective atmosphere. Exposure of powders during or after milling to atmospheres containing O_2 , H_2O etc. is lethal and must therefore be avoided (Ivey et al. 1983). Thus the powders are often processed and handled under argon atmosphere of high purity, i.e. in a glove box.

In this respect, ECAP processing, a recent process that has been employed in the processing of hydrogen storage alloys, is quite attractive since the new surfaces generated in this process are negligibly small. The process normally involves a material in bulk form extruded through a die with two channels of equal cross-section, intersecting at an angle. The method has been used for hydrogen storage

purposes for alloys such as Mg-Ni (Loken et al. 2007) with the result that ECAP processing has a positive effect on hydrogenation kinetics.

A different method for production of hydrogen storage alloys may be nanopowder synthesis. Although it is expected that nanopowders should have improved hydrogen storage properties due to their high surface area they have not been widely studied yet.

Of the various techniques of nanopowder synthesis, thermal plasma route has the advantage that it can be adapted to volume production (Suresh et al. 2008). Plasma, a fourth state of matter, can yield temperatures as high as 10000 K in a suitably designed torch. At these high temperatures, powders fed to the torch evaporate and then condense further down in the reactor. Since the materials condense from the vapor phase, resulting powders are in the nanometer range. This nanosized powders are expected to have improved hydrogenation properties but have not yet been studied.

To sum up, the studies conducted over the last ten years or so show that for the improved hydrogenation properties, the storage material (Mg) should be in the form of small sized particles. The studies also show that for improved kinetics it is necessary to have catalytic additives that need to be finely distributed over this particulate structure.

In this thesis, an investigation was carried out on alternative production methods which could be used in the processing of Mg-Ti. First we review, Chapter 2, the production methods that could be used for hydrogen storage alloys. Results of the experimental programs are given in Chapters 3-5. These cover *mechanical milling*, milling under argon as well as milling under hydrogen i.e. reactive milling, *ECAP processing* and *thermal plasma synthesis*. Chapter 6 gives a comparative summary of the results obtained from each of these processing routes.

CHAPTER 2

LITERATURE REVIEW

2.1. Introduction

For an effective hydrogen storage system, the storage alloys should satisfy certain specific criteria. The main criteria are high gravimetric and volumetric storage capacities, low sorption (absorption and desorption) temperature, fast reaction kinetics and resistance to degradation. Specific targets have been set in various research programs that are currently in progress (DOE-2001, NESSHY-2006).

Lightweight elements of periodic table are particularly relevant for satisfying the requirement with respect to high gravimetric capacity. Of these elements, only C, Ni, Li, Na, Mg, Al form stable compounds and have sufficiently high hydrogen content. LiH and NaH are too stable for practical applications. Ammonia and methane are not reversible in the practical sense, and AlH_3 requires very high pressures for reversibility. Another potential candidate for light hydrogen storage is based on the $[\text{AlH}_4]^-$ anion as in NaAlH_4 . Achieving reversible hydrogenation in such complex hydrides is known to be complicated and has rather slow reaction kinetics (Gross et al. 2002). Within these elements, Mg appear to be the only candidate that reacts with hydrogen in reversible manner, though its hydride is relatively stable and reaction rate is rather sluggish.

Mg and Mg based alloys can store large quantities of hydrogen up to 7.6 wt % (Pedersen et al., 1983). The binary phase diagram of Mg-H is given in Figure 2.1 (Manchester et al. 1988). Mg has a hexagonal crystal structure (hP2) with lattice parameters of $a=0.321$ nm $c=0.521$ nm in the elemental form. The hydrogenation takes place via a primary dissolution of H in Mg. Maximum solubility of H in $\text{Mg}(\alpha)$ is

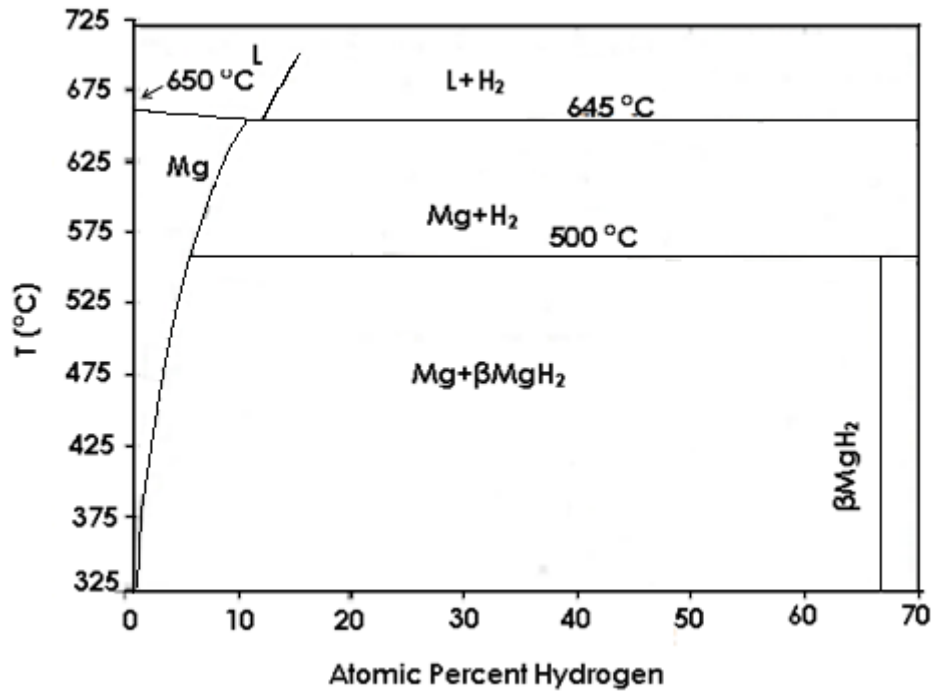


Figure 2.1. Phase diagram of Mg-H system (Manchester et al. ,1988).

9.1 at %. More dissolution of H in Mg (α) leads to the formation of $\text{MgH}_2(\beta)$. This phase has a body centered tetragonal structure (tP6) with lattice parameter of $a = 0.452 \text{ nm}$ $c = 0.302 \text{ nm}$. Thus the full conversion of Mg to MgH_2 leads to 32.57 % volume expansion.

The conversion of Mg to MgH_2 may be followed in pressure composition temperature (PCT) diagram given in Figure 2.2. Here the diagram refers to isotherms at $\sim 300 \text{ }^\circ\text{C}$. As seen in the diagram, the pressure rises very rapidly with little absorption of hydrogen and the pressure then remains constant throughout the extended range. At the end of the plateau where Mg to MgH_2 transformation is complete, the pressure rise leads to very little change in the absorbed hydrogen. Upon reversal, i.e. decreasing the pressure, PCT follows a similar pattern. The plateau pressure has a somewhat lower value implying hysteresis in the reaction.

Figure 2.3 is adapted from Manchester et al. and refers to different isotherms determined at 340, 350 and 375 °C for Mg. Values of plateau pressure determined

at different temperature may be used to obtain the enthalpy and entropy of the reaction using Van't Hoff equation.

$$\ln P = \frac{\Delta H}{RT} - \frac{\Delta S}{R} \quad (2.1)$$

Here, P is the equilibrium pressure ΔH and ΔS are enthalpy and entropy change, respectively. R is gas constant and T is the equilibrium temperature. Following the data given in Figure 2.3, Manchester et al. determines $\Delta H=74.9$ kJ/mol- H_2 and $\Delta S=135.1$ J/Kmol- H_2 respectively. It should be emphasised that entropy change from molecular hydrogen in gas state to hydrogen in the solid state is constant for all metal hydrides and has a value of approximately $\Delta S_f=-130$ J/Kmol- H_2 (Züttel et al., 2004). In dehydriding reaction the entropy change is expected to have the same value ($\Delta S_f =130$ J/Kmol- H_2). Therefore, the stability of formed hydride could be measured by the enthalpy of the reaction only. Assuming an enthalpy value of 74.9 kJ/mol- H_2 for dehydriding reaction i.e. value given by Manchester et al. (1988), it is necessary to reach 576 K to desorb hydrogen from MgH_2 . For metal hydride that could desorb hydrogen in ambient conditions (300 K, 1 bar) it is necessary that the enthalpy of the dehydriding reaction should be reduced down to 39.2 kJ/mol- H_2 .

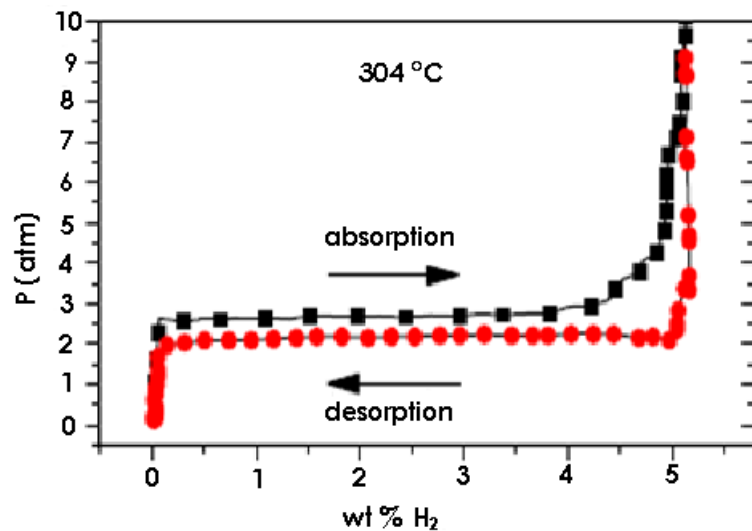


Figure 2.2. Pressure composition isotherm of Mg- MgH_2 system (Milonas,2009).

For hydrogen to react with metals it is necessary that the molecular hydrogen should be split into atomic form. Once this is achieved hydrogen atoms can diffuse into the lattice forming the stable hydride. Normally, the surface of metal powders is covered by oxides or other contaminants and therefore the surface is not active enough to split the hydrogen molecule. Therefore Mg, like other hydrogen storage alloys, requires an activation treatment. This usually involves several hydriding-dehydriding treatments under severe conditions, i.e. relatively high temperatures, high pressures, and low vacuum (Selvam et al. 1986). As a result, fresh surfaces are created in the metallic powders. This process may be helped by self pulverization of powders which occurs due to a volume change associated with hydriding and dehydriding reaction (Zaluska et al. 1999).

Dissociation of hydrogen molecules into the atomic form is often helped by the addition of the so-called catalytic elements. Pd is a well-known catalyst for hydrogen dissociation reaction (Zaluska et al. 1999, Gutfleisch et al. 2005). The hydriding properties are enhanced by Pd nanoparticles attached to Mg surface. Due to high cost of Pd, often other transition metals are used for the same purpose. Of these, the elements Ti, V, Nb are most common (Barkhordarian et al., 2003). The catalytic additions are not limited to pure elements. Transition metals (Hanada et al. 2005), oxides (Oelerich et al. 2001), carbides(Immamura et al. 2009),or nitrides(Luo et al. 2004) may also be used for the same purpose.

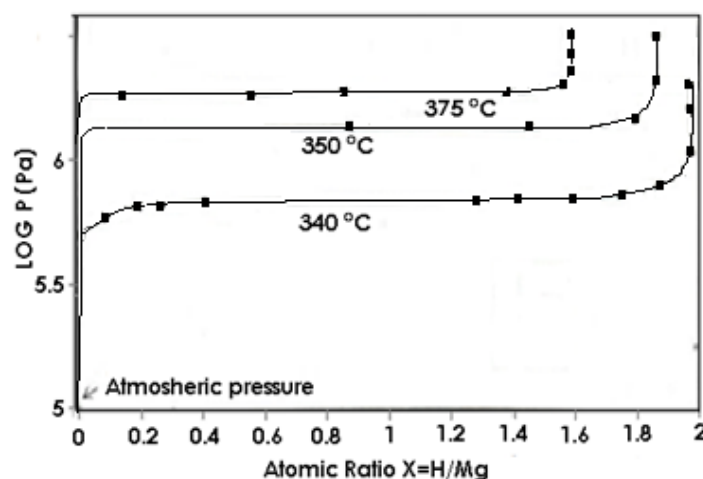


Figure 2.3. Pressure-composition-temperature diagram of Mg-H system (Manchester et al.1988)

2.2. Processing of hydrogen storage alloys

Hydrogen storage alloys may be produced in a variety of ways. These may be categorised as solid-state, liquid-state and vapour phase processes. The solid state processes cover electroreduction of oxides, mechanical alloying and severe plastic deformation, i.e. equal channel angular pressing. Arc melting and vacuum induction melting which may be followed by rapid solidification are liquid state processes. Thin film deposition and thermal plasma synthesis involve processing in vapour phase.

2.2.1. Solid State Processing

2.2.1.1. Direct Synthesis of hydrogen storage alloys from their oxides

Solid state electroreduction of oxides is a method to extract metals from their oxides. The method, also referred to as electro-deoxidation, was first proposed by Chen et al. in the late 1990s and originally employed to produce Ti from TiO_2 . The method was used for other oxides and more recently, for $\text{TiO}_2\text{-Fe}_2\text{O}_3$ and MgO-NiO for the synthesis of FeTi (Örs et al. 2009) and Mg-Ni (Tan et al. 2010) compounds as hydrogen storage alloys.

In this method, a cathode is made from slightly sintered pellets of metal oxides, placed on or attached to a collector. The electrolysis is performed between this cathode and an inert anode, such as graphite, in a bath of molten salt, such as CaCl_2 , which has a decomposition voltage higher than that required for the electrodeoxidation of the oxide. The main characteristics of this method, in contrast to conventional electrolytic methods, are that metal is not deposited from electrolyte onto the cathode; rather it is left at the cathode in the solid state. During the process, the oxygen in cathode is ionized, enters the electrolyte and is subsequently discharged at the anode.

In electrodeoxidation process, number of factors affects the ease of reduction achieved. The oxides of low reduction potential are reduced easily such as NiO, Cr_2O_3 , Fe_2O_3 . The reduction is affected by oxygen diffusivity in the solid state. Since the diffusion of oxygen is slow in metallic lattice, the rate slows down when the

metallic state is achieved. The advantage of this process is that the resulting material is in the powder form of small size. The size reported for FeTi alloy (Örs et al. 2009) is 1-2 μm .

The synthesis of Mg or Mg rich compositions from their oxides seems to be rather complicated. This is attributed to high stability of MgO, low melting point of Mg, and conductivity problems (Tan et al. 2010).

2.2.1.2. Mechanical Milling

Mechanical milling is a common technique used in the processing of hydrogen storage alloys. The method often aims at homogeneous mixing and refining of the base powder with the additives. In certain cases, the aim is material synthesis, i.e. elemental powders are milled heavily so as to obtain alloy phases including solid solutions, quasi-crystalline and crystalline intermetallic phases, and amorphous alloys.

Mechanical milling, as used for particle refinement and the material synthesis, have been reviewed by Suryanarayana (1995) in detail. For this reason only a brief description will be presented here.

Equipment used for mechanical milling of hydrogen storage alloys are normally of high-energy type. These cover spex shaker mill, planetary ball mills, and attritor mills (Yamada and Koch, 1993). Spex mills which handle about 10-20 g of powder at a time are most commonly used for laboratory investigations. The vial follows infinity sign (∞) as it moves and due to high rotation speeds, the impact force of the balls are quite high. Planetary mills involve two movements. These vials are arranged on a rotating disk and a special drive mechanism causes them to rotate around their own axes. Since the vials and the supporting disk rotate in opposite directions, the centrifugal forces alternately act in similar and opposite directions. This results in both frictional and impact effects.

The nature of the initial powder combination i.e. ductile-ductile, ductile-brittle, or brittle-brittle have an important effect on the resulting microstructure and phases observed.

Ductile-ductile mixtures are particularly suitable for alloying. The alloying usually achieved due to repeated cold welding and fracturing processes that take place throughout milling. According to Benjamin and Volin (1974), initially the powders are flattened by micro-forging process. The flattened particles are then cold welded together and form composite lamellar structure. This leads to an increase in the particle size. With continued milling, composite lamella is strain hardened and as a result the lamella is subjected to ductile fracture. Normally milling is continued until a steady state is reached where there is a balance between the cold welding and fracturing process.

In the process of milling, the alloying occurs due to decreased diffusion distance, increased defect concentration and heat. With further milling, true alloying occurs in atomic level in the form of solid solutions, intermetallics, or amorphous phase.

In ductile-brittle systems, while the ductile component is flattened, brittle one becomes fragmented. With further milling, the ductile component work hardened and the lamella get convoluted and refined. The composition of the individual particles converges with the overall composition. Under such conditions whether alloying can occur depends on the solubility of a brittle phase within the ductile component. If the phase has limited solubility then the alloying is not expected.

In brittle-brittle systems, both constituents are fragmented and their particle size is reduced. At very small particle size, the powder particles behave in non-brittle fashion. It has been observed that harder (more brittle) phase get fragmented and embedded into the softer phase. Further alloying occurs similar to described in ductile-brittle systems.

Within the overall framework described above, important parameters of milling are milling media, i.e. ball diameter, ball to powder ratio, milling time and the environmental control.

Hardened steel, stainless steel, WC, zirconia, alumina are the most common materials used as the grinding media. The density of the grinding balls together with their size determines the severity of milling. The density should be high enough so that the balls create enough impact force on the powders. The size of the

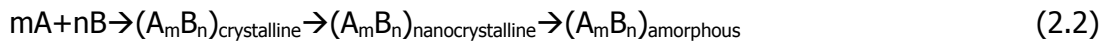
grinding medium also has an influence on the milling efficiency. According to Lai et al. (1998) in Ti-Al system solid solution is successfully obtained using 15 mm diameter balls. The use of larger diameter balls (20-25 mm), despite their high impact energy, was less successful in yielding the solutionized structure. A similar result was reported by Padella et al. (1991) where Pd-Si powder mixture was successfully converted to amorphous phase with smaller balls (2 mm as opposed to 8 mm).

Ball to powder weight ratio could vary from 1:1 (Chin et al., 1997) to 220:1 (Kis-Varga, 1996). Though the values are commonly around 10:1 for laboratory scale milling process. Ball to powder weight ratio has an effect for the milling efficiency of the material; the higher the ratio shorter is the milling time.

The powders are usually milled under inert atmospheres, e.g. Ar (Rochman et al. 1999) or He (Varin et al. 2004). Normally filling and unloading of the vial is carried out in a glove box under Ar atmosphere. The powders that are ductile tend to weld together and an anti-sticking agent e.g. NaCl, stearic acid or graphite is usually added at a level of 1-5 wt%. Cryogenic conditions have also positive effect on the grindability of ductile powders (Huang et al., 1996).

The first report on the formation of a nanostructured material synthesized by high energy ball milling is from Thompson and Politis in 1987. According to Suryanarayana (1995) at the early stages of milling, shear bands were observed due to the high deformation rates experienced during milling. With continued milling, the average local strain increases due to the increasing dislocation density. At a certain dislocation density within these heavily strained regions, the crystal disintegrates into subgrains that are separated by low angle grain boundaries. According to Suryanarayana, this results in a decrease of the lattice strain. On further processing, deformation occurs through shear bands located in the previously unstrained parts of the material. The grain size decreases steadily and the shear bands coalesce. The small angle boundaries are replaced by higher angle grain boundaries, implying grain rotation. Consequently, dislocation free nanocrystalline grains are formed.

Amorphous phase formation is also possible with this method in binary, ternary and higher order alloy systems. In the synthesis of amorphous phase, the milling can start from the blended elemental powder mixtures, prealloyed powders and/or intermetallics, mixtures of intermetallics and elemental powders. Suryanarayana (1999) states that for the amorphous phase formation from a mixture of powders (A and B) two routes are possible:



Occurrence of amorphization by both routes can be found in the literature (Huot et al. 1998 and 1999, Gennari et al. 2001, Liang et al. 1999)

Amorphization in mechanical milling is not purely a mechanical process and that a solid-state reaction occurs (Schward and Johnson 1983). During mechanical milling, however, destabilization of the crystallite phase is thought to occur by the accumulation of structural defects such as vacancies, dislocations, grain boundaries, and anti-phase boundaries. The continued decrease in grain size (and consequent increase in the grain boundary area) and the lattice expansion would also contribute to the increase in the free energy of the system. It has been reported that the stored energy during mechanical milling can be about 50 % of the enthalpy of fusion. (This value in cold rolling and wire drawing is only a small fraction of the fusion energy; Eckert et al, 1992). These defects raise the free energy of the intermetallic system to a level higher than that of the amorphous phase and consequently, it becomes possible for the amorphous phase to form.

Increased milling energy (achieved by a higher ball to powder ratio, increased speed of rotation, etc.) is normally expected to introduce more strain and increase the defect concentration in the powder and thus leads to easier amorphization. However, higher milling energies also produce more heat (and higher temperatures) and this can result in the crystallization of the amorphous phase. Therefore, a balance between these two effects will determine the nature of the final product phase. There have been conflicting reports on the effect of milling temperature on the nature of phases formed. Generally a lower milling temperature is reported to

promote amorphization process. For example, the time required for amorphization in NiTi was 2 hours at -190 °C, 13 hours at 60 °C (Suryanarayana, 2001). For the characterisation of milled powders X-ray diffraction techniques are frequently used. Nanocrystalline phases give very broad peaks, it is difficult to differentiate either the phase is crystalline or amorphous or the combination of both.

In some systems, it was reported that on mechanical alloying of the blended elemental powder mixture, the sequence of phase formation with time was solid solution, intermetallic and amorphous phase (Oleszak et al., 1993 and Bonetti et al. 1993). Whether an intermetallic or a solid solution phase forms before amorphization depends on the relative free energies of solid solution and the intermetallic phases.

The degree of solutionizing is usually determined by extrapolating the lattice parameter vs. solute content. According to Suryanarayana, supersaturated solid solution formation is possible with mechanical milling and the formation of it is promoted in solid immiscible systems rather than miscible ones. Extensive solid solubility has been observed in Cu-Co (Gente et al. 1993), Fe-Cu (Huang et al. 1994) and Mg-Ti (Liang et al. 1999). They claimed that the presence of structural defects is responsible for the formation of supersaturated solid solutions.

The mechanical milling procedure has been used for Mg based hydrogen storage systems for several reasons. The studies conducted within last ten years or so, show that for the improved hydrogenation properties, the storage material (Mg) should be in the form of small particles with a uniform distribution of fine catalytic additives. Mechanical milling procedure results in the creation of defects, micro/nanostructures and reduction in the size of particulate structure. The high defect content together with increased surface area aid the diffusion process and results in fast hydrogenation kinetics. For instance Huot et al. (1999) reports faster hydrogenation kinetics in milled MgH₂ as compared to unmilled one with the former having 10 fold increase in surface area.

In addition to increase in the surface area, the role of mechanical milling is to distribute the catalytic additives in the host material. For instance Liang et al. (2001)

attributed fast hydriding dehydriding rates in Mg-V to the homogeneous distribution of catalytic additive, i.e. V, achieved by ball milling.

The milling procedure can be applied either under inert or hydrogen atmosphere. With the application of hydrogen pressure, in situ conversion of Mg to MgH_2 is possible. For instance Huot et al. (1999) produced MgH_2 from pure Mg under H_2 atmosphere. This more brittle hydride phase results in faster size reduction and shorter milling time. Pulverisation and deformation process occurring together in this route plays a major role in the hydriding properties.

2.2.1.3. Equal Channel Angular Pressing

ECAP developed by Segal et al. in the 1980s and has become a widely used procedure for the severe plastic deformation of the materials. In this method, plastic deformation is induced by repetitive pressing of material through equal channels intersecting at an angle Φ , Figure 2.4. Typically Φ vary from 45° to 157.5° , though 90° and 120° are the most common ones. The channel and therefore the material to be deformed can be either square or circular in cross section. Since the cross sectional area of the sample does not change, the same material can be pressed repetitively in this method. There are basically four routes that can be followed in repetitive pressing; route A (the sample is not rotated between passes), B_C (clockwise 90° rotation after each pass), B_A (counter-clockwise 90° rotation after each pass), and C (180° rotation between passes) (Stolyarov et al., 2001).

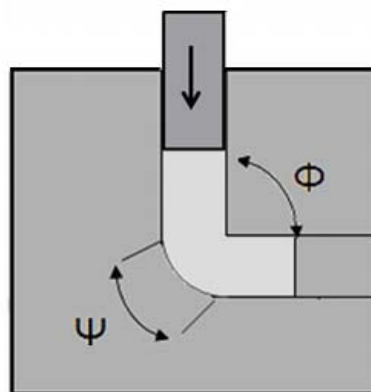


Figure 2.4. Die used for equal channel angular pressing. Φ refers to channel angle, Ψ refers to the angle of curvature

ECAP die angle is important for microstructural refinement. A series of experiments on pure Al have shown that the ultrafine microstructures can be obtained when the die angle was close to 90° (Nakashima et al. 1998).

Although the pressing can be repeated a number of times, substantial refinement in the average grain size occurs after only a single passage through the die. For instance, Liu et al. (2003) starting from $95\mu\text{m}$ Mg-3.3Li alloy decreased the grain size to $2\mu\text{m}$ after only one pass. The misorientation between subgrains increases with increasing number of ECAP passes. For instance, in the Al-3%Mg alloy the grain size was effectively reduced to $1\mu\text{m}$ from initial grain size of $500\mu\text{m}$ after first pass and to $0.2\mu\text{m}$ is observed after an effective strain of ~ 4 passes (Munoz-Morris, 2004).

Chakkingal et al. (1998) have found that using the die angle $\Phi = 90^\circ$ and route B_C microstructure evolves most rapidly into equiaxed grains separated by high angle grain boundaries. When $\Phi = 120^\circ$, route A found to be more effective indicating that choice of processing route influences the effectiveness of the die angle (Shin and Kim, 2000).

Smaller grain sizes are achieved when ECAP deformation is carried out at low temperatures (Yamashita et al. 2001, Kim et al. 2003). So, to obtain refined grain structure, temperature should be lowered to a level which maintains the materials ductility. Mg, however, with its hexagonal structure has limited ductility so temperatures of at least around 200°C are needed in order to ensure sufficient ductility (Yamashita et al. 2001).

ECAP processing has also been used for the consolidation of powders (Matsuki et al. 2000 and Senkov et al. 2005). This is normally achieved by high temperature pressing in conventional powder metallurgy. Matsuki et al. (2000) reports that even single pass ECAP deformation is sufficient to consolidate the powder sample.

Within the context of hydrogen storage alloys, Sprinyuk et al. (2006, 2010) and Loken et al. (2007) have used ECAP processing for Mg-Ni and Mg-Mn-Ni observing faster hydrogenation kinetics.

2.2.2. Melt Processing

The melt processes that are used in the production of hydrogen storage alloys normally involve vacuum induction melting and arc melting.

Vacuum induction melting uses electromagnetic induction to melt the charge. Since most hydrogen storage alloys have high affinity to oxygen, the melting process is carried out under vacuum atmosphere. The alloy systems; Mg_2Ni (Terashita et al. 2001), $TiV_{1.1}Mn_{0.9}$ (Yonkeu et al. 2008), $Zr_{0.55}Ti_{0.45}V_{0.54}Mn_{0.24}Ni_{0.88}Co_{0.16}Cr_{0.16}$ (Kim et al. 2009) are some of the examples that have been produced with this method.

Arc melting is another method that have been used for production of hydrogen storage alloys. This method is particularly suitable for difficult-to-melt alloys and intermetallic compositions. In this method, the charge material is exposed to an electric arc where the current passes through the charged material. The melting environment is usually an inert gas, normally argon. The material obtained is in the bulk form. Zr alloys (Beal et al. 1955), AB_5 type alloys ($MINi_{4.0}Al_{0.3}Cu_{0.5}Zn_{0.2}$), CoB (Song et al. 2009), FeTi (Chen at al., 2002), Ti-Cr-V (Kawasuso et al. 2009) are some of the metal alloy systems that have been produced with this method. Hydrogen storage alloys produced by arc melting include Ti-V-Mn BCC alloys (Wang, 2009) Mg_2Ni (Shao et al., 2004), Mg (Choe et al., 2010), Zr-Ti-Ni alloys (Mingfen et al., 2002), FeTi (Khatamian et al., 1983), Nb-Zr-Fe alloys (Okuyama et al., 2007).

The materials both in induction melting and arc melting are obtained in the bulk form. To use the material for hydrogen storage purposes it is necessary to pulverize them with methods such as mechanical milling. In order to decrease the energy and time for the milling operation, melting of the alloy may be followed by rapid solidification methods. This involves contact of the molten metal with the cooling medium which has high thermal conductivity. Molten metal is solidified into a thin strip or small droplets. The rapid extraction of thermal energy allows the system to be cooled far from equilibrium. This results in the formation of metastable phases as well as in the extension of the solubility limit. The process leads to sharp reduction in grain size and often in the formation of nanocrystalline and/or amorphous structure (Jones et al. 1982, Liebermann et al. 1983, Cahn et al. 1991). The amorphization rules described in mechanical milling section is also valid in rapid

solidification. So, the selection of suitable solute element is essential to obtain amorphous or nanocrystalline alloys. Examples of hydrogen storage alloys that involve rapid solidification include Mg₂Ni (Zhang et al. 2010), Mg-Al alloys (Urgnani et al. 2009), V₃₅Ti₂₅Cr₄₀ (Pei et al. 2009), LaNi_{5-x}Si_x (x=0.1, 0.3, 0.5)(Srivastava 1998), Ti-V (Yu et al. 2004).

2.2.3. Vapour Phase Processing

In vapour phase processing, materials are evaporated and then condensed into solid form. This evaporation-condensation process is very common for thin films studied for hydrogen storage purposes. However, the similar approach has recently been applied for powder production with the thermal plasma synthesis.

2.2.3.1. Thin Film Processing

In the 80's, storage of hydrogen in thin films has become quite popular due to their high surface area with improved hydrogenation kinetics. Thin films have several advantages over bulk materials. Typical deposition techniques such as sputtering, thermal evaporation or electron-beam evaporation allow the evaporation of more than one element at a time. Moreover by controlling deposition parameters, it is possible to exercise compositional control in the resulting films. Although the amount of material deposited is very low, it helps to identify compositions suitable for hydrogen storage.

Thin films have shorter diffusion distances and hence better hydrogenation properties. For instance, Mg thin films, capped with Pd overlayer, desorption temperature could be as low as 100 °C (Higuchi et al., 2002). In such films kinetic improvements have been also observed which may be due to Pd as catalyst. The main problem with this method is the limited amount of material that can be produced. Furthermore, the films are usually not stable and deteriorate during cycling (Remhof and Borgschulte, 2008).

For thin films that are amorphous, it is difficult to obtain thermodynamic properties as they display no clear plateau in their PCT. Such a case was reported by Ingason

et al. (2007) for 25 nm thin film co-sputtered Mg-C. Ingason et al.(2005) further claimed that the films thicker than 300 nm show similar properties to bulk counterparts.

Favourable hydrogenation properties in thin films (Akyıldız and Öztürk, 2010) imply that nanosize Mg could have improved storage properties. A method for this could be thermal plasma synthesis which allows the production of nano powders.

2.2.3.2. Thermal Plasma Processing

Thermal plasma synthesis is a new approach for the production of hydrogen storage alloys (Çakmak et al. 2010). So the method will be described in some detail.

Plasmas can be divided into two broad categories; equilibrium (thermal) plasma and non-equilibrium (cold) plasma. In thermal plasma, both heavy particles and electrons are in thermal equilibrium and therefore they have high energy densities. This is unlike cold plasma where only electrons have high temperature which are used for etching purposes.

Thermal plasma, due to its high energy density is suitable for powder synthesis, coating process and spheroidization treatment. The source can be in the form of direct current (DC), radio-frequency (RF) or microwave. In DC arc plasma, the arc is generated between the cathode and the anode which ionizes the plasma gas. The temperatures reached varies from 8000 to 15000K. In arc spraying; the arc is generated between the tips of two continuously fed metallic wires. The tips of the wires melt by the arc and spray atomised by an overlaid gas flow. Wires of the same metal, different metals or hollow wires filled with ceramics or hard metals can be used. Normally powder particles are injected radially or directly behind the nozzle into the plasma jet.

In an RF torch, energy coupling to the plasma is accomplished through the electromagnetic field of the induction coil. A schematic representation of a typical RF torch is given in Figure 2.5. Here, plasma gas is fed into a quartz tube. The tube is separated from the induction coil by a sheath gas that flows in between. The purpose of this is to protect the torch from high temperature generated in the

plasma. Powder is fed into the torch by carrier gas via a probe placed axially into the torch. The probe is usually a water cooled stainless steel tube of a small diameter.

Typically there are three zones in RF systems used for nanopowder synthesis. These are plasma torch, reactor and powder collector (see Figure 5.1). The torch (as well as the reactor) is maintained either at atmospheric conditions (Tendero et al., 2006) or under a slight vacuum (Katva et al., 2004). The reactor is normally a water cooled stainless steel chamber. This chamber also accommodates a quenching zone where normally nitrogen gas of relatively high flow rate is fed into the chamber (Kumar, 2008). The reactor is connected to the collector where nanopowders produced are collected in a filter system.

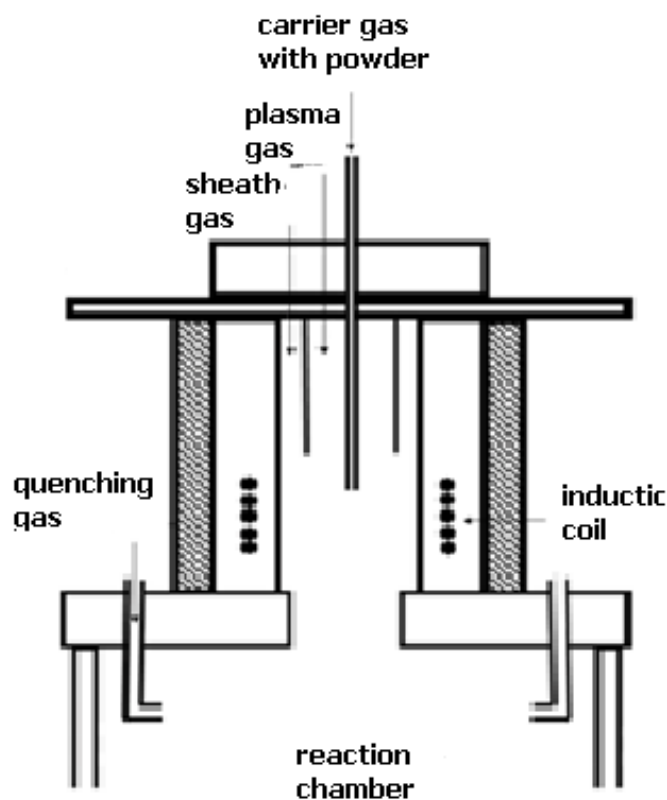


Figure 2.5. Schematic diagram of an RF plasma torch.

Metallic powders of similar melting and boiling points, good thermal conductivity and a high vapour pressure can be processed at moderate temperatures. Examples in this category include copper (Kobayashi et al. 2007), iron (Kumar et al 2008), and Nickel (Shanmugavelayutham et al. 2004,2007). By optimising the quenching conditions, i.e. feed rate of metallic powder and flow rate of quenching gas, the particle size can be modified. This so-called flash vaporization process can also be used for non metallic powders such as alumina (Hu et al., 2007) and silica (Hu et al., 2007).

If the aim in synthesis is a mixed composition, i.e. compound or solid solution, it is necessary to consider the differences between melting and boiling temperatures of the elements involved. If they differ from each other with respect to these temperatures, then the precursors can be fed into the torch-reactor at different zones.

Since the thermal plasma synthesis involves rapid quenching, this may lead to the formation of metastable phases (Szépvölgyi et al. 2007, Hu et al. 2007). For instance Hu et al. (2007) in synthesising alumina observed the metastable phases γ , θ , δ instead of alpha-alumina. Also because of quenching process the formation of quasicrystals was reported(Kumar et al. , 2006).

Thermal plasma reactor can also be used to obtain metallic powders from their precursors via a reduction process. For instance, Bai et al.(2009) used hydrogen gas in the chamber to obtain Ni powder from the nickel hydroxide/carbonate precursors. Hydrogen was also used as a carrier gas in the system. In this method, the precursors underwent vaporization and reduction and then the resulting metallic Ni species condensed and formed nanoparticles as a result of high quenching rate.

The method can also be applied for the synthesis of nitrides, oxides and chlorides. This process usually requires some specific gases in the reaction chamber to provide estimated reactions to take place. Direct oxidation reaction is also possible in plasma synthesis (Szépvölgyi et al., 2008). Ikeda et al.(2007) used this approach to obtain TiO₂ particles. In this study, liquid precursors were used containing titanium

terabutoxide and diethanolamine. The precursors were fed into the system with the use of Ar and O₂. The size of resulting particles was controlled by the parameters of the quenching process for which Ar, O₂, He were used. Similarly, thermal plasma can also be used for nitriding reaction (Kobayashi et al., 2007)

Powder particles collected either from the cyclone or from the walls of the reactor are often agglomerated. With the application of high power levels, the tendency for agglomeration is diminished. For instance Szépvölgyi et al.(2007) obtained 30-70 nm FeAl particles with 15 kW, whereas the same system operated at 5 kW yielded highly agglomerated particles.

2.3. Summary

It has been shown that Mg is one of the most attractive options for hydrogen storage and meets most criteria for practical application. However, there are two main problems with this option; high stability of MgH₂ and slow reaction kinetics.

It has been shown that there are a variety of methods that can be used for the processing of hydrogen storage alloys. These cover solid state processings; electroreduction of oxides to metallic powders, mechanical milling under inert or hydrogen atmosphere and ECAP processing. It is also possible to produce hydrogen storage alloys using liquid phase processing, namely induction melting and arc melting. This is often followed by rapid solidification and/or mechanical milling. Thermal plasma synthesis is a vapour phase process yielding nanopowders.

For Mg based hydrogen storage alloys, studies reviewed above show that it is highly desirable to produce the alloy with as small a particle size as possible. For improved reaction kinetics, catalytic additions are often necessary. Studies further show that it is necessary to distribute the catalytic addition in the particulate material as homogeneously as possible.

CHAPTER 3

THE PROCESSING OF Mg-Ti FOR HYDROGEN STORAGE WITH MECHANICAL MILLING

3.1. Introduction

Mechanical milling by high energy ball milling is a common method for the synthesis of hydrogen storage alloys in magnesium based systems (Zaluska et al. 1999). The main aim is usually to refine powders to extremely small sizes.

Mechanical milling of pure Mg was studied by Zaluska et al. (1999), Schulz et al. (1999) and Orimo et al. (2001). These studies all showed that the milled powders have better sorption properties than unmilled one. Schulz et al. (1999) claimed that the main reason for this was an increase in surface area of the powders. They mentioned that mechanical milling has a positive affect for lowering the activation energy barrier for desorption of hydrogen.

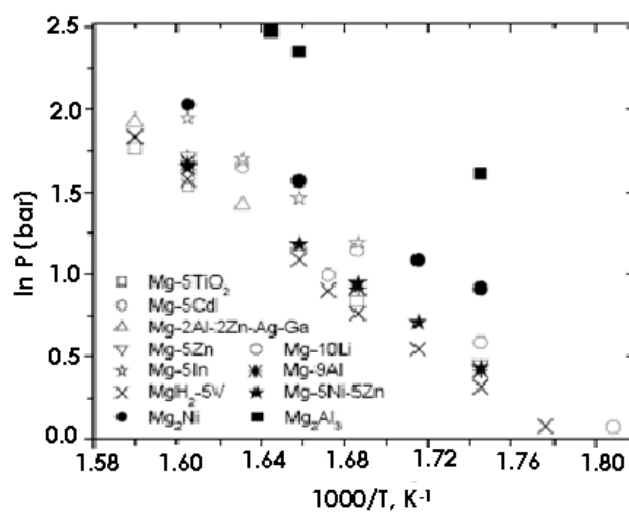


Figure 3.1. Van't Hoff plot of Mg based storage materials. (Liang 2004)

The plateau pressure is the measure of stability for hydrogen storage alloys and this value can be changed by alloying additions. Some additions increase the plateau pressure, whereas the addition of elements such as V and Cd decreases it (Liang et al. 2004). The effect of additions on such thermodynamic properties can be followed by the Van't Hoff plots. (Liang et al. 2004). It is seen from Figure 3.1 that the addition of TiO₂, V, or Li does not change the stability of MgH₂, whereas Zn, Al or Ni decreases the stability, i.e. dehydrogenation takes place at lower temperature.

The transition metals are good catalysts for chemisorption of hydrogen and have often been added to Mg to improve their sorption properties. For instance, Liang et al. (1999) have added Ti, V, Mn, Fe, Ni to MgH₂. This produces little effect on thermodynamics, but kinetics were improved considerably. Absorption and desorption kinetics were fastest in the case of Ti addition. They also found that powders could be hydrogenated without activation. In terms of effectiveness, Ti was followed by V and then by Ni. The effectiveness of Ti was also verified in a latter study (Ershova et al. 2008).

Mechanical milling, in addition to synthesizing elements into compounds or to the mixtures, leads to the introduction of defects e.g. dislocations, stacking faults etc. into the structure as well as to particle fragmentation which results in an increase in the surface area. Most metallic powders, however, are difficult to mill due to their ductility. Bobet et al. (2005) in order to improve the milling ability added hard oxide powders to Mg. Hard/brittle powders that have been added to the Mg systems are V₂O₅ (Yermakov et al. 2006), Nb₂O₅ (Friedrichs et al. 2006, Barkhordarian et al. 2004), Al₂O₃ (Güvendiren et al. 2004, Friedrichs et al. 2006), also SiC (Güvendiren et al. 2004), VH₂ (Yermakov et al. 2006, Güvendiren et al. 2004). The addition of these hard particles has been found to have a positive effect on the sorption kinetics. However, desorption temperatures of Mg were little affected by these additions. Table 3.1 gives some examples of magnesium based hydrogen storage systems produced by mechanical alloying with various additions.

A common technique used as an aid in milling is to carry out the milling operation under hydrogen atmosphere (Bobet et al. 2000) or to start the milling process with MgH₂ rather than Mg (Liang et al. 2004). Milling under hydrogen leads to in-situ

conversion of Mg to MgH_2 . Such reactive milling therefore leads to very rapid fragmentation of the powders due to the brittleness of hydrides.

Table 3.2 gives some examples of reactively milled magnesium based hydrogen storage materials together with their hydrogenation properties. The lowest desorption temperature reported for Mg is about 280°C which is achieved by milling MgH_2 under 10 bar pressure (Klassen et al. 2006).

The mechanical milling leads to a size reduction as well as to substructure development. The size reduction is measured by variety of methods e.g. laser method, direct measurement from electron microscope image, or from the measurement of surface area with BET (Brunauer, Emmett and Teller) method. The substructure, i.e. coherently diffracting volume sizes, is measured usually using X-ray diffraction methods.

The size results obtained with the methods named above varies from micron to 20-30 nm range for Mg based systems. For instance Zaluska et al. (1999) having spex milled Mg granules for 20 hours reported particles that are only 20 μm in size. Values reported by Bystrycki et al.(2005) for Mg powders mixed with Mo, Co, Zr, V magneto-milled for 20 hours are in the range of 20-30 μm . Scale of substructure that evolves as a result of these processings; however, is much finer. Zaluska et al. (1999) reported a "cell size" of 20-30 nm for the milled Mg measured directly with TEM. In most studies the values are derived from the X-ray diffraction profile and are in the range of 40-65 nm (Bystrycki et al., 2005; Liang et al., 2003; Riktor et al., 2009).

For the hydrides milling leads to very rapid fragmentation resulting in a large increase in the surface area (Huot et al., 1998). For instance Chen et al. (2001) have milled MgH_2 particles of initially 5-15 μm in size was reduced them to 2 μm only after 1 hour of milling. Varin et al. (2005) have carried out extended milling (100 hours) and reported an average particle size of 0.6 μm . Similar values were reported in milling of MgH_2-TiH_2 (Charbonnier et al., 2004; Choi et al., 2008), MgH_2-Co (Chen et al., 2001), MgH_2-V (Liang et al., 1999) for which the milling time varied between 10 and 60 hours. Reactive milling of Mg, i.e. milling under hydrogen atmosphere, is almost as effective as starting with hydrides. Tessier et al. (1999)

Table 3.1. Some examples of hydrogen storage systems produced by mechanical alloying.

| Reference | Material | Miller | | B/P | Controlling Agent | Activation | Absorption | | Desorption | | Amount wt % |
|--------------------|-----------------------|--------------------------|-------|------------------|---|------------------|------------|-----------|----------------------|---------|-------------|
| | | Type and Duration | T | | | | P | T | P | | |
| Zaluska (1999) | Mg+Pd | 20 h | - | - | - | 300 | 10 | 330 | 1 | 5 | |
| Liang(2003) | Mg-20Ti | Spex 31 h | 10:1 | - | 290°C 10atm H ₂ | 290 °C | 10 atm | 290 °C | | 5 | |
| Liang (2004) | Mg+Li V | | 10:1 | graphite | Evacuated 20 min | 350 °C | 13.5 atm | 350 °C | 1.5 atm | 6 | |
| Liang (2004) | Mg+20 Cd | Spex 20+20h | 10:1 | 2.5V graphite | Evacuated 20 min | 300 °C | 10 atm | vacuum | 1 atm | 3 | |
| Czujko (2006) | Mg+V Zr Y | Magnetic ball mill 5-20h | 10:1 | - | Vacuum 350 °C, 1.5 hrs Abs; 23 atm 50 min 350 °C | 350 °C 90 min | 23 atm | 300-350°C | Atmospheric pressure | 5 | |
| Bystrzycki (2005) | Mg+Y | Magnetic ball mill 20h | - | - | 350 C 10 bar | 300 | 10 | - | - | 5 | |
| Takasaki (2007) | C100- xMgx (0? x? 40) | planetary ball mill. | 8:1 | - | - | 40 | 40 | - | - | 0.1-0.4 | |
| Khrussanova (2001) | Mg+Ti V Fe | 20 h | 10:1 | | Vacuum activation | 350 °C | 10 atm | 350 °C | 1.5 atm | 6 | |
| Hashimoto (2006) | Mg+In | | 100:1 | NaCl | 10 atm hydrogen | 330 °C | | 340 °C | 2.5 atm | ? | |

Table 3.2. Reactively milled Mg based systems and their storage results.

| Reference | Material | Milling hydrogen pressure | Miller type duration | B/P | Activation | Absorption T | Absorption P | Desorption T | Desorption P | Amount wt % |
|----------------|---|---------------------------|--------------------------|-------|---|------------------|--------------|--------------|----------------------|-------------|
| Bobet (2006) | Mg+V Zr Y | 11 | Magnetic ball mill 5-20h | 10:1 | Vacuum 350 °C, 1.5 hrs Abs; 23 atm 50 min 350 °C | 350 °C 90 min | 23 atm | 300-350 °C | Atmospheric pressure | 5 |
| Gennari (2001) | Mg | 5 | 50 | 44:1 | - | - | - | 350 | - | 4.7 |
| Castro (2004) | Mg-5 at.%Nb | 30 | 25-48 h | 40:1. | - | 350 | - | - | - | - |
| Castro (2004) | Mg + WO3 | 11 | 16 h | 9.8:1 | - | 300 | 11 | 330 | 0.4 | 6 |
| Bobet (2000) | Mg+ Ni Co Fe | 11 | Planetary mill 5 h | 10:1 | - | 350 | 16 | 350 | 1.5 | 5 |
| Bobet (2005) | Mg + 5wt.%Cr-2O3 | 11 atm | Planetary mill 30 h | - | - | 300 | 10 | 300 | 0.25 | 6 |
| Song (2005) | Mg+10 wt Fe ₂ O ₃ | 10 atm | 6 h | ? | 5 cycle | 320 | 12 | 320 | 1-1.8 | 3.43 |

have milled Mg under 10 bar hydrogen for 40 hours reported that 25 % of Mg was converted to MgH₂ yielding quite small particles. In similar studies, values of 1.3- 0.57 μm (Bobet et al., 2002) were reported for MgH₂. Although the particle sizes that are reported are quite small for hydride milling or with reactive milling, all these values are quite small as compared to those achieved with direct milling of Mg based powders. As for the crystallite size, however, the difference is rather diffuse. This value as measured with X-ray diffraction falls in the range 15- 66 nm. For instance Bobet et al. (2000) reports a crystallite size of MgH₂ 12 nm in Mg-Co system milled under hydrogen for 10 hours. They report almost the same value when the mixture was milled under argon

3.1.1. Hydrogen Storage in Mg-Ti system

Ti is one of the most widely used additives in the processing of Mg for hydrogen storage purposes. Mg and Ti both have hexagonal close packed (HCP) structure at ambient conditions. Ti transforms to a body centered cubic structure above 1155 K. Solubility of Mg in Ti is less than 2 at % and Ti has no solubility at all in Mg. No Mg-Ti intermetallic compound is formed in this binary system, Figure 3.2 (Nayeb-Hashemi et al. 1998). Ti has been added to Mg especially for their catalytic effects, i.e. splitting of hydrogen molecule into atomic form, ready for diffusion into the host metal. Since normally Ti has no solubility in Mg lattice, in order to obtain this catalytic effect the surface of the Mg powders should be covered by Ti particles of extremely small size.

Such refined structure is very difficult to achieve using melting methods. Mechanical milling and thin films are the only processing techniques that can be used for this purpose. Under such conditions, some degree of solubility as well as metastable phase formation are possible (Akiba et al. 2009) in both bulk form (Liang et al. 1999) or as in thin film samples (Kyojima et al. 2004). Liang et al. (2003) have synthesized Mg_xTi_{100-x} alloys by means of ball milling using Spex mill. They have used stainless steel balls and pot with a ball to powder ratio of 10:1 under argon atmosphere. No new phase formation has been reported. But they observed dissolution of Ti in Mg which could be as much as 12.5 at % Ti. This was reflected

to a decrease in c/a ratio of the crystal. Liang et al.(2003) conclude that the extended solubility improves the kinetics of hydrogenation. It has been shown that the supersaturated solid solution obtained by milling is not stable and decomposes upon exposure to elevated temperatures. During hydrogenation the single phase alloy has been transformed to MgH_2 and TiH_2 . So the incorporation of Ti into Mg was temporary and disappeared with the first cycle.

Asano et al. (2009) have studied wide range of Mg-Ti mixture spanning all compositions; Mg_xTi_{100-x} x ranging from 25 to 80. The powders were milled in argon atmosphere with planetary mill up to 150 hours. They observed two-phase Mg-Ti HCP structure in Mg rich composition down to $x=60$. Between $X=60$ to 50 they observed a BCC phase with a lattice parameter of $a=0.345$ nm, and $a=0.342$ nm at $x=60$ and at $x=50$ respectively. Beyond $X=50$ no BCC phase was observed. In a separate study, the same group reports also the formation of FCC phase(Asano 2009). In this study they have milled the powders using zirconia or stainless steel balls. With stainless steel balls and pot, the results have confirmed that Mg rich end had a two phase HCP structure which was followed by BCC phase starting from $X=80$. When they used zirconia balls however, the resulting phase was FCC.

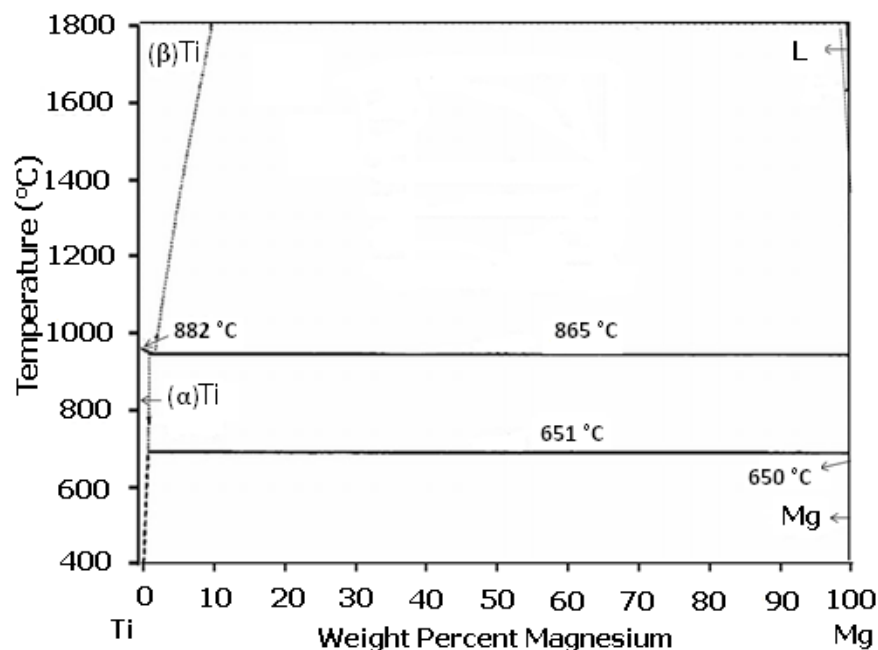


Figure 3.2. Binary Phase Diagram of Mg-Ti, Nayeb-Hashemi et.al.(1998)

They proposed that the HCP phase was formed by solution of Ti into Mg and, BCC phase by solution of Mg in Ti. FCC phase was stabilized by introduction of stacking faults into the HCP structure.

FCC and BCC phases reported by Akiba and co-workers were not stable upon hydrogenation. The BCC phase can be hydrogenated to 5.0 wt % at 423 K and to 3.9 wt % at 303 K. The FCC phase (including MgH_2) had a hydrogen content of 4.7 wt % and the chemical formula of $\text{Mg}_{42}\text{Ti}_{58}\text{H}_{177}$.

A Mg-Ti compound with FCC structure was also produced by a high pressure synthesis (Rönnebro et al. 2005). This phase synthesized from MgH_2 and TiH_2 powders had a unit formula $\text{Mg}_7\text{TiH}_{16}$ with Fm3m (225) space group. The basic structural building block is claimed to be face centered cubic unit cell; $a = 4.76(6)$ Å, which is close to the $\text{TiH}_{1.9}$ structure $a = 4.44(8)$ Å, The compound with the formula of $\text{Mg}_7\text{TiH}_{16}$ had 7 wt % hydrogen. In a similar study, Kyoji et al. (2004) have synthesized $\text{Mg}_7\text{TiH}_{16}$ FCC hydride using a high pressure anvil cell by reacting a mixture of MgH_2 and TiH_2 . This FCC hydride phase had a Ca_7Ge type superstructure. The compound releases its hydrogen at around 332°C by decomposing into Mg and $\text{TiH}_{1.9}$ whereby releasing 4.7 wt % of hydrogen.

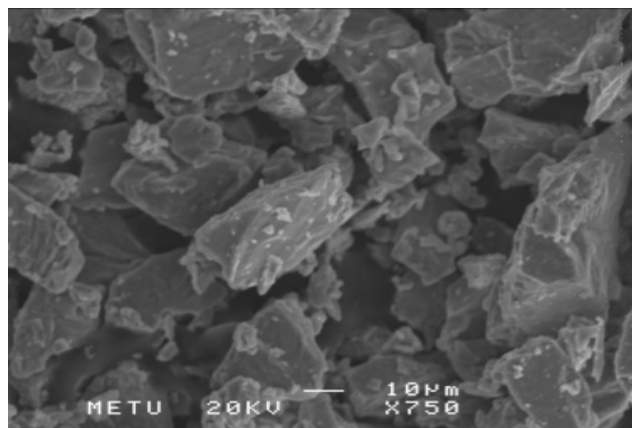
Mg-Ti compositions can also be synthesized by thin film processing. Vermeulen and co-workers (2006) have synthesized Mg-Ti thin films by sputtering. These thin films, which had a two phase HCP structure, covered with Pd, were hydrogenated by means of both electrochemical method and solid-gas reactions. Broederz et al. (2008) have produced Mg thin films doped with Ti. They found that hydrogenated film with alloy compositions between $\text{Mg}_{65}\text{Ti}_{35}$ and $\text{Mg}_{86}\text{Ti}_{14}$ had FCC structure. However, enthalpy of these hydrides were found to differ little (-65 kJ/mol- H_2) from that of rutile MgH_2 . The enthalpy of the thin films compositions incorporating less than 14 at % Ti was however -61 kJ/mol- H_2 which is less than that of pure MgH_2 (74.06 kJ/mol). This shows that Mg-Ti hydrides could be less stable than pure MgH_2 . The authors have reported that the Mg-Ti compositions mentioned above have good optical switching properties and excellent hydrogenation kinetics.

Following the favorable characteristics of Mg-Ti system, the present work concentrates on Mg-10 vol %Ti alloy and aims to process this alloy via mechanical

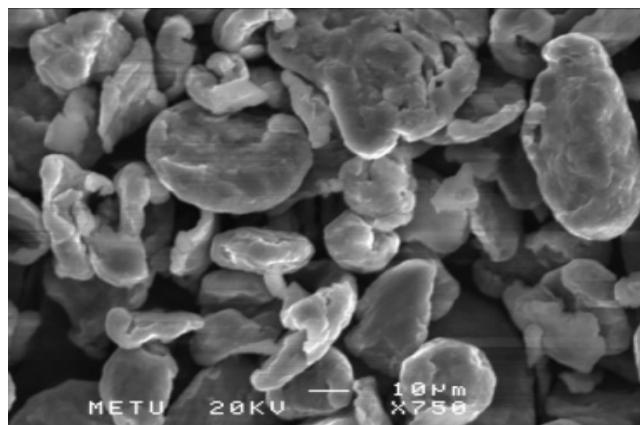
milling. The aim is to produce a nanostructured Mg-Ti where both Mg and Ti are formed as nanosized particles. The study involves processing in two conditions; i) milling of Mg-Ti under inert atmosphere ii) reactive milling of Mg-Ti, i.e. milling under hydrogen atmosphere.

3.2. Experimental Procedure

Starting materials were elemental powders (Alfa Aesear) of Mg and Ti. All were provided in $\leq 44\mu\text{m}$ (-325 mesh) with a purity of 99.8 %. Scanning Electron Microscope (SEM) images of the starting powders are given in Figure 3.3.



(a)



(b)

Figure 3.3. SEM images of starting powders a) Ti ($\leq 44\mu\text{m}$) and b) Mg ($\leq 44\mu\text{m}$).

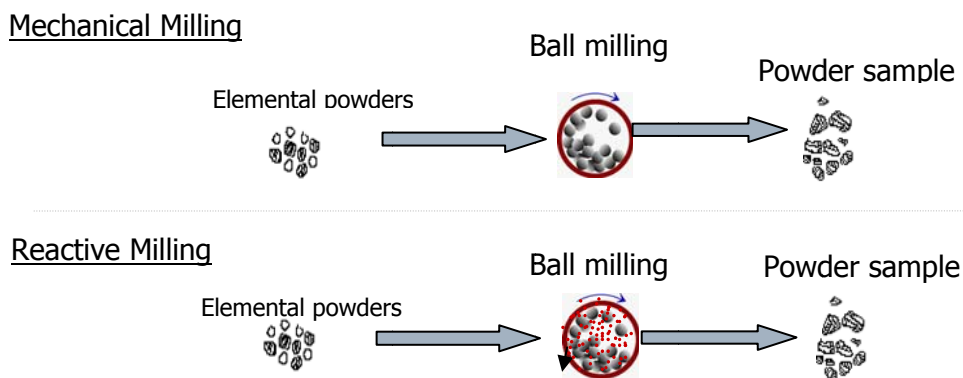


Figure 3.4. Schematic representation of processing routes in mechanical milling and reactive milling used in the study.



Figure 3.5. Vials used for mechanical milling and reactive milling.

XRD analysis was performed with Rigaku diffractometer using Cu K α radiation. Data were collected over a 2θ range of 20–90° with a step of 0.02°. A 3 s acquisition time was used at each step. X-ray data were refined with Rietveld method using MAUD program (Lutterotti, 2002). Standard Si sample was used to estimate the instrumental parameters for Rietveld refinement.

Morphological and microstructural examination was carried out with scanning electron microscope (JEOL-JSM6400, FEI-NOVA nanosem). The specific surface area

of the powder was measured using the BET method (Quantachrome Autosorb-1-C/MS analyzer). The method determines total surface area of the material using the physical adsorption of gas over the surface area of the material. The samples were out gassed at 573 K for 6 hours before the experiments and the measurements are carried out at 77 K. The particle size was measured using laser diffraction technique by comparing a sample's scattering pattern with an appropriate optical model.

Hydrogenation experiment is carried out with Sievert type apparatus. Photograph and schematic representation of the apparatus are given in Figure 3.6 (a) and (b), respectively. The volumetric hydrogen storage apparatus contains a pressure gauge, hydrogen and Ar gas inlets connected to the cylindrical reservoir and to the sample system with several valves. A filter with the a hole diameter of 1 μm is placed to the gas inlet/outlet part of the reactor system. The temperature of the reactor system, reservoir and filter is monitored separately using three thermometers at each point. The reactor is inserted into a furnace to set the temperature for intended application. Here the apparatus can be divided into three regions; i) the reservoir, ii) filter and iii) reactor. The reservoir and the filter region had volumes of 72 and 8 cm^3 respectively. The reactor volume varied depending on the amount of sample place inside, but typically had a value of 2.5 cm^3 .

Before starting the sorption experiments, samples were activated. (for the samples milled under hydrogen atmosphere no activation was necessary.) Activation involved several cycles of hydriding and dehydriding. For this purpose, furnace is set to the desired temperature (e.g. 350°C) and after stabilization of the temperature, hydriding is carried out by exposing the sample to 10 bar of hydrogen pressure for 3 hours. For dehydriding the system is taken under vacuum and waited for 3 hours.

Measurement of the PCT was carried out by hydriding the sample at different levels of hydrogen pressure. Pressure levels studied varied from 0.5 to 10 bar at an interval of 0.5 atm. At a given level, change in pressure was monitored. The experiment was terminated when no change in pressure occurred for a period of 5 minutes. Drops in pressure are added together to find the total absorption for that level. The pressure is adjusted to a new value and the whole process is repeated until the maximum pressure is reached (usually 10 bar).

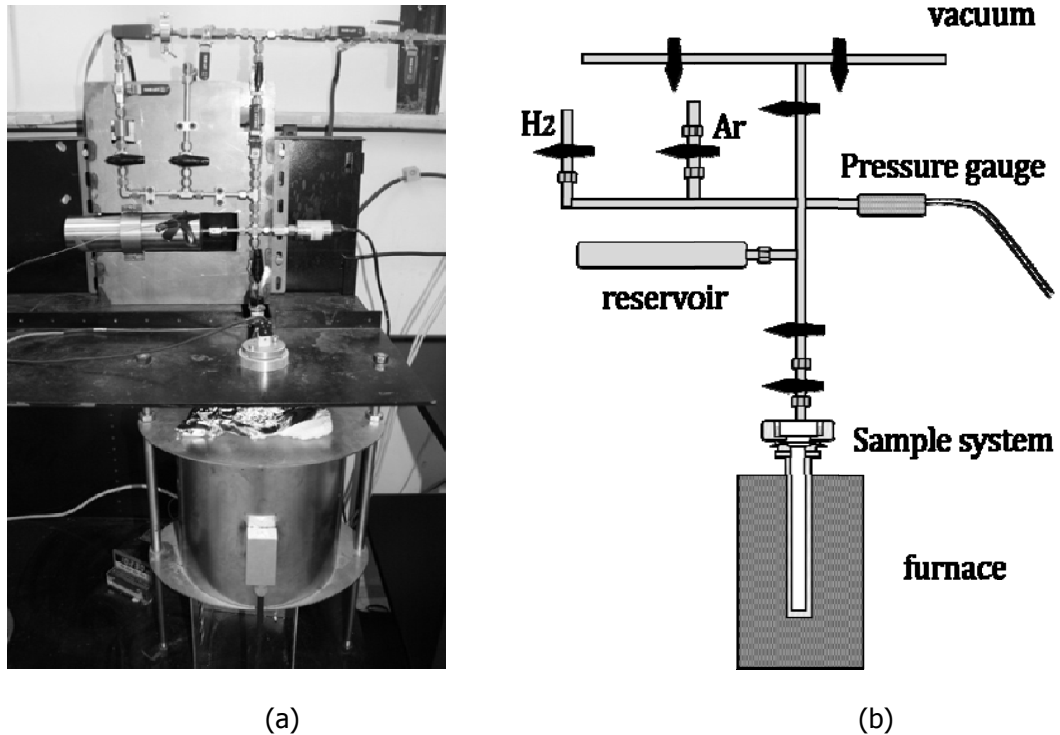


Figure 3.6. (a) General view of the apparatus used for experiment. (b) Schematic diagram of the sample reactor.

The measurement of absorption kinetics was carried out in the same apparatus but the reservoir was changed and the volume was increased to 400 cm³. The hydrogen at a selected pressure in the reservoir volume was released to reactor by opening the sample valve and the pressure change was monitored as a function of time. Reaction was considered to be complete when no drop in pressure occurs for a waiting period of 1 hour. Pressure values were selected as 10 bar and 0.1 bar for absorption and desorption, respectively.

3.3. Results and Discussion

3.3.1. Structural Observations: X-ray diffractogram of the sample which is milled under inert atmosphere is given in Figure 3.7. It is seen from the figure that no new phase formed between Mg and Ti. Thus, the pattern is made up of peaks of Mg and Ti.

The pattern of reactively milled sample is given in Figure 3.8 after 30 hours of milling. The pattern covers peaks of TiH_2 , MgH_2 as well as Mg. From the diffractogram, it appears that Ti is totally converted to its hydride; while the conversion of Mg is only partial.

Various structural parameters derived from Rietveld refinement of X-ray data for samples milled under argon as well as those milled under hydrogen are reported in Table 3.3. Rietveld refined pattern of samples after 30 hours of milling are given in Figure 3.9. The goodness of fit value (R) value is 6.5 and 7.4 for mechanically milled and reactively milled samples, respectively. According to Luterotti (2002), the value should be less than 10 for a usable fit. As seen in Table 3.3, the lattice parameter of Mg remains almost the same after milling. Thus, Mg does not dissolve Ti to any significant extent. Values of crystallite size reported in table 3.3, show that Mg and Ti in have quite comparable values.

SEM images of milled samples are given in Figure 3.10. Mg-Ti milled under Ar appears to be little affected by milling in terms of its appearance. The particles after

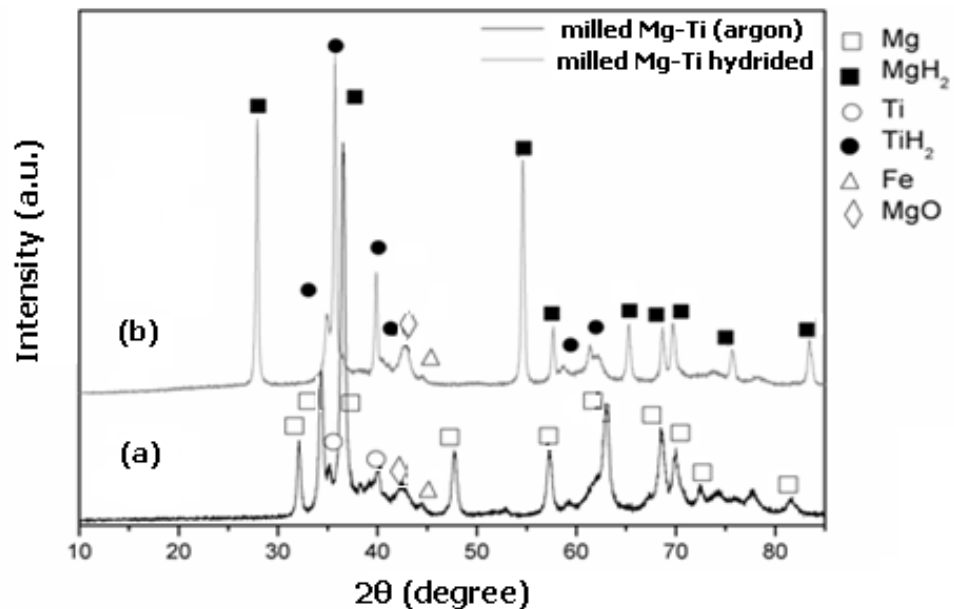


Figure 3.7. X-ray diffractogram of the milled sample before (a) and after hydrogenation (b).

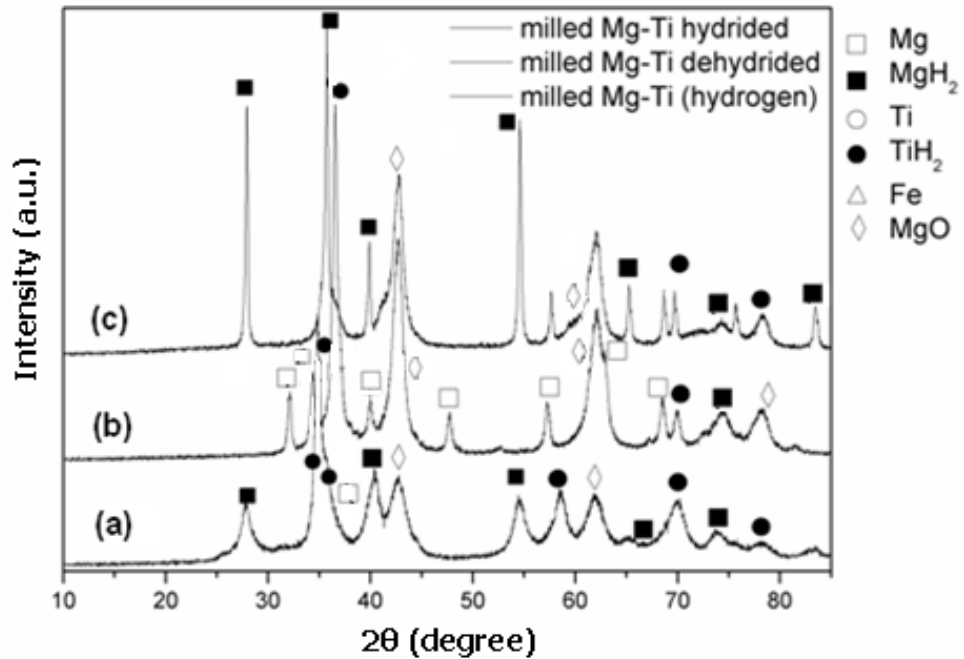


Figure 3.8. X-ray diffractogram of reactively milled sample(a). Figure also shows the diffractogram of dehydrided(b) and rehydrided (c) samples.

milling appear to be even larger than the initial ones; compare Figure 3.10 (a) and Figure 3.10 (b). Particles seem to be in the form of agglomerates probably formed by a cold welding process. BET measurement of this sample yields a value of 1.76 m²/g.

Mg-Ti milled under hydrogen atmosphere develops extremely refined structure, as shown in Figure 3.10 (c). BET measurement carried out on the milled sample yields a value of 9.86 m²/g. The most particles are micron and submicron in size, but some are coarse in the order of 30-40 μm. It is probable that these relatively coarse particles are Mg which were not converted to MgH₂.

In conclusion, it appears that milling under hydrogen and argon are quite different in terms of particulate structure they produce. While milling under hydrogen leads to the development of particles of extremely small size (< 1μm), milling under argon does not produce such an effect. The particles in the latter case agglomerate and results in particles that are even larger than the initial ones.

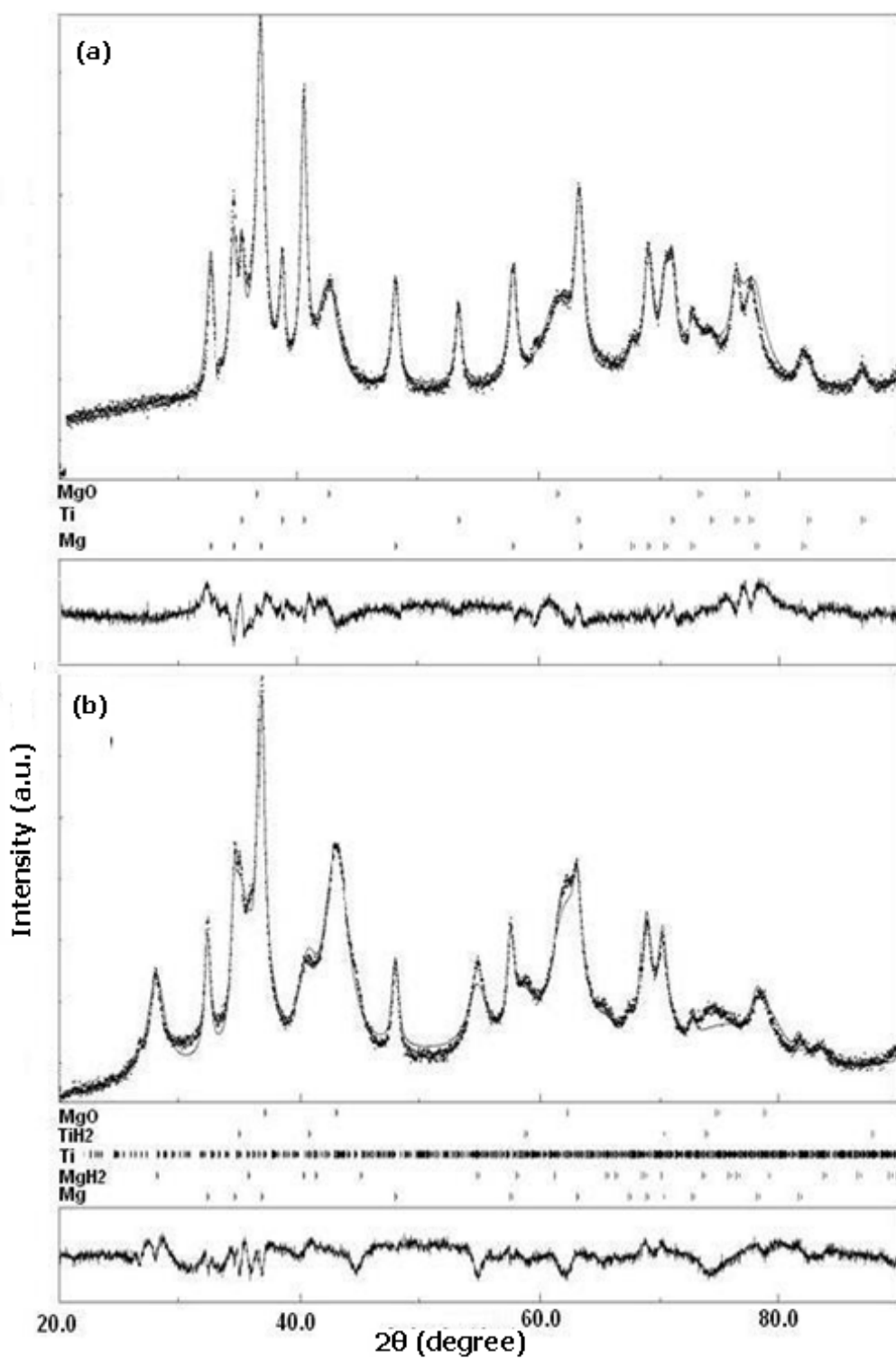
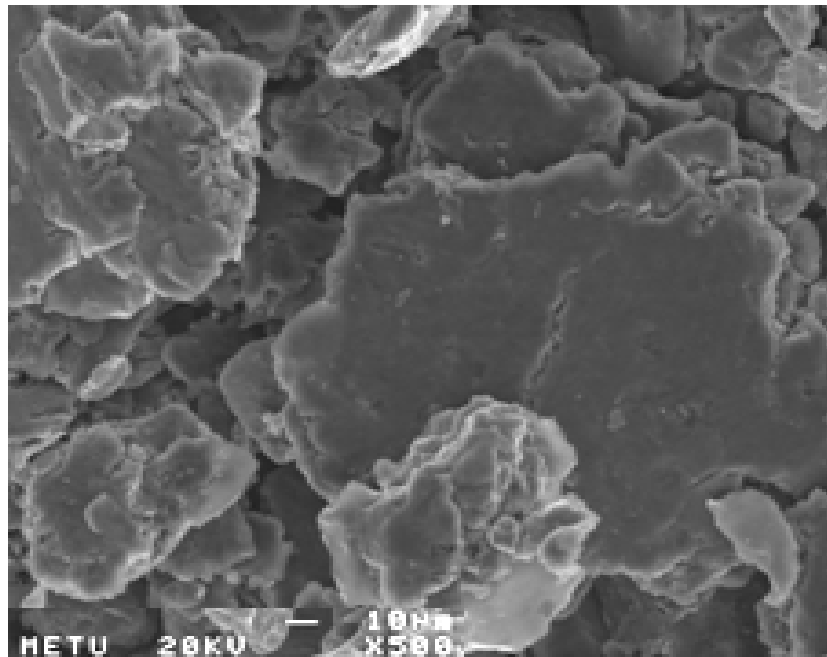


Figure 3.9. X-ray diffractograms of mechanically milled samples (a) argon (b) hydrogen.

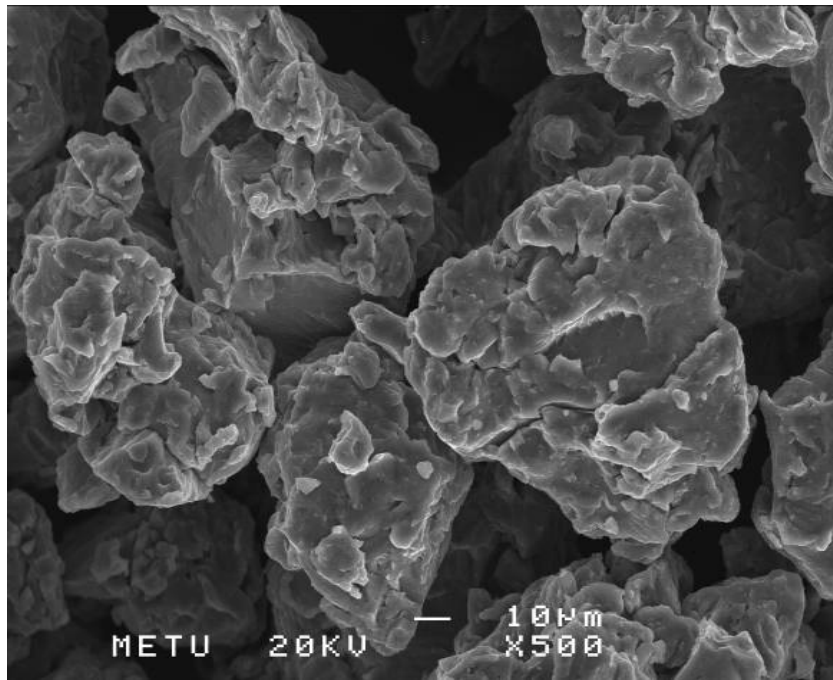
Table 3.3. Structural characteristics of Mg-10 vol%Ti powders processed via mechanical milling under argon and hydrogen atmosphere.

| | | Argon atmosphere | Hydrogen atmosphere |
|----------------------------------|---------------------|------------------|---------------------|
| surface area (m ² /g) | | 1.76 | 9.86 |
| volume fraction of phases | Mg | 70.94 | 39.82 |
| | Ti | 19.28 | 0.79 |
| | MgH ₂ | - | 38.50 |
| | TiH ₂ | - | 5.27 |
| | MgO | 9.77 | 15.58 |
| Average crystallite size (nm) | Mg | 20.78 | 25.09 |
| | Ti | 25.06 | 33.63 |
| | MgH ₂ | - | 20.05 |
| | TiH ₂ | - | 25.04 |
| lattice parameters (Å) | Mg-a | 3.21(3) | 3.21(4) |
| | Mg-c | 5.21(8) | 5.21(9) |
| | Ti-a | 2.95(6) | 2.95(8) |
| | Ti-c | 4.69(3) | 4.69(9) |
| | MgH ₂ -a | - | 4.49(8) |
| | MgH ₂ -c | - | 3.05(9) |
| | TiH ₂ | - | 4.46(1) |

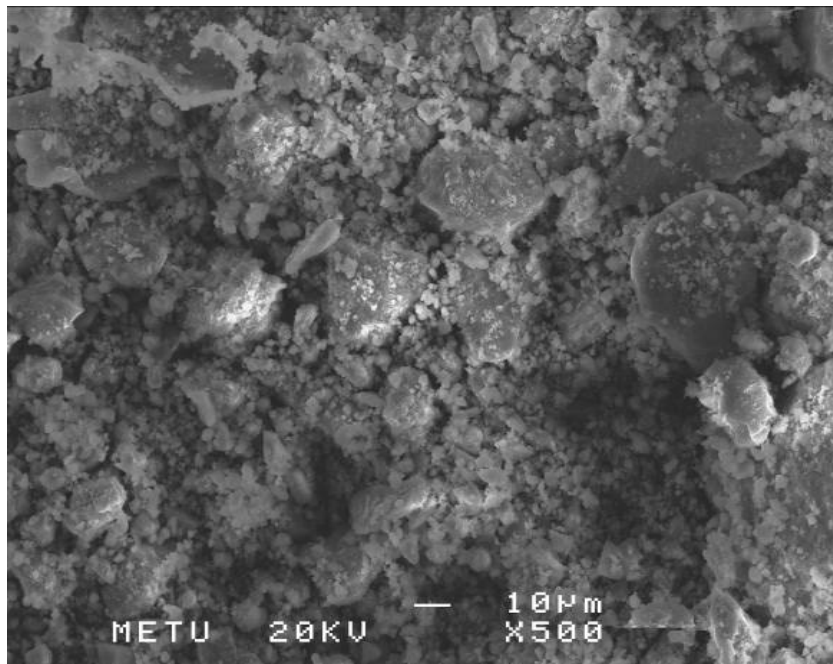


(a)

Figure 3.10. The microstructure of Mg-10 vol%Ti samples (a)unmilled (b) milled under argon (c) milled under hydrogen (10 bar).



(b)



(c)

Figure 3.10. *Continued,*

3.3.2. Hydrogenation Experiments: Following milling of Mg-Ti under argon and hydrogen, each for 30 hours, the samples were subjected to various hydrogenation experiments.

The sample milled under Ar was hydrogenated at 300 °C using the procedure described above. Figure 3.7(b) shows the X ray diffractogram of the sample after hydrogenation. It can be seen that the peaks for Mg and Ti which were present in the milled sample are replaced by those of MgH₂ and TiH₂ after hydrogenation. Thus the phases were totally converted into hydrides.

Before hydrogenation experiments, an activation procedure was applied to Mg-Ti samples milled under Ar. This consisted of 3 cycles of hydriding and dehydriding treatment carried out at 350 °C. Following activation PCT curves were determined at two different temperatures, namely 320 °C and 280 °C. The curves obtained for absorption and desorption are given in Figure 3.11. These curves give plateau pressures of 0.99 bar at 280 °C and 3.05 bar for 320 °C for absorption. The values for desorption are 0.98 bar and 2.6 bar in the same order.

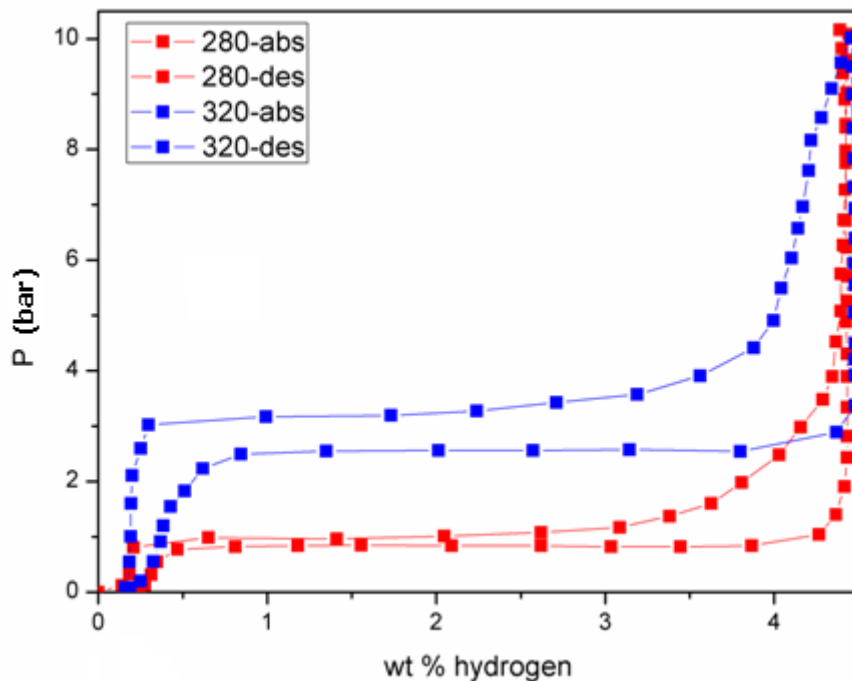


Figure 3.11. PCT diagram of Mg-10 vol % Ti milled under argon.

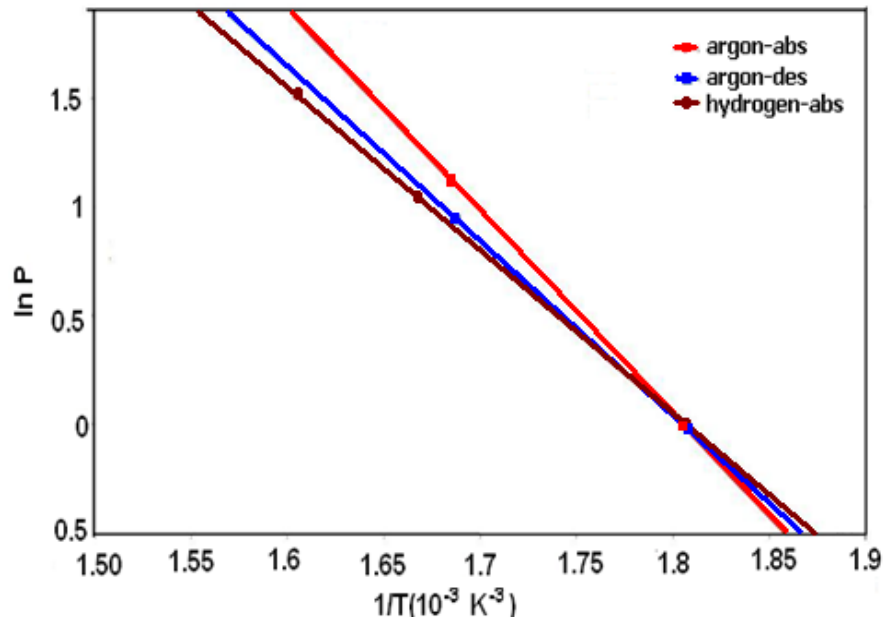
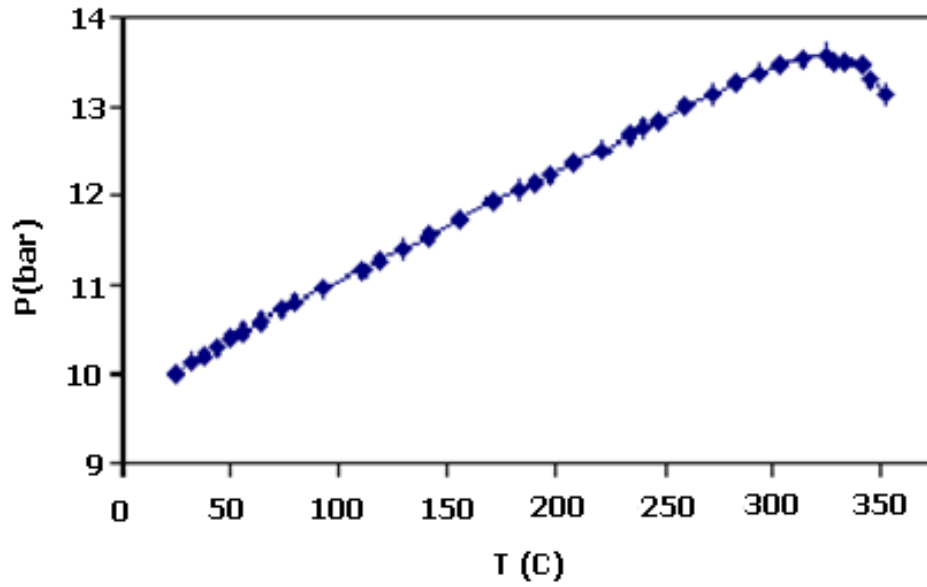


Figure 3.12. Van't Hoff plot of the mechanically milled samples; milled under argon, milled under hydrogen.

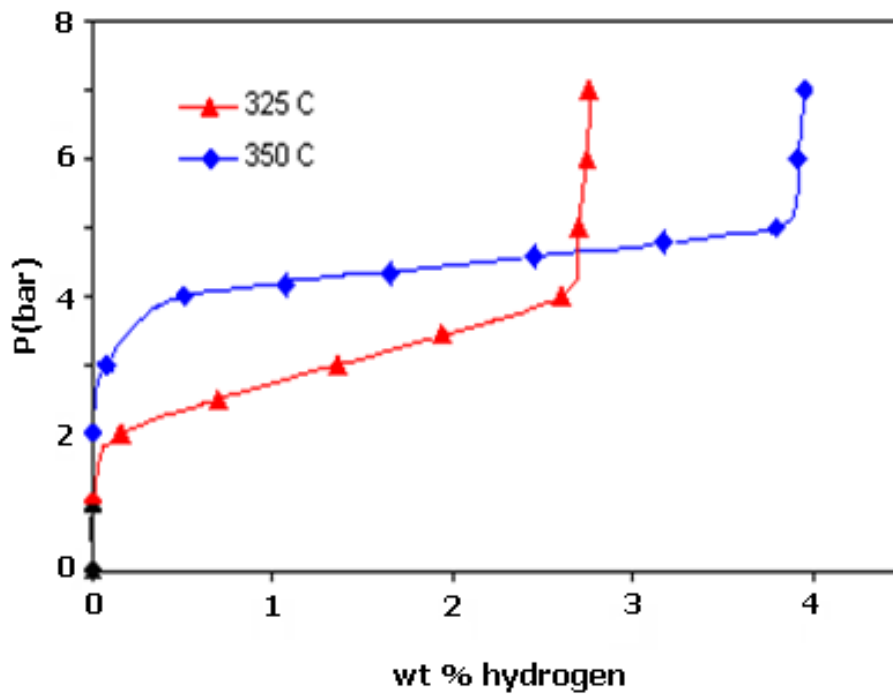
The temperature dependence of plateau pressure (P) can be described by van't Hoff equation.

$$\ln P = \frac{\Delta H}{RT} - \frac{\Delta S}{R} \quad (3.1)$$

here ΔH and ΔS are enthalpy and entropy of dehydrogenation, R is the gas constant and T is the temperature. Plateau pressure determined at 320 and 280 °C are shown plotted in Figure 3.12. This yields enthalpy and entropy values of -76.74 kJ/mol-H₂ and -138.64 J/K.mol-H₂ for absorption and 66.54 kJ/mol H₂ and 120.12 J/K.mol H₂ for desorption, respectively. For 1 bar of hydrogen pressure, this corresponds to a hydrogen release temperature of 280 °C. This value is not far off the lowest desorption temperature reported for powder processed Mg based alloys (Oelerich et al. 2001). Thus, it appears that even though Mg milled under argon have yielded quite coarse particles size the processing was successful in that the mixture had a desorption temperature which was one of the lowest reported in the literature.



(a)



(b)

Figure 3.13. (a) Pressure change (hydrogen) as a function of temperature in Mg-10 vol. % Ti milled under hydrogen, (b) PCT diagram of Mg-10 vol % Ti milled under hydrogen.

No activation was necessary for Mg-Ti milled under hydrogen. This can be seen by the temperature programmed sorption curve given in Figure 3.13 (a). This curve was determined under 10 bar of hydrogen pressure and the pressure change was recorded as a function of temperature, i.e. temperature programmed sorption. It is seen that there is a clear pressure drop at temperatures close to 300 °C.

Hydrogenation behavior of the reactively milled Mg-Ti was further evaluated by determining its PCT (absorption). Figure 3.13(b) show this diagram at, 325°C and 350 °C. Van't Hoff plot for this sample is also shown plotted in Figure 3.12. The enthalpy and entropy values obtained from this curve is -62.42 kJ/mol H₂ and -112.91 J/K.mol H₂, respectively. The enthalpy of hydrogenation here is slightly less than that of the sample milled under Argon.

3.4. Discussion

Results reported above show that the processing of Mg-Ti via mechanical milling under argon and hydrogen differ from each other in several respects. The most important difference is that milling under hydrogen leads to extremely small particle size. Mg is converted to MgH₂ and due to its brittleness and they are fragmented into particles of extremely small size. BET measurement yields a surface area value which is an order of magnitude larger than that of the sample milled under argon. This implies that the particle size is an order of magnitude less in milling under hydrogen. For the Mg particles mechanically milled under argon, higher particle size was obtained implying the agglomeration of the initial particles. Ti particles seem to be distributed homogeneously throughout the Mg particles.

Mg agglomerates as well as Ti fragments are made up of coherently diffracting volumes of approximately 20-25 nm in size for both mechanically and reactively milled sample.

Hydrogenation experiments have shown that mechanically milled Mg-Ti sample can be hydrogenated after an activation treatment, whereas reactively milled samples does not require activation. After activation, both samples can be hydrogenated

easily. From the PCT diagram for desorption of mechanically milled samples, enthalpy and entropy values are calculated to be $-76.74 \text{ kJ/mol-H}_2$ and $-138.64 \text{ J/K.mol-H}_2$ for absorption and 66.54 kJ/mol-H_2 and $120.12 \text{ J/K.mol H}_2$ for desorption respectively. The enthalpy and entropy of hydrogenation obtained for reactively milled sample yields values of $-62.42 \text{ kJ/mol-H}_2$ and $-112.91 \text{ J/K.mol-H}_2$ in the respective order.

3.5. Conclusions

The current study on the processing of Mg-Ti for hydrogen storage has shown that Mg-Ti can be processed quite successfully using mechanical milling both under argon and under hydrogen.

Milling under argon has shown that:

- i. Mg powders agglomerate to sizes which are larger than the initial ones, while Ti is fragmented into pieces homogeneously distributed throughout the structure.
- ii. Mg agglomerates as well as Ti fragments are made up of coherently diffracting volumes of approximately 20-25 nm in size

The processed powders following an activation treatment reacts with hydrogen. The enthalpy of hydrogen desorption has a value of 66.54 kJ/mol which means that the processed powders can desorb hydrogen at $280 \text{ }^\circ\text{C}$ against 1 bar of hydrogen pressure. This is close to lowest desorption temperature reported for Mg based powders processed with additives (Oelerich et al.2001).

The milling of Mg-Ti under hydrogen atmosphere has shown that:

- iii. Mg and Ti are partially converted into their hydrides and they are milled down to extremely small sizes, while untransformed fraction remains as coarse particles in the order of 30-40 μm .

CHAPTER 4

THE PROCESSING OF Mg AND Mg-Ti WITH SEVERE PLASTIC DEFORMATION

4.1. Introduction

A number of routes are available for structural refinement of metallic materials e.g. mechanical milling (Suryanarayana, 2001), repetitive rolling (Pedneault et al., 2008), equal channel angular pressing (ECAP) (Segal, 1999) etc. Of these, mechanical milling is a well established method, used widely for the processing of metallic powders. The method not only induces severe plastic deformation but also, quite often, leads to particle fragmentation. In fact the milling with its associated structural refinement has established itself as an efficient method of material synthesis for hydrogen storage alloys (e.g. Güvendiren et al. 2004).

Although the effectiveness of mechanical milling is well established in the processing of hydrogen storage alloys especially in intermetallics or intermetallic forming mixtures, it is often very difficult to employ this in ductile powders (Huang et al. 1995). Mg and Mg based powders are not brittle enough and therefore, as illustrated by Çakmak et al. (2010) they agglomerate during milling with the resultant increase in particle size. The role of additives is then to help make material brittle so that the milling may lead to particle fragmentation rather than agglomeration. Still, the milling of Mg or Mg based powders to small particulate sizes is an extremely difficult task (Hwang et al. 2001, Zaluska et al. 1999).

A drawback in the synthesis of hydrogen storage alloys is the necessity to process the material under a protective atmosphere. Exposure of powders during or after milling to atmospheres containing O_2 , H_2O etc are lethal and must therefore be avoided [(e.g. Ivey et al. 1983). Thus the powders are often processed and handled

under argon atmosphere of high purity, i.e. in a glove box. The problem is aggravated by the fact the milling, when successful, leads to a rapid generation of new surfaces, so the environment to which they are exposed to is of paramount importance.

Clearly an alternative method of material synthesis which would not require a protective atmosphere would be extremely beneficial. In this respect, ECAP processing appears to be the an obvious candidate since the new surfaces generated in this process are negligibly small. In fact, ECAP have already been employed in the processing of Mg based hydrogen storage alloys (Loken et al. 2007, Skripnyuk et al. 2007,Çakmak et al. 2007). The process normally involves a material in bulk form extruded through a die with two channels of equal cross-section, intersecting at an angle. The passage of material through the channels produces a simple shear deformation. This method, first used in 1972 by Segal , has since been developed in a number of respects; see Valiev and Langdon (2006). Though various forms of ECAP are available, the essence of the process is still the same, i.e. the cross-section of the material does not change during the passage, and so the process may be repeated many times enabling the accumulation of extremely large strains. It has been shown for many bulk metallic systems that the ECAP processing leads to drastic structural refinements often leading to the formation of submicron or nanoscale structures (e.g. Komura et al. 1999, Pushin et al. 2002).

The current work explores the possibility of employing ECAP processing in lieu of mechanical milling in an effort to develop a cost-effective processing route for hydrogen storage alloys.

4.2. Material and Method

Elemental powders used in this work were Mg and Ti, each 99.5 wt % pure with - 325 mesh size (see Figure 4.8 for particle size distribution). Samples were prepared from pure Mg and Mg-10%vol Ti powders. Two sets of samples were prepared for each; one was processed with ECAP and the other with mechanical milling.

For ECAP processing, the powder was first Spex milled for 10 minutes and then compacted with a pressure of 200 MPa into 8 mm diameter pellets. For ease of handling, the compacted powders were encapsulated in a copper block. The block was either square in its cross-section 14x14 mm, or round with 18 mm diameter. This was achieved by drilling a hole of 8 mm diameter from one end. Four pellets, each approximately 20 mm in length, were fitted into the hole. The block was then closed by pressing a copper insert into it. The block was 130 mm in length, so approximately 25 mm at each end was solid copper.

ECAP was carried out by feeding the copper block into a special die. Two die geometries were employed. One was a single zone 90 ° die that enabled batch processing, and the other was a two-zone 120° die that allowed continuous deformation, as shown in Figure 4.1.

A single zone die had two identical channels with 14x14 mm cross section intersecting at an angle of $\phi=90^\circ$. The inner corner of the intersection was kept sharp while the outer corner was rounded with $\psi =20^\circ$, Figure 4.1(a). Samples were deformed by feeding the copper block into die cavity and pressing the punch onto the block. To eliminate seizure, the punch was forced into the channel, typically by 25 mm, and then removed. A deformable insert was placed into the channel and the operation was repeated in the same manner as before. This continued until the block was forced through the deformation zone and came out from the exit end of the channel. For the geometry in question, i.e. $\phi=90^\circ$ and $\psi =20^\circ$, the passage through the deformation zone, imposes a true strain of $\epsilon= 1.00$ (Kim et al. 2001). After the passage, the copper block was re-fed to the die by rotating the sample 90°, i.e.the so-called B_c route, see García-Infanta et al. (2008).

Two-zone die had circular cross-section. The channel angle was 120° in both zones arranged in such a manner that the entry and exit channel was parallel to each other, Figure 4.1 (b). Each zone, in this die, could impose a strain of $\epsilon=0.60$ giving a total value of $\epsilon =1.2$. The process was automated, i.e. sample was pushed backward and forward in the die a number of times ,until the desired level of strain was achieved. The advantage of this parallel die was that it allowed the application

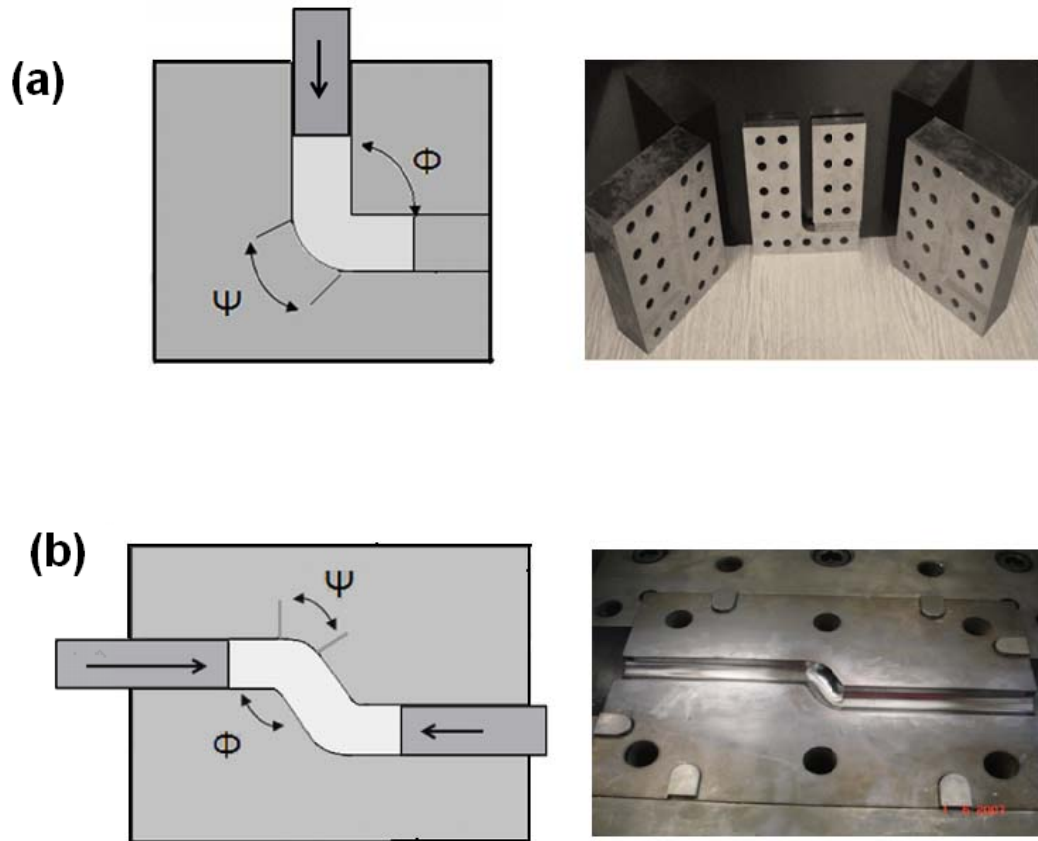


Figure 4.1. Dies used for equal channel angular pressing of compacted powder samples. Φ refers to channel angle, Ψ refers to the angle of curvature. (a) Single zone die with $\Phi = 90^\circ$, (b) Two-zone parallel die with $\Phi = 120^\circ$. The sample (white) is shown in a partially deformed state.

of back pressure on opposing punch so that deformation can be carried out with high hydrostatic pressure.

Mechanical milling of ECAPed samples as well as of the initial powders was carried out with a planetary ball mill using 5 mm diameter balls. Due to limited amount of ECAP samples, milling was carried out with a ball-to-powder ratio of 20:1. 1 wt % graphite was added to the powder mixture as anti-sticking agent. Where necessary, the particle size is measured with laser scattering using ethanol as dispersant.

Density of the powder compacts were measured by Archimedes principle. Since Mg reacts with water, ethanol was used for volume measurement. Microstructural

characterization was carried out using a field emission SEM. Structural refinement in samples was measured in terms of the size of coherently diffracting volumes. For this purpose, X-ray diffractograms were measured in a step scanning mode (0.02° for 3 seconds) $20^\circ < 2\theta < 80^\circ$ using CuK α radiation (typically 40 kV, 40mA). Standard Si sample was run at each session of X-ray measurements so as to correct angular shift that might occur in peak positions. The crystallite size, the lattice parameters as well as volume fractions were obtained from the Rietveld refinement of X-ray data.

4.3. Results

4.3.1. ECAP Processing of Mg and Mg-Ti

The regime of ECAP deformation employed in this study normally involved a single zone die with passage of samples 1, 2, 3 and finally 4-times. This corresponds to true strain values of $\epsilon=1, 2, 3$ and 4, respectively. Figure 4.2 shows a typical diffractogram recorded from a Mg sample deformed to $\epsilon =4$. The goodness of fit(R) value for the Rietveld refinement of the data was 5.25. Structural parameters derived from X-ray data for Mg and Mg-Ti are given in Table 4.1 and Table 4.2, respectively. Crystallite size, reported in this table, shows that the powders have been strained as a result of ECAP deformation. The values are such that there is a monotonic decrease with increasing level of strain, both for Mg and Mg-Ti. The size which is initially in the order of 140 nm for Mg decreases to a value of 80 nm after the fourth pass, i.e. a true strain of $\epsilon=4.0$. This decrease in the size of the coherently diffracting volumes is also true for Mg-Ti, Mg is reduced down to 72 nm and Ti had a size of 41 nm at the end of fourth pass.

Table 4.1 and Table 4.2 also contain data from mechanically milled powders. The crystallite sizes of Mg and Mg-Ti, determined after 5 hours of milling, are 80 and 70 nm in the respective order. Thus, in terms of coherently diffracting volumes, i.e. crystallite size, both ECAP deformation and mechanical milling leads to similar sizes. It can therefore be concluded that ECAP deformation is as efficient as mechanical milling in terms of size reduction in coherently diffracting volumes.

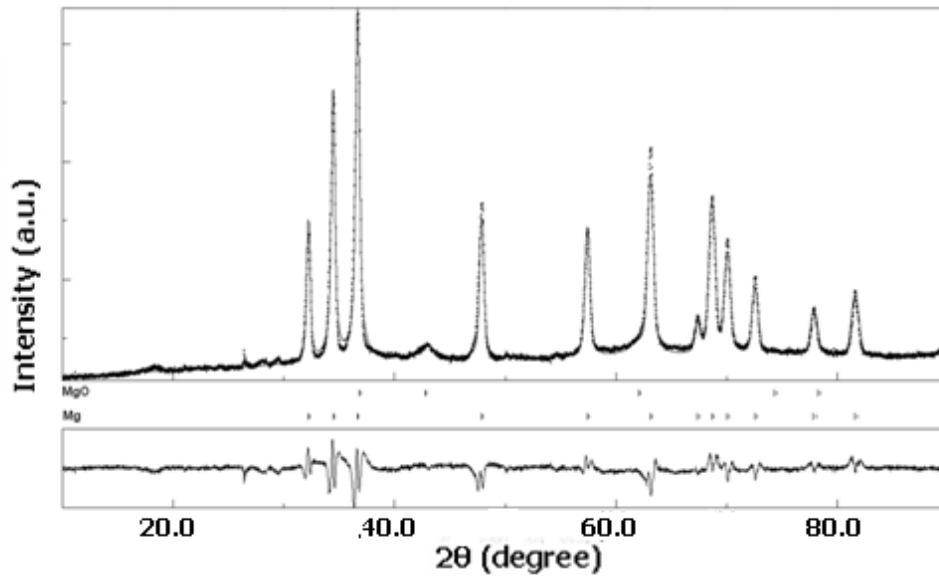


Figure 4.2. X-ray diffractogram (Rietveld refined) of Mg ECAP deformed to a true strain of $\epsilon=4.0$.

Table 4.1. Structural characteristics of Mg powder compacts ECAP deformed to true strains of $\epsilon=1, 2, 3$ and 4. The same mixture milled for 5 hours are also included for comparison

| | | ECAP deformation (ϵ) | | | | | Milled |
|-------------------------------------|--------|---------------------------------|---------|---------|---------|---------|---------|
| | | 0 | 1 | 2 | 3 | 4 | 5h |
| Crystallite size (nm) | Mg | 138.8 | 118.8 | 100.2 | 89.6 | 77.6 | 79.7 |
| | MgO | 2.0 | 1.4 | 1.4 | 1.5 | 1.5 | 2.4 |
| Volume fraction of phases | Mg | 98.0 | 98.6 | 98.6 | 98.5 | 98.5 | 97.6 |
| | MgO | 2.0 | 1.4 | 1.4 | 1.5 | 1.5 | 2.4 |
| Lattice Parameters (\AA) | Mg (a) | 3.21(6) | 3.21(5) | 3.21(5) | 3.21(4) | 3.21(4) | 3.21(4) |
| | Mg (c) | 5.22(1) | 5.21(7) | 5.21(6) | 5.21(7) | 5.21(7) | 5.21(7) |

Table 4.2. Structural characteristics of Mg-10 vol%Ti powder compacts ECAP deformed to true strains of $\epsilon=1, 2, 3,$ and 4. The same mixture milled for 5 hours are also included for comparison.

| | | ECAP deformation (ϵ) | | | | | powder |
|-------------------------------------|--------|---------------------------------|---------|---------|---------|---------|---------|
| | | 0 | 1 | 2 | 3 | 4 | 5 h |
| Crystallite size (nm) | Mg | 140.2 | 97.39 | 75.51 | 72.06 | 69.85 | 72.0 |
| | Ti | 179.3 | 57.66 | 56.35 | 47.98 | 40.4 | 70.8 |
| Volume fraction of phases | Mg | 91.09 | 90.10 | 89.95 | 90.06 | 89.79 | 90.35 |
| | Ti | 8.18 | 8.41 | 8.51 | 8.63 | 8.93 | 7.85 |
| | MgO | 0.73 | 1.49 | 1.54 | 1.31 | 1.27 | 1.79 |
| Lattice Parameters (\AA) | Mg (a) | 3.21(2) | 3.21(0) | 3.21(1) | 3.21(2) | 3.21(3) | 3.21(4) |
| | Mg (c) | 5.21(4) | 5.21(4) | 5.21(3) | 5.21(6) | 5.21(7) | 5.21(6) |
| | Ti (a) | 2.95(3) | 2.95(2) | 2.95(2) | 2.95(3) | 2.95(4) | 2.95(5) |
| | Ti (c) | 4.68(7) | 4.68(6) | 4.68(6) | 4.68(8) | 4.69(0) | 4.68(8) |

It should be pointed out that the crystallite sizes reported above are not unlike to those reported for ECAP deformed solid samples (Dinkel et al. 2008, Mathis et al. 2005). For instance Mathis et al. has deformed cast AZ91 alloy (Mg-9 wt % Al) with a 90° die and found a crystallite size of approx. 60 nm after a total strain of $\epsilon= 9.2,$ i.e. 8 passes. To check this, a fully dense Mg sample was prepared from the current Mg powders. The sample hot compacted under 200 MPa at 350 °C for 3 hours, was subjected to 4 passes using the single zone die. The sample has yielded a crystallite

size of 83 nm, which is quite close to the value obtained with the powder compacts (77 nm).

The fact that both powder compact and the fully dense sample yield essentially similar crystallite sizes imply that in ECAP, the powders even when loosely packed respond to the shape change by plastic deformation rather than being re-accommodated as rigid particles. The latter is a possibility since loose powders could flow through the deformation zone simply by translation and rotation without being subjected to plastic deformation. Figure 4.3 shows a powder compact that has been removed from the Cu block after the first pass. The piece appears to be quite solid with visible shear markings on its surface. Thus, the powder compact seems to have been consolidated as a result of ECAP deformation.

Samples following ECAP deformation were subjected to density measurement so as to establish the level of particle consolidation. The values measured after each pass are shown plotted in Figure 4.4. Here, the compact which initially had a density of 1.673 g/cm^3 consolidates to a value of 2.029 gr/cm^3 after the first pass. This value

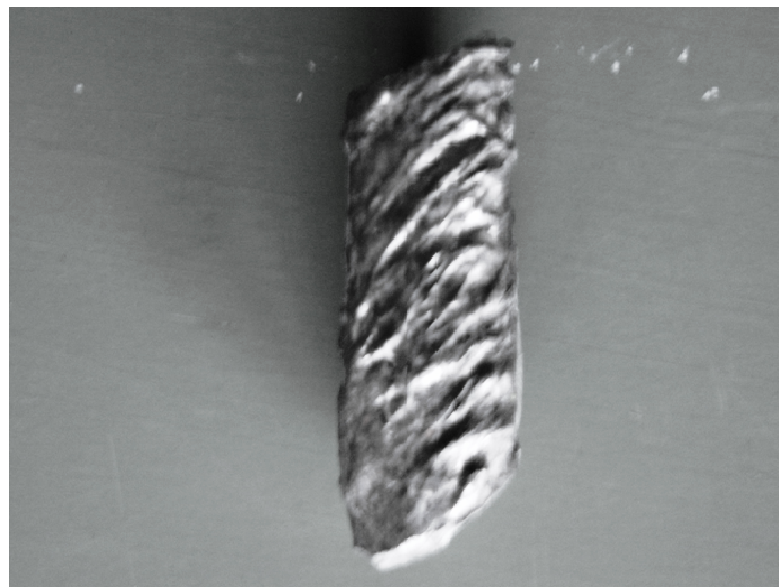


Figure 4.3. Structural characteristics of Mg-10 vol%Ti powder compacts ECAP deformed to true strains of $\epsilon=1, 2, 3,$ and 4. The same mixture milled for 5 hours are also included for comparison.

increases in subsequent passes reaching a value of 2.073 gr/cm³ after the fourth pass. The value is quite close to the density of the hot compacted sample (2.0997gr/cm³) shown by the horizontal line in Figure 4.4. Consolidation of powder compacts via ECAP deformation is a well known phenomenon that has been previously reported for Mg (Wu et al. 2007, Moss et al. 2007) as well as for the other powder systems (Xia et al. 2005, Quang et al. 2007).

Observations reported above imply that feeding of material in powder form does not significantly modify the nature of ECAP deformation. The powders are sufficiently consolidated even in the first pass so that the process results in the formation of nanosize volumes in much the same way as in the solid samples.

Microstructures in the ECAP processed powder compacts are given Figure 4.5 and Figure 4.6. Figure 4.5 (b) refers to a longitudinal section of a pure Mg after the

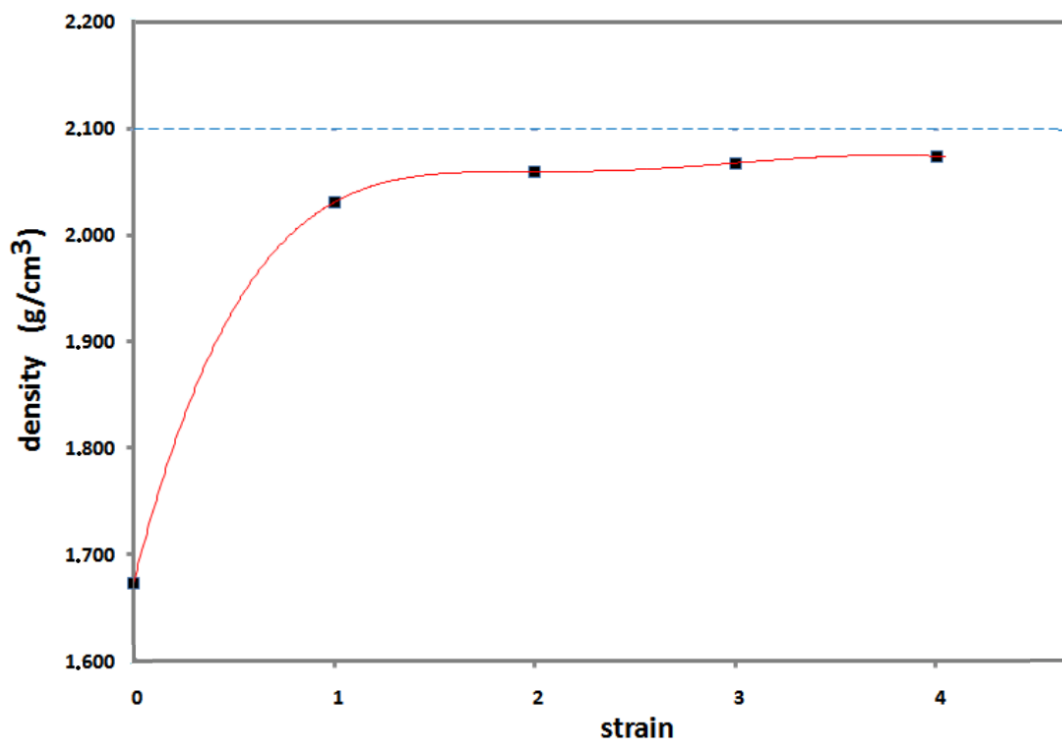
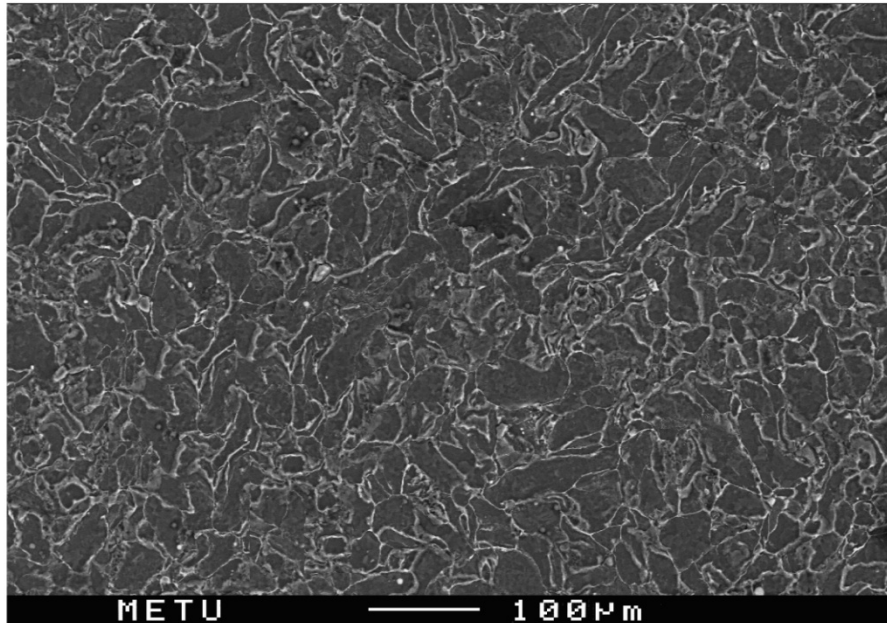


Figure 4.4. The variation of density in Mg-10 vol.%Ti with ECAP deformation. Note that the density increase in the first pass is quite high.

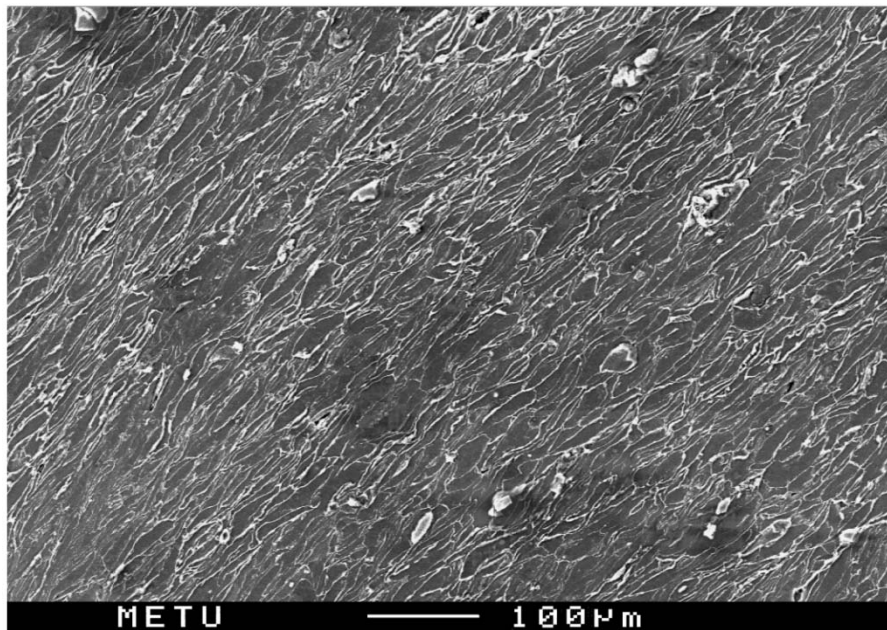
fourth pass. Here grains originating from the powder particles which are initially equiaxed, Figure 4.5 (a), seem to have been inclined at an angle to the shear (longitudinal) direction. Angular distortions of grains are also apparent. Microstructure of the same sample at the transverse section is given in Figure 4.5 (c). It is worth noting that in Figure 4.5 (c) is still comparable to that of Figure 4.5 (a). This is despite the fact that the latter sample was subjected to a very high strain ($\epsilon=4$).

Microstructures in Mg-Ti display similar features. Figure 4.6(a) and (c) refer to the transverse section of the sample before and after ECAP deformation, respectively. Here, the length scales are again quite comparable to each other, despite the heavy strain imposed. In addition, Ti particles seem to have been deformed less than Mg. This is quite clear in Figure 4.6 (b), which shows the longitudinal section of the deformed sample. Here, Ti particles seem to have been translated without much sign of distortion. Inset in Figure 4.6 (b) shows a locality in this sample, where Mg was subjected to a complex flow pattern, presumably to accommodate the Ti particles that remains un-deformed or deformed less.

Particulate structures resulting from milling of Mg are shown in Figure 4.7 (a) to (e). It should be noted that the milling does not reduce the particle size. The Mg particles seem to have been agglomerated and have sizes which are in fact larger than the starting powder, as shown in Figure 4.8. In Mg-Ti, Mg particles behaved in a similar manner. Ti particles on the other hand, have been refined quite drastically. They appeared as small fragments that have been distributed throughout the particulate structure. The agglomeration of Mg particles in the one hand and the disintegration of Ti particles, on the other, imply that the structure, under the repeated impacts of the balls, is determined by a balance between the fragmentation arising from ductile fracture and agglomeration resulting from the cold welding process. The result of these repeated impacts is that the particulate structure are heavily mixed and refined. This is well illustrated in Figure 4.9 where the particulate structure shown refers to Mg-Ti after 1 hour milling. Thus, even when Mg is agglomerated Ti has been refined and distributed uniformly over the structure.

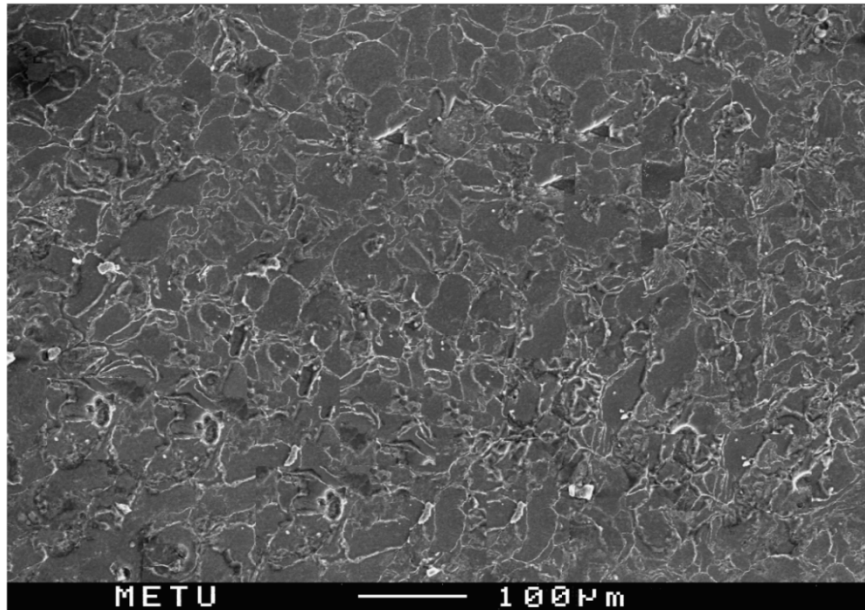


(a)



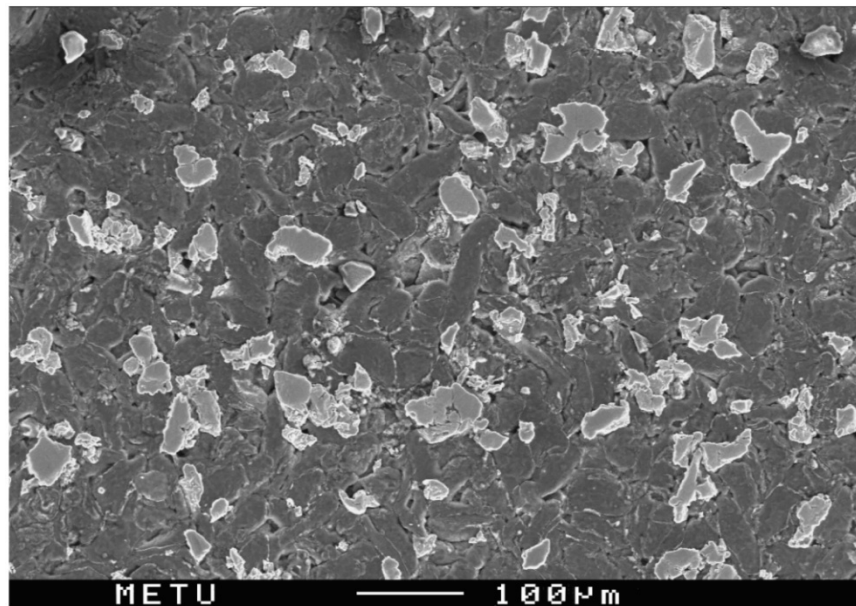
(b)

Figure 4.5. Microstructures in Mg powder compact a) Initial structure(transverse section), b) after ECAP deformation (longitudinal section), c) after ECAP deformation (transverse section)



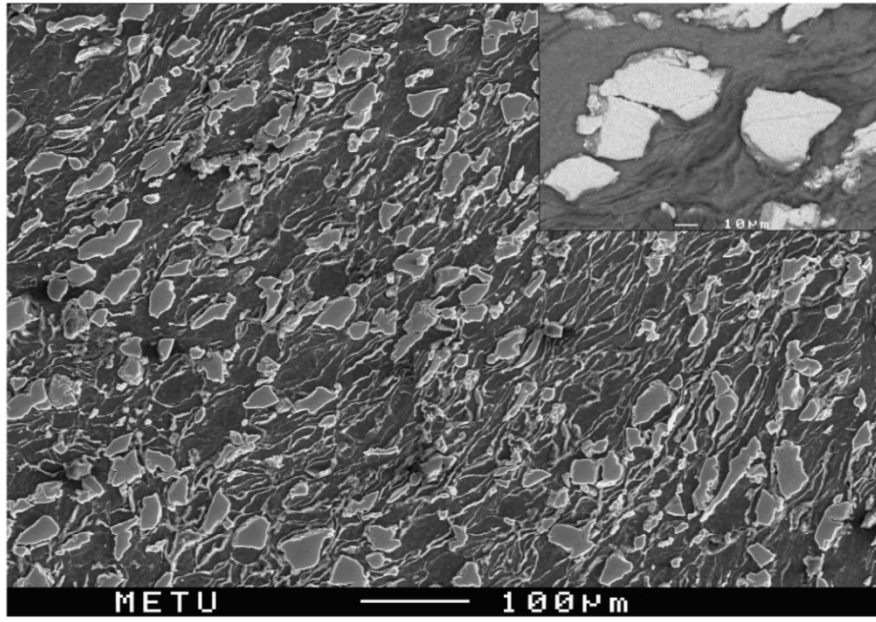
(c)

Figure 4.5. *Continued,*

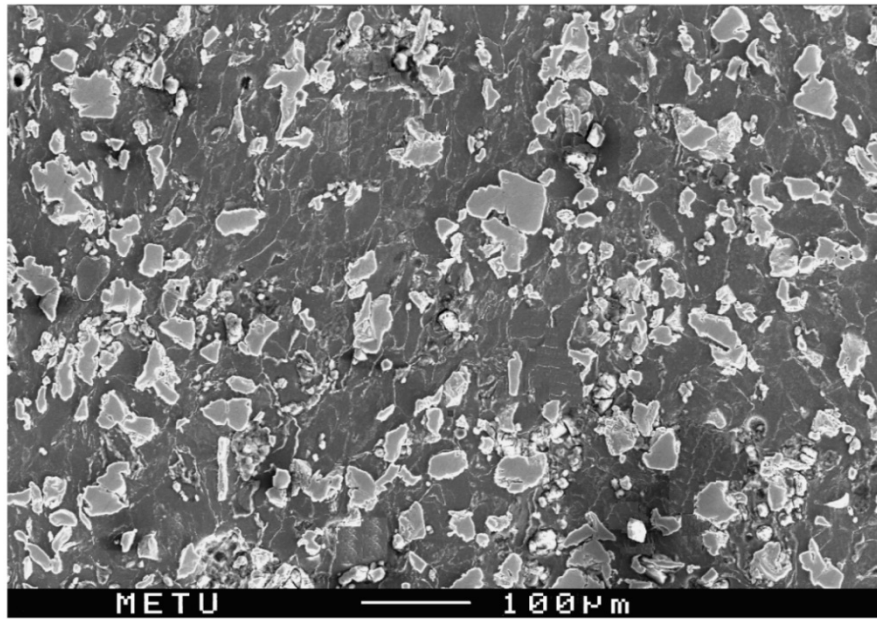


(a)

Figure 4.6 Microstructures in Mg-10 vol % Ti powder compact a) Initial structure (transverse section), b) after ECAP deformation $\epsilon=4$ (transverse section). and c) after ECAP deformation $\epsilon=4$ (logitudinal section)



(b)



(c)

Figure 4.6. *Continued,*

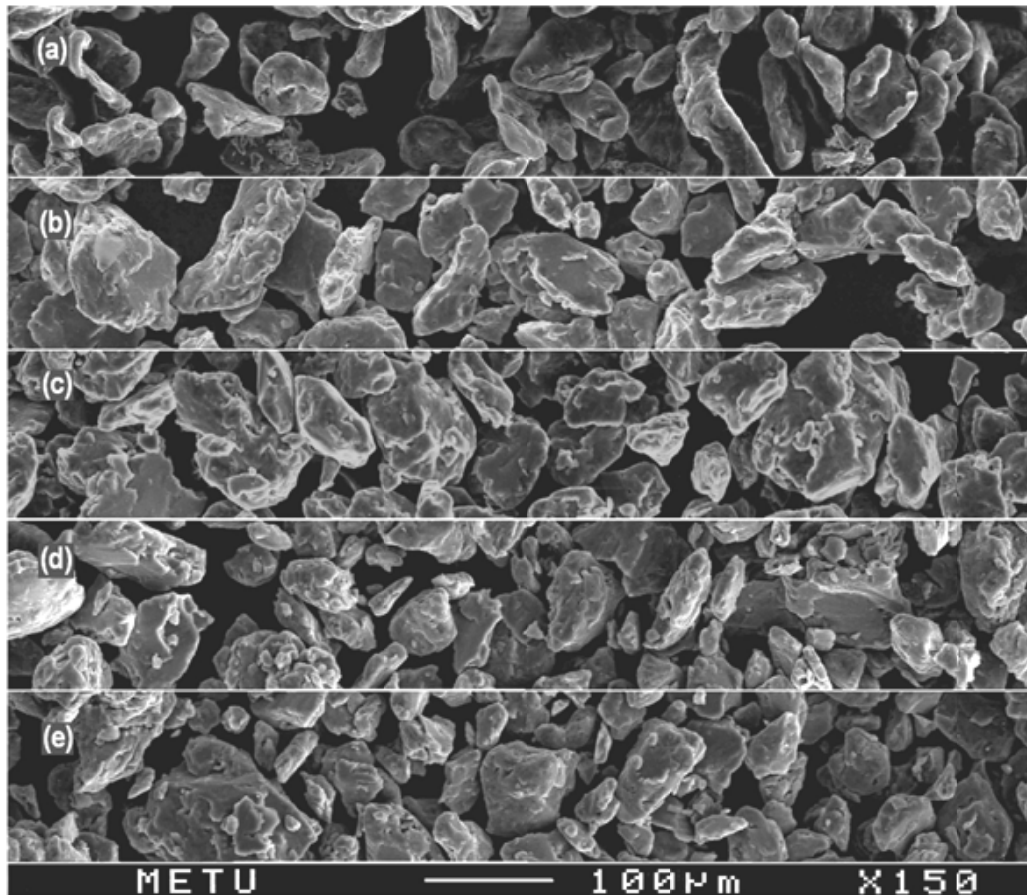


Figure 4.7. SEM micrographs of Mg powder after milling for (b)0.5 h (c) 1 h (d) 2 h (e) 5 h.(a) refers to the starting powder.

The observations made above show that ECAP processing and mechanical milling differ from each other quite drastically in terms of resulting micro/particulate structure. While in milling, the volume elements are mixed together and re-distributed continuously. This is not the case for ECAP processing. This difference is well reflected in the distribution of Ti constituent in both samples. In Figure 4.9, Ti appears as tiny pieces formed as a result of repeated impacts in milling. In Figure 4.6(c) which refers to ECAP deformed sample, the phase is very large in comparison and appears in sizes which are only slightly less than the initial particles size, Figure 4.6(a).

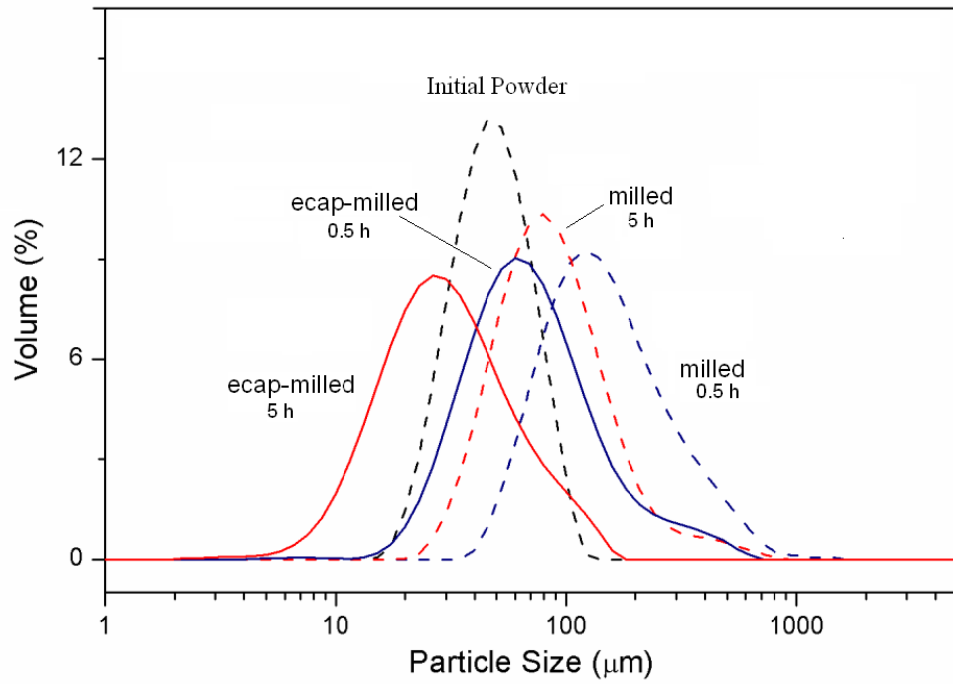


Figure 4.8. Particle size distribution of Mg powders obtained after direct milling (dotted lines) and milling after ECAP deformation ($e=4$) (continuous lines). Note that ECAP deformed Mg yields finer particles with milling.

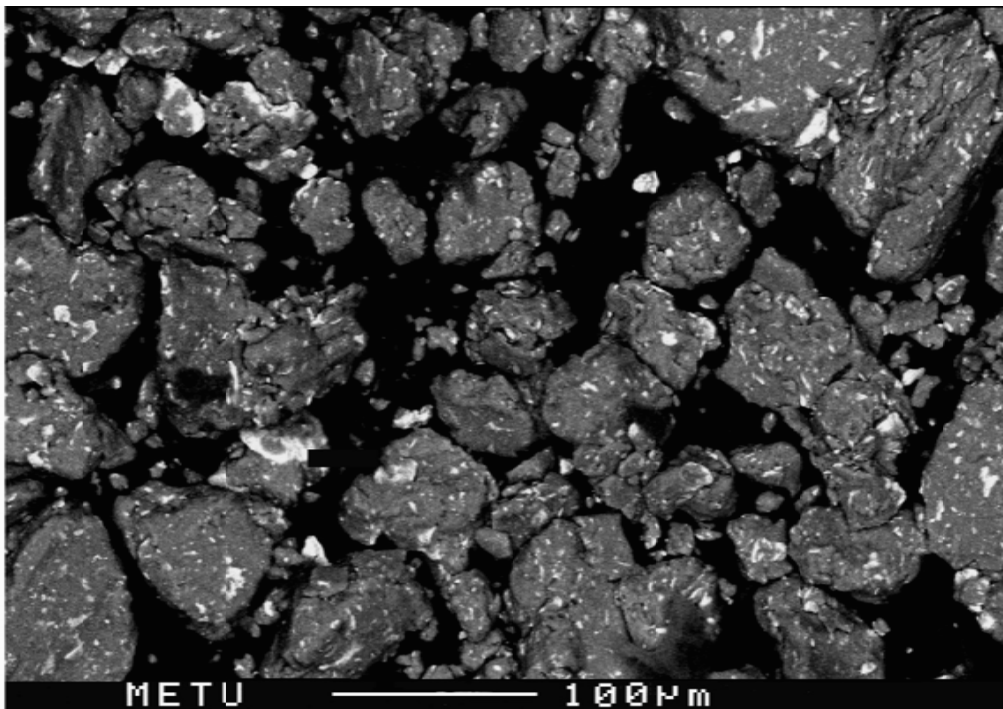


Figure 4.9. SEM micrograph of Mg-10 vol % Ti milled for 1 hour. Bright phase is Ti.

The size reduction achievable with plastic deformation is not necessarily small. This has been well demonstrated in rolling deformation of metal-metal systems (Öztürk et al. 1994). For instance, in Fe-Cu multilayer, Shighu et al. (2001) reports a size reduction of 1:100 obtained after a rolling deformation of $\epsilon=4$, i.e. final size of 500 nm obtained from 45 μm thick layers. The deformation imposed in this study is quite comparable to the strain imposed in the present work.

The preservation of the initial length scale though surprising when contrasted with the more conventional processing techniques, is the direct result of simple shear deformation. An important parameter in this respect is the interfacial area, i.e. the rate with which it increases with the imposed strain. A grain or a phase, cubic in shape, for instance when subjected to a true strain of $\epsilon=4.0$, i.e. the same strain that was imposed in this work, the interfacial area increases by a factor of roughly 8. The same deformation when imposed in for instance in rolling on the other hand, the area increases by a factor of more than 100. Thus to reach a similar degree of refinement, much higher strain would be needed in ECAP deformation.

To test this, a Mg-Ti sample was prepared and deformed in parallel ECAP die. A total of 10 pair of passes have been imposed which corresponds to a true strain of $\epsilon=24$. Figure 4.10 shows the transverse section of this sample. Here, Mg grains seem to have been heavily distorted in a complicated pattern. Ti particles seem to have been refined in a manner as if they have been eroded by Mg flow around them. This erosion is consistent with the presence of tiny Ti fragments as well as rounded shapes of the larger fragments. Thus, the structure obtained after a true strain of $\epsilon=24$ is not unlike to that obtained after milling.

The mixing and refinement of structure that takes place with heavy ECAP deformation were also reported in Mg-Mm-Ni (Loken et al. 2007) and Mg-Ni (Skripnyuk et al. 2007). In the former study, Loken et al. converted the heterogonous as-cast structure into a fine microstructure via ECAP deformation with a true strain of $\epsilon=8$. Moreover, Skripnyuk et al. noting the presence of Ni gradient near Mg_2Ni particles, implied mixing at much finer scale.

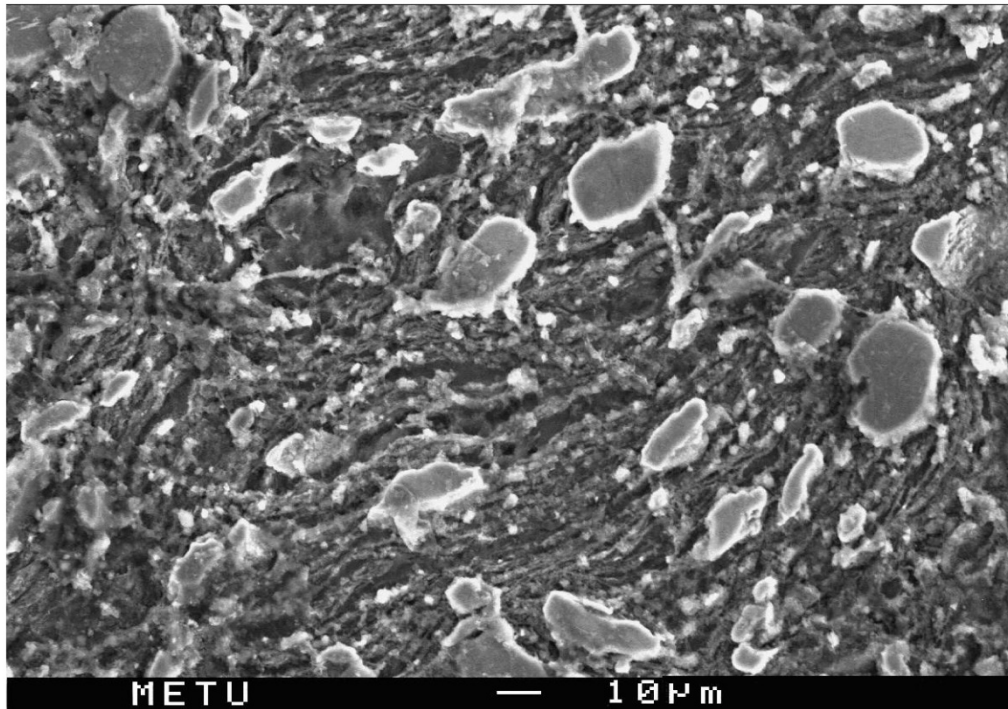


Figure 4.10. Microstructure of Mg-Ti deformed to $\epsilon = 24$ (10 pair of passes) using the parallel die

4.3.2. Milling after ECAP deformation

Since hydrogen storage alloys are used in particulate form, it is necessary to convert the consolidated materials resulting from ECAP deformation into a granular form. Figure 4.11 shows the particulate structures obtained after mechanical milling of ECAP deformed Mg sample. Of these, Figure 4.11 (a) refers to the structure after 30 minutes of milling. The average particle size has a value of 71 μm . This value is significantly less than the sizes obtained with direct milling of Mg powders. To verify this, ECAP deformed samples were subjected to the milling operations using the same conditions and durations as above. Thus, milling was extended to 5 hours, samples being taken after 60 and 120 minutes. Particle size distribution determined for these samples are included in Figure 4.8. It is seen that the size distribution of milled ECAPed samples centres on values which are significantly less than those obtained by direct milling. For instance after 5 hours of milling, milled ECAPed sample has $d_v(0.5) = 31 \mu\text{m}$. This should be compared with $d_v(0.5) = 88 \mu\text{m}$ obtained with direct milling.

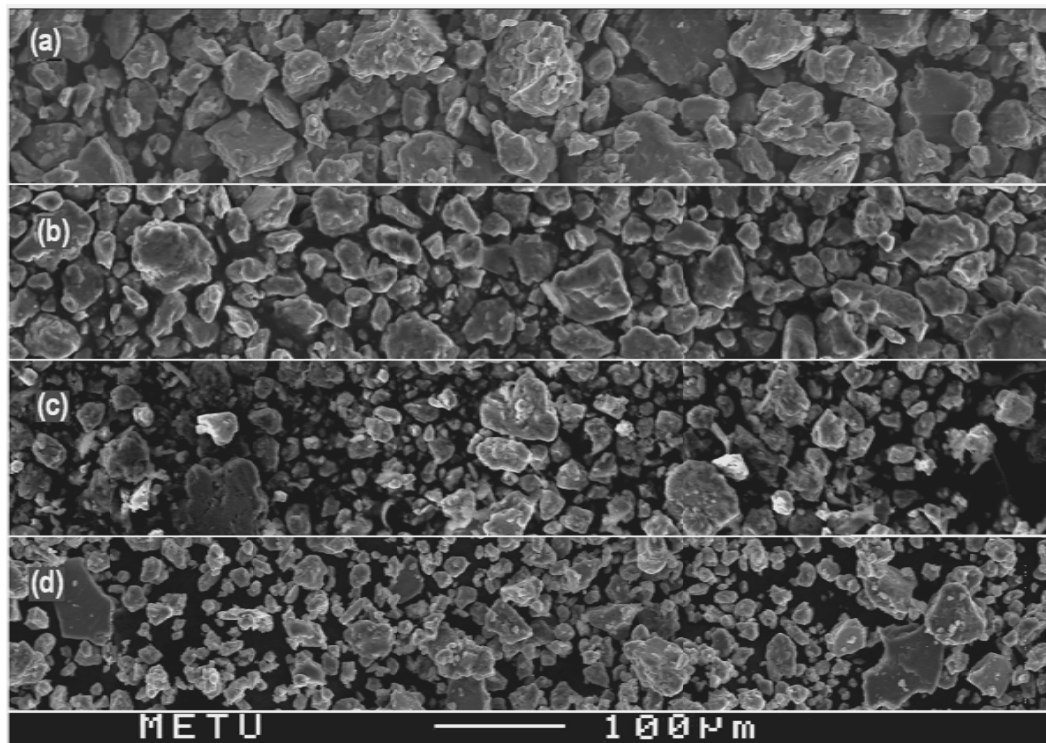


Figure 4.11. SEM micrographs of Mg powder compacts ECAP deformed to $\epsilon=4$ and milled for (a) 0.5 h (b) 1 h (c) 2 h (d) 5 h.

4.4. Discussion

The advantage of ECAP processing over mechanical milling is that the particles embedded in the sample, except those at the very surface, are isolated from the environment in which the processing is carried out. This is of considerable advantage in the processing of hydrogen storage alloys since they are poisoned when exposed to atmospheres that contain O_2 , H_2O etc. Thus the efficient refinement and mixing of phases achieved in ECAP processing is of considerable advantage implying that ECAP can be employed as a technique of material synthesis.

The fact that ECAP deformed sample has a better milling ability is quite important and provides a new approach in the milling of ductile powders. Ductile powders are difficult to mill due to cold-welding of particles which leads to agglomeration, i.e. increase in particle size with milling, rather than particle fragmentation, as was the case above.

Based on the observations reported above, a processing route for ductile powders might involve two steps. In the first step, the powders in loose form could be fed into a die, similar to those depicted in Figure 4.1(b) and subjected to several cycles of ECAP deformation. In the second step, the solid piece removed from the die in strain hardened form may be subjected to mechanical milling of a short duration.

4.5. Conclusions

In the current work, the possibility of employing ECAP processing in lieu of mechanical milling was explored for the purpose of both structural refinement and material synthesis. Mg and Mg-Ti powder compacts encapsulated in copper were subjected to ECAP deformation. The study has shown the following;

- i. ECAP processing leads to consolidation of powder compacts producing almost fully dense samples. As a result, the particles in the compact deform in much the same way as grains in the bulk material.
- ii. ECAP processing leads to structural refinement of powder particles resulting in coherently diffracting volume sizes that are comparable to those obtained with mechanical milling.

In this respect, ECAP processing and mechanical milling are quite similar. ECAP processing, however, does not seem to be very efficient in generating or expanding the inter-particle boundaries. Thus for efficient mixing of phases, required for such purposes as material synthesis, it is necessary to employ extremely high strains.

Finally, for size reduction, it appears that ECAP processing even with several passes may be employed quite usefully for the purpose of the improving the milling ability of the powders.

The last point implies a two step approach in the processing of hydrogen storage alloys. The powder mixtures may be first processed with ECAP in open atmosphere and then by a short duration of mechanical milling carried out under protective atmosphere.

CHAPTER 5

THE PROCESSING OF Mg-Ti FOR HYDROGEN STORAGE; PLASMA SYNTHESIS

5.1. Introduction

Hydrogen storage alloys may be synthesized in a variety of ways. Synthesis in the liquid state is the most common, i.e. elements in suitable proportions are melted together, normally under protective atmosphere, which are then cast into a suitable form or preferably pulverized for further processing. An alternative method would be solid-state synthesis. This may start from elemental powders (Sakintuna et al. 2007) or from oxide mixtures. In the latter, the oxides are mixed together in the required proportions and then reduced electrochemically in the solid state yielding the alloy or compound in powder form (Schlapbach et al. 2001, Tan et al. 2009). Final stages in the processing, whether the alloy is produced from the liquid or from the solid route, almost always involve mechanical milling. In this case, the synthesized alloy mixed with additives, is milled for extended period of time (Güvendiren et al. 2004). The aim of the milling is to distribute the additives homogeneously in the one hand, and refining of the particle size on the other hand. The degree of nano-structuring achieved as a result of this milling is extremely important, since for a given chemistry, this seems to be the only way to modify the hydrogenation characteristics of the alloy.

Gas-phase synthesis of hydrogen storage alloys, so far, has been confined to thin film deposition. Though commercially, thin films have a limited scope, the method is highly versatile in that the precise control could be exercised with regard to both the composition and the structure of the films. Tailored structures which can be produced in this way, have superior storage characteristics. This was demonstrated

for Mg where 300 nm thick films, was shown to absorb and desorb hydrogen near ambient conditions (Akyıldız and Öztürk 2010).

Thermal plasma synthesis is a relatively new method which essentially is similar to thin film deposition. This method has the added advantage that it can be adapted to volume production. In thermal plasma the temperatures are sufficiently high to vaporize the starting material which then condenses in the quenching zone of the reactor to nano-size powders (Szepvolgyi et al. 1996). The method has been used for the synthesis of metallic and ceramic nano-powders for a variety of purposes (Suresh et al. 2008, Bystrzejewski et al. 2009)..

In this study, we process Mg-Ti powder mixture for the purpose of hydrogen storage making use of two routes; mechanical milling and thermal plasma synthesis. In the former we make use of conditions to ensure efficient milling of the powder mixture. In the latter, i.e. in thermal plasma processing, a set of experiments were conducted so as to produce Mg powders of extremely small size.

5.2. Experimental Procedure

Starting powders were Mg (Alfa Aesar, 99.8 %) and Ti (Alfa Aesar, 99.5 %) with an average particles sizes $d(0.5)$ of 47 and 32 μm , respectively. The powder mixtures Mg-10 vol% Ti were prepared and processed via mechanical milling and plasma synthesis.

Mechanical milling was carried out in a planetary ball mill given in Figure 3.5 (Fritsch-Pulverisette 7 Premium Line) under argon atmosphere. 1 wt % graphite was added as anti-sticking agent to the initial powder mixture. 15 mm stainless steel balls were used with ball to powder ratio of 10:1. The mill was operated at a speed of 700 rpm. Thus, the conditions employed in milling were quite severe. The milling was carried out for 1, 5, 10, 15 and 30 hours using a program of 30 minutes milling and 30 minutes rest time.

Thermal plasma processing of the powder mixture was carried out in a Radi-Frequency(RF) system. The system is made up of a plasma torch (TEKNA Plasma

System Inc, PL-35), an RF generator (3-5 MHz, 30kW), a powder feeding system, reaction chamber connected to a filter system and a vacuum pump

A schematic representation of the RF plasma unit is given in Figure 5.1. The plasma torch uses five turn induction coil, a water cooled ceramic tube with 36 mm inner diameter and another ceramic tube with 40 mm diameter separating plasma gas from the sheath gas, Figure 5.1. Plasma (central) gas was a mixture of Ar (15-23 slpm) and He (5-8 slpm) and sheath gas was Ar (35-40 slpm) mixed with H₂ (4-5 slpm). Mixed powders were fed with a carrier gas He (6 slpm) and injected into the Ar-He plasma via a water cooled stainless steel probe. The probe was positioned axially into the torch down to the first turn of the coil. Reaction chamber, water cooled, was cylindrical in shape 200 mm in diameter and 1005 mm in length and contains viewing ports for in-situ process observations. Typically, the system and the reaction chamber were maintained at a pressure of 900 mbar (absolute). Where necessary, quenching was carried out by feeding He gas with 60 slpm at a position approx. 70 mm below the fifth (last) turn of the coil.

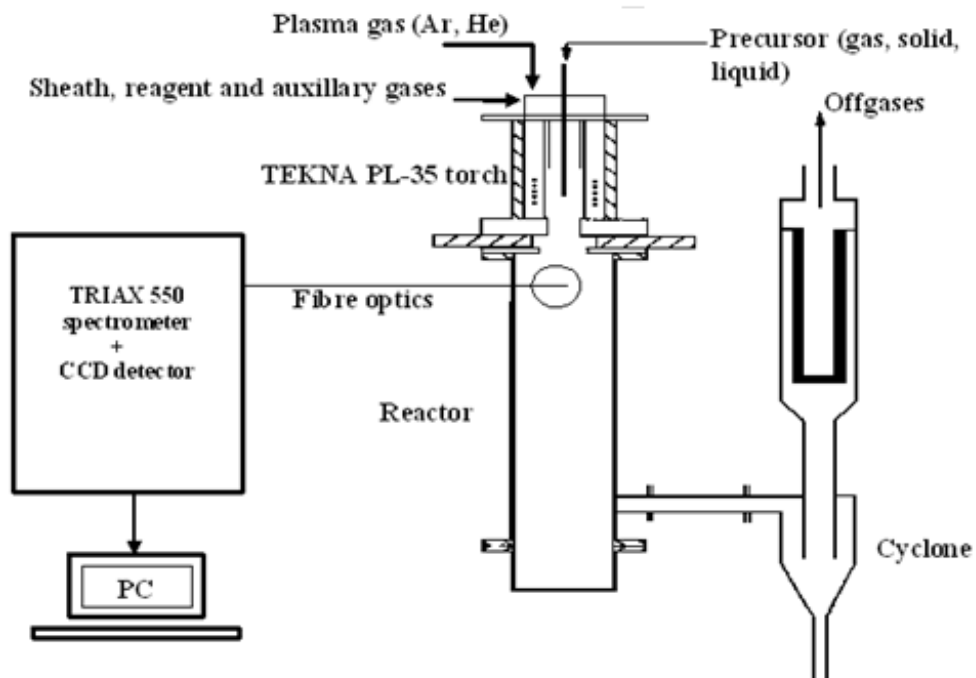


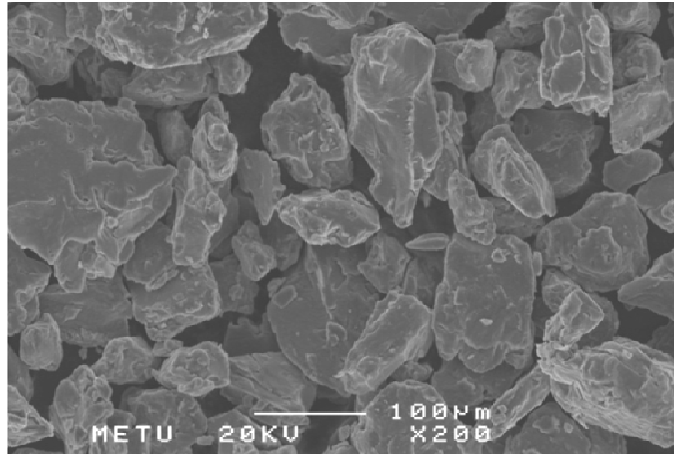
Figure 5.1. Schematic representation of RF plasma system.

The amount of powders processed in each experiment was rather small (typically 15 g). As a result, powders were collected from the wall of the reaction chamber rather than from the filter system. Experimental conditions for each set of sample is given in Table 5.1.

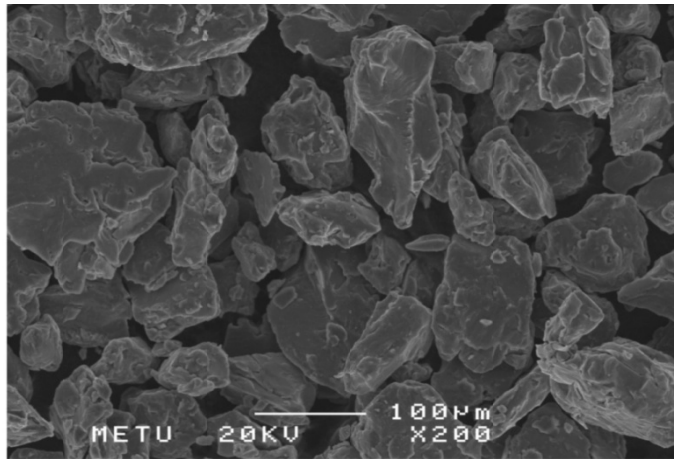
Powders following both mechanical milling and plasma synthesis were characterized with respect to their size and structure. Powders in mechanically milled samples were rather coarse and were characterized with laser scattering. Wet method was employed with 500 mg sample using ethanol as dispersant. Plasma synthesized powders characterized by multi-point BET analysis due to their small size. Particles were examined in field emission SEMs both in secondary electron and in back – scattered image mode. The powders were structurally characterized by X-ray diffraction using CuK α radiation (typically 40 kV, 40mA). Diffractograms were obtained in a step scanning mode (0.02° for 3 seconds) 20° <2 θ <80°. Standard Si sample was run at each session of X-ray measurements so as to correct angular shift that might occur in peak positions. The volume fraction of phases, the lattice parameters as well as crystallite size of samples were obtained from the Rietveld refinement of X-ray data (Luterotti et al.,1999).

Table 5.1. Experimental conditions for thermal plasma synthesis

| Material | sheat gas flow rate (l/min) | plasma gas flow rate (l/min) | carrier gas flow rate (l/min) | plate voltage (kV) | plate current (A) | quench gas (l/min) | feed rate g/min |
|----------------|-----------------------------|------------------------------|-------------------------------|--------------------|-------------------|--------------------|-----------------|
| Ti | 35 Ar 5 H ₂ | 6 He 15 Ar | 6 He | 8.4 | 3.2 | - | 1.01 |
| Ti | 35 Ar 5 H ₂ | 5 He 15 Ar | 6 He | 7.6 | 2.8 | - | 1.166 |
| Mg | 40 Ar 4 H ₂ | 8 He 23 Ar | 6 He | 7.6 | 2.8 | - | 2.932 |
| Mg-10 vol % Ti | 40 Ar 4 H ₂ | 8 He 23 Ar | 6 He | 8.3 | 3.2 | - | 1.805 |
| Mg-10 vol % Ti | 40 Ar 4 H ₂ | 15.5 Ar | 1.8 Ar | 8.3 | 3.2 | 60 He | 1.843 |
| Mg-10 vol % Ti | 40 Ar 4 H ₂ | 15.5 Ar | 1.8 Ar | 8.3 | 3.2 | 60 He | 1.843 |



(a)



(b)

Figure 5.2. SEM micrographs of Mg-10 vol% Ti a) the initial mixture and (b) after 30 hours of milling.

5.3. Results

5.3.1. Mechanical Milling

In mechanical milling, the powder mixtures of Mg-10 vol % Ti were milled for durations of 1, 5, 10, 15 and 30 hours. SEM micrographs of the initial Mg powders and of the mixture after 30 hours of milling are given in Figure 5.2. Particle size distribution at various stages of milling are shown plotted in Figure 5.3. Both these

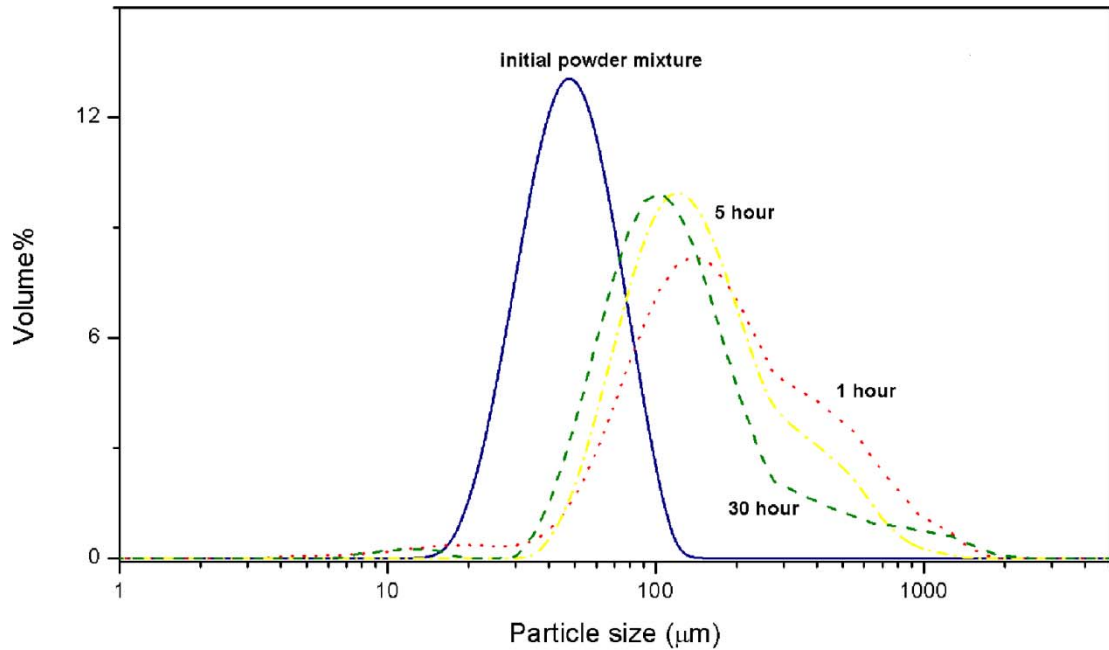


Figure 5.3. Particle size distribution of Mg-10vol% Ti powders milled for 1,5 and 30 hours. The initial distribution is also shown.

distributions and the median values, dv_{50} , reported indicating that there is an increase in particle size. Table 5.2 show little sign of particle refinement by milling. The particle size are quite comparable to the initial mixture, compare Figure 5.2 (a) and Figure 5.2 (b). In fact dv_{50} values are larger This is not unexpected since Mg powders are quite ductile and can join together during milling, getting larger in size. Thus the actual particle size is the result of a balance between fragmentation arising from ductile fracture and agglomeration resulting from the cold welding process.

X-ray diffractogram of the powders after 30 hours of milling is given in Figure 5.5 together with that of the initial powder mixture. Except a small amount of MgO and Fe and an FCC phase, each less than 2 vol%, there is no new phase formation in the powder mixture. Thus, the milled powder has two-phase HCP structure, the same as the initial powder mixture. The presence of this two- phase structure in milled samples is consistent with previous reports made on milling of Mg-Ti by Liang and Shultz (2003) and Asano et al. (2009), though in the latter by modifying Ti content and the conditions of milling, the formation of new phases with BCC or FCC structure was reported.

Table 5.2. Structural Characteristics of Mg-10 vol%Ti powders processed via mechanical milling

| Time (hours) | | 0 | 1 | 5 | 10 | 15 | 30 |
|-------------------------------------|--------|---------|---------|---------|---------|---------|---------|
| Particle size (μm) | | 50.5 | 158.6 | 138.9 | 196.2 | 115.7 | 116.4 |
| Volume fraction of phases | Mg | 91.24 | 89.45 | 87.56 | 81.29 | 80.69 | 81.28 |
| | Ti | 7.82 | 8.41 | 6.82 | 6.04 | 5.87 | 4.8 |
| | MgO | 0.94 | 2.24 | 5.63 | 10.61 | 13.12 | 13.69 |
| Crystallite size (nm) | Mg | 140.7 | 70.1 | 30.15 | 26.02 | 26.71 | 26.46 |
| | Ti | 187 | 65 | 23.1 | 14.2 | 6.8 | 7.8 |
| Lattice Parameters (\AA) | Mg (a) | 3.20(7) | 3.20(0) | 3.19(8) | 3.19(8) | 3.19(5) | 3.19(4) |
| | Mg (c) | 5.20(7) | 5.19(9) | 5.19(8) | 5.19(6) | 5.19(2) | 5.19(1) |
| | Ti (a) | 2.94(9) | 2.94(2) | 2.94(6) | 2.96(9) | 2.96(3) | 2.99(5) |
| | Ti (c) | 4.68(1) | 4.68(1) | 4.68(3) | 4.68(8) | 4.68(8) | 4.70(3) |

Various structural parameters derived from Rietveld refinement of X-ray data are reported in Table 5.2. This shows that the volume fraction of MgO can be as high as 14 % after 30 hours of milling. This was due to partial oxidation of the sample during milling. This, unfortunately, could not be prevented under the current experimental conditions, due to less than perfect sealing of the lid. The lattice parameter of Mg remains almost the same during milling. Thus, Mg does not dissolve Ti to any significant extent. It is known that such dissolution is possible under extreme milling conditions, as has been shown by Liang et al. (2003). Unlike Mg, the lattice parameter of Ti changes during milling. The lattice volume expands presumably due to accommodation of some Mg atoms in Ti crystal lattice.

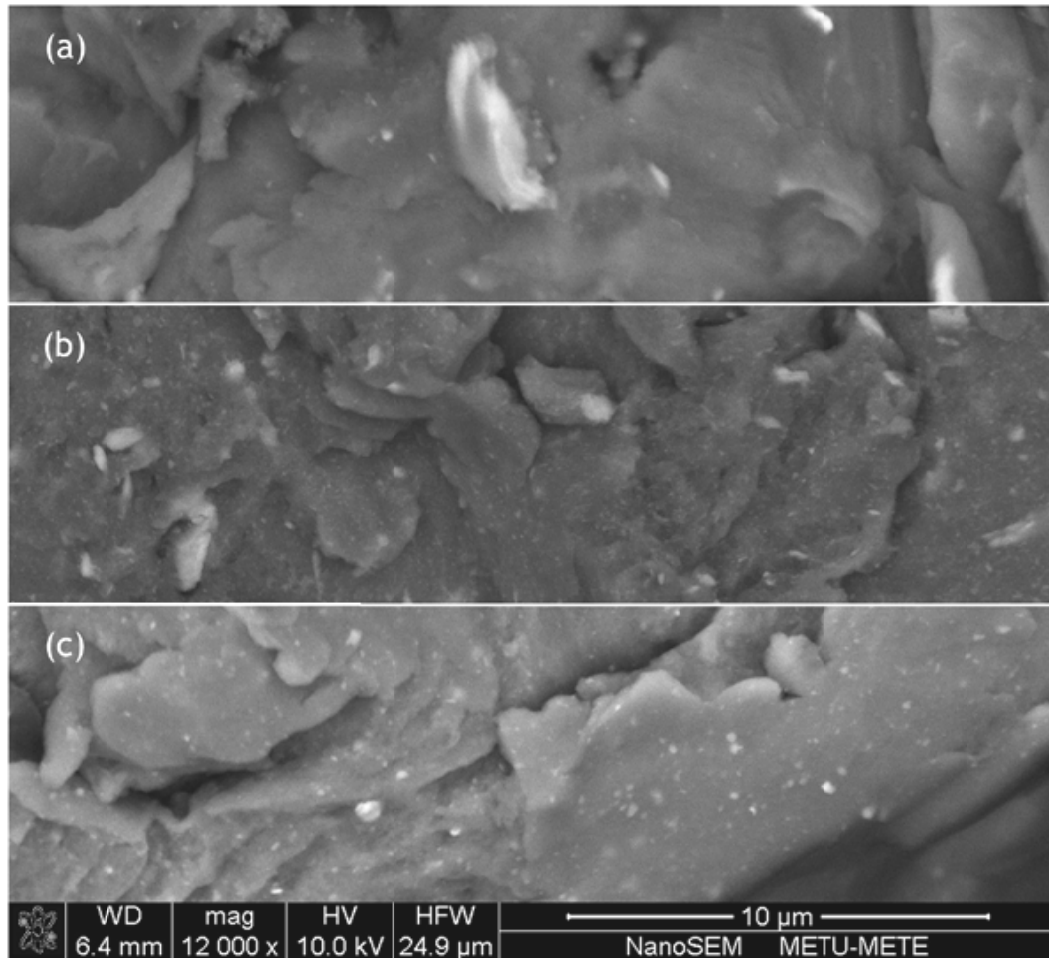


Figure 5.4. SEM micrographs of Mg-10%vol Ti after milling for a) 1 hour (b) 5 hours (c) 30 hours recorded in back-scattered image mode. Ti appear bright in a dark background of Mg agglomerates.

X-ray patterns in milled Mg-10 vol% Ti show a pronounced peak broadening as a result of milling, when Figure 5.5 (a) and (b) are compared. Data reported in Table 5.2 confirms this by showing a systematic decrease in the crystallite size of milled samples. Crystallite sizes have values of 70, 30, 26 nm for 1, 5 and 30 hours of milling. This size refers to coherently diffracting X-ray volumes, i.e. subvolumes that, together, make up Mg particles of large size, i.e. those shown in Figure 5.2 (b). The values of crystallite size reported show that the refinement is quite fast and almost complete within the first 5 hours of milling as the crystallite size changes very little afterwards.

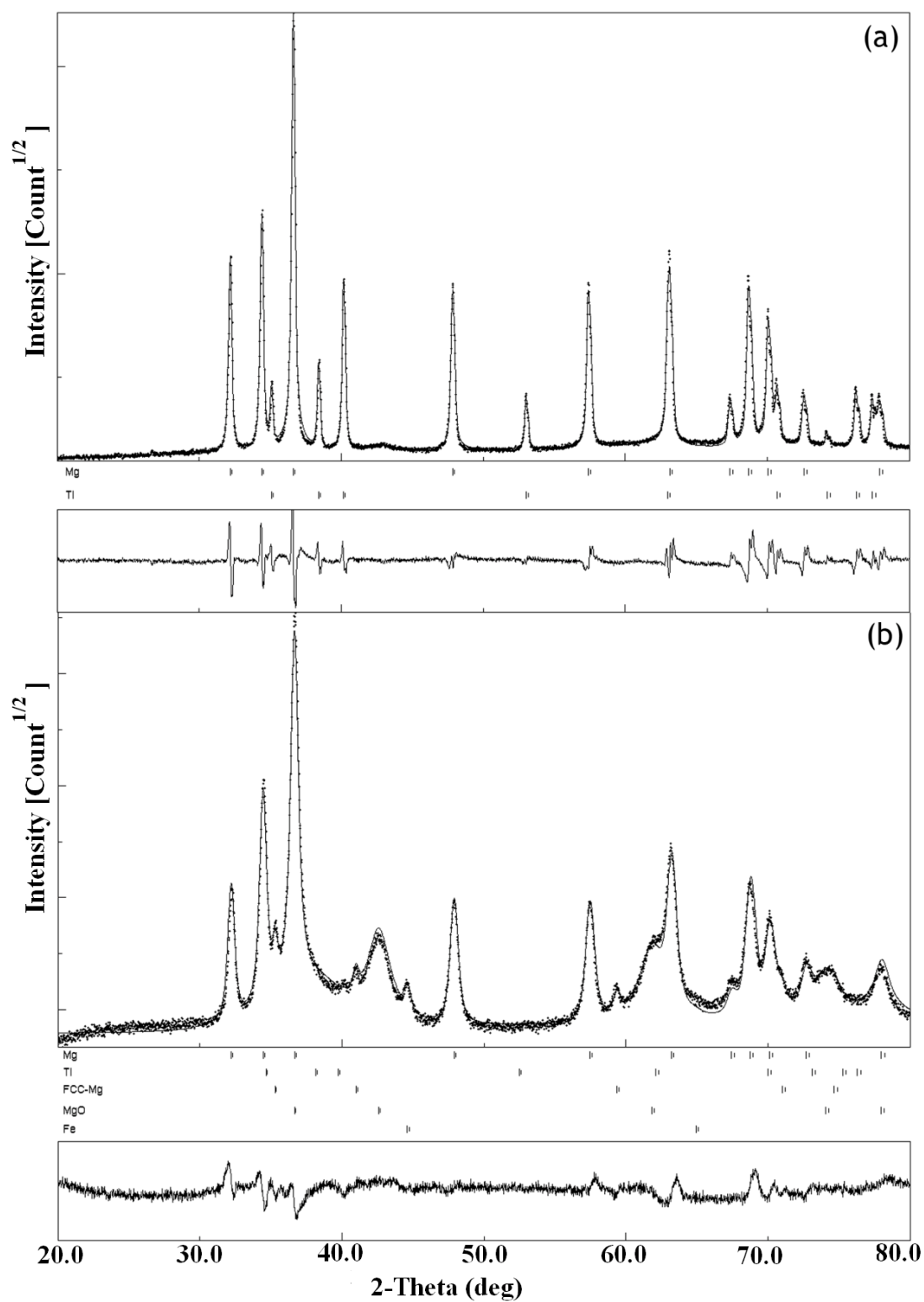


Figure 5.5. X-ray diffractograms of Mg-10vol%Ti (Rietveld refined). (a) the initial powder mixture (b) after 30 hours of milling.

In conclusion, it appears that mechanical milling yields a particulate structure in which Mg powders are quite large, i.e. nearly 0.1 mm. They incorporate Ti particles of approx. 1 μm in size embedded at their surface and in their volume. It appears that the individual Mg particles are made up of coherently diffracting volumes of extremely small size, i.e. 26 nm.

5.3.2. Thermal Plasma Processing

Thermal plasma processing was carried out first with pure powders and then with the powder mixtures. Conditions employed are given in Table 5.3. Here, the powders which were fed into the torch melt/vaporize and further below in the reaction chamber, condense into solid particles. BET values of plasma processed powders are included in Table 5.3. Particle sizes derived from BET values are in the range of 75-300 nm. These values are nearly three orders of magnitude smaller than those obtained with mechanical milling (90-100 μm). It should be pointed out that powders are collected from the walls of the reaction chamber, rather than from filters, and the BET values measured are probably less than the real values due to improper sampling. Thus, particle sizes are probably much less than the values derived from BET measurement.

SEM micrographs of pure Ti particles processed with 21 kW with a powder feeding rate of 3g/min are given in Figure 5.6(a) and (b). It is seen that there is a range of particles sizes; some Ti particles are relatively large in size. They are spherical in shape and most probably originate from initially coarse Ti particles which are melted rather than vaporized. Greater portion of powders obtained from plasma processing, however, are quite fine in the order of 80 nm, as shown in Figure 5.6 (b)

Mg powders which are plasma processed under the same condition are given in Figure 5.6(c) Here particles are more homogenous in size. Even though there are fine particles comparable to Ti, most are approximately 1 μm in size.

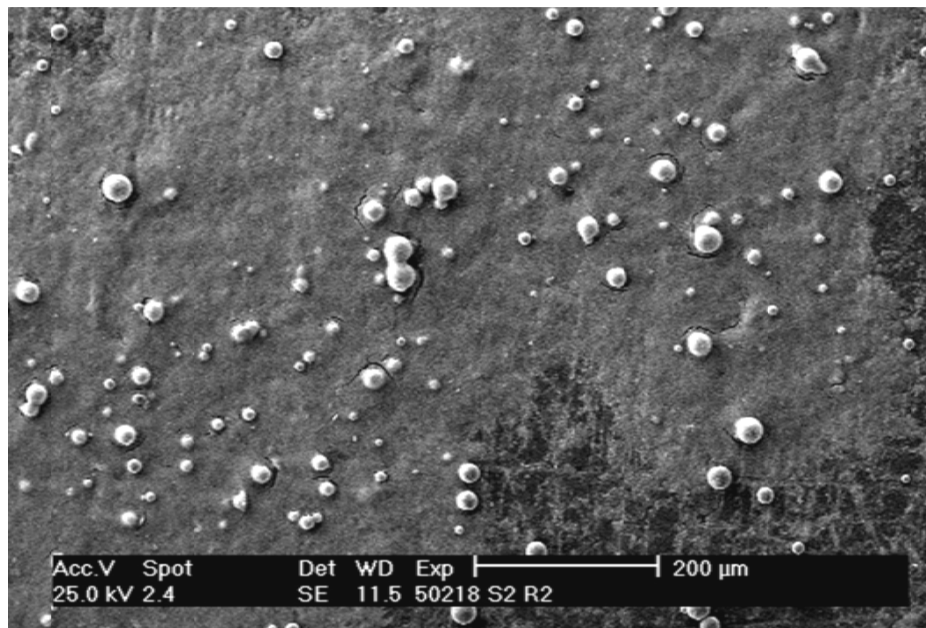
Table 5.3. Structural characteristics of mg-10 vol % Ti obtained with plasma processing

| Applied power/ feeding rate | | 21kW, 3gr/min (Mg) | 21 kw, 3gr/min (Ti) | 27 kw, 2gr/min (Mg-Ti) | 27 kw, 2gr/min (Mg-Ti) quenched | 27 kw, 1gr/min (Mg-Ti) quenched |
|-------------------------------------|------|--------------------------|---------------------------|------------------------------|--|--|
| Surface area (m ² /g) | | 11.5 | 11.6 | 10.3 | 12.1 | 28.2 |
| Particle size (BET) (nm) | | 299 | 105 | 238 | 182 | 78.1 |
| Volume fraction of phases | Mg | 69 | - | 80.67 | 70.09 | 64.69 |
| | Ti | - | 83.41 | 4.97 | 5.58 | 2.67 |
| | MgO | 31 | | 14.34 | 24.33 | 32.64 |
| Crystallite size (nm) | Mg | 215 | - | 291.6 | 73.1 | 74.2 |
| | Ti | - | 90.9 | 99.8 | 91.6 | 98.78 |
| Lattice Parameters (Å) | Mg-a | 3.21(8) | - | 3.21(0) | 3.20(9) | 3.20(9) |
| | Mg-c | 5.21(0) | - | 5.21(2) | 5.21(1) | 5.20(9) |
| | Ti-a | - | 2.96(0) | 2.96(1) | 2.96(6) | 2.94(3) |
| | Ti-c | - | 4.67(2) | 4.67(4) | 4.67(3) | 4.67(2) |

Initial experiments with plasma processing made use of Mg and Ti powders and involved different power loading as well as feeding rates. Accordingly a power loading in excess of 20 kW and a feeding rate less than 4 g/min were selected as a suitable window for operation. Following initial experiments, the program of study undertaken has focused on feeding rate as the main parameter, see Table 5.3. Figure 5.7 refers to a feeding rate of 2 g/min (27 kW) and shows a spheroidized Ti

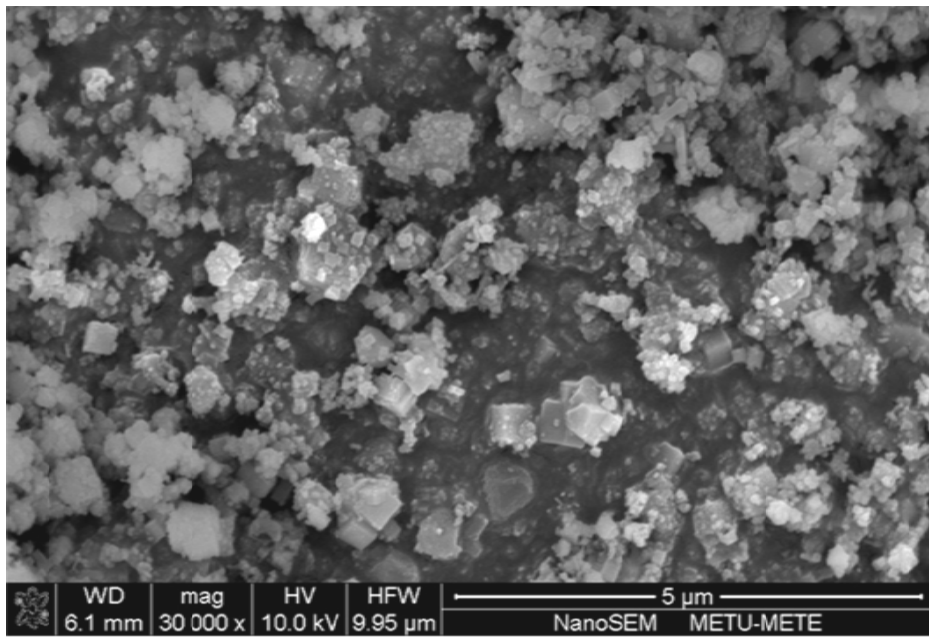
particle partially covered with Mg nanopowders. A higher magnification image of Mg powders is also given, Figure 5.7(b). Here, Mg powders are of, on average, 85 nm in size. A similar micrograph obtained with the use of quenching gas, feeding rate being reduced to its minimum, 1g/min, is given in Figure 5.7(c).

X-ray diffractograms taken from plasma processed powders showed the presence of a two phase mixture. There is, however, MgO as an additional phase, due to post-passivation treatment carried out, which could reach a value of 33 vol %. Structural parameters derived from Rietveld refinement of X-ray data are included in Table 5.3. It is seen that there is no significant change in the lattice parameters of both Mg and Ti. Thus, powders following vaporization condense into solid form with a very little mixing of atoms. This might be due to a large difference in the boiling points of Ti (3560 K) and Mg (1363 K). The evaporation of Ti may be difficult in the presence of Mg since the latter evaporates easily reducing the heat content left for the evaporation of Ti.

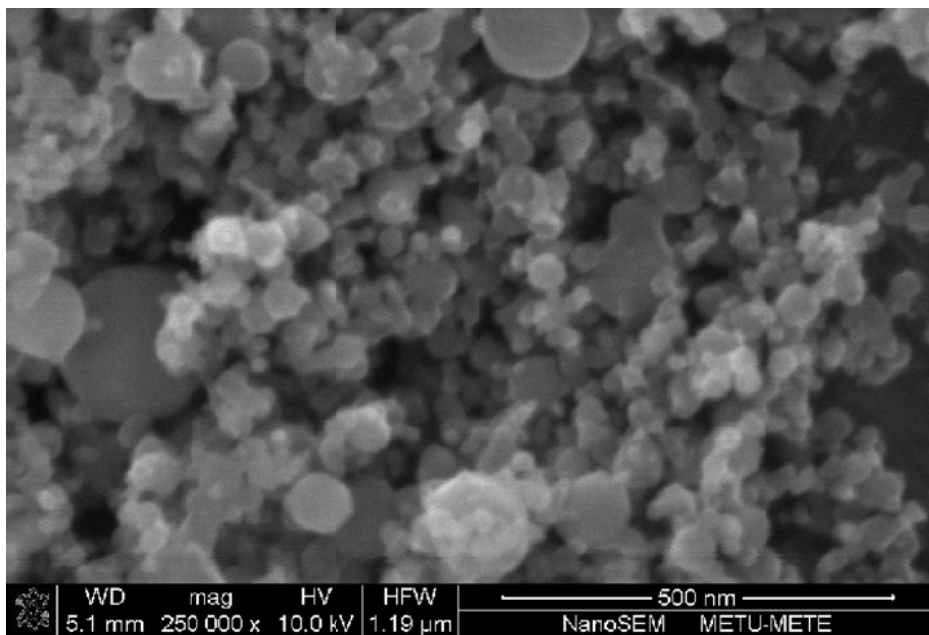


(a)

Figure 5.6. SEM micrographs of pure powders after plasma processing. (a), (b) Ti powders and c) Mg powders.

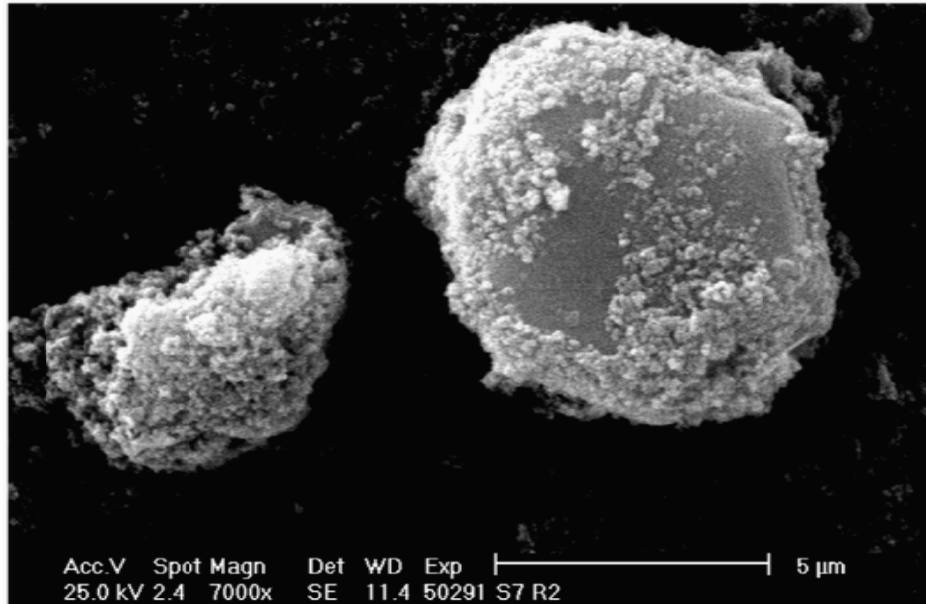


(b)

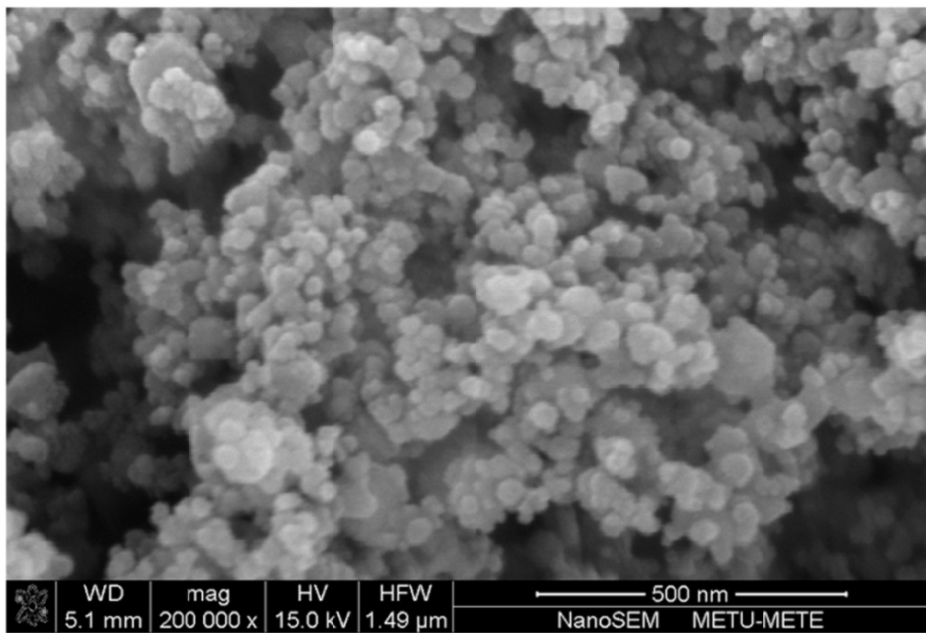


(c)

Figure 5.6. *Continued,*

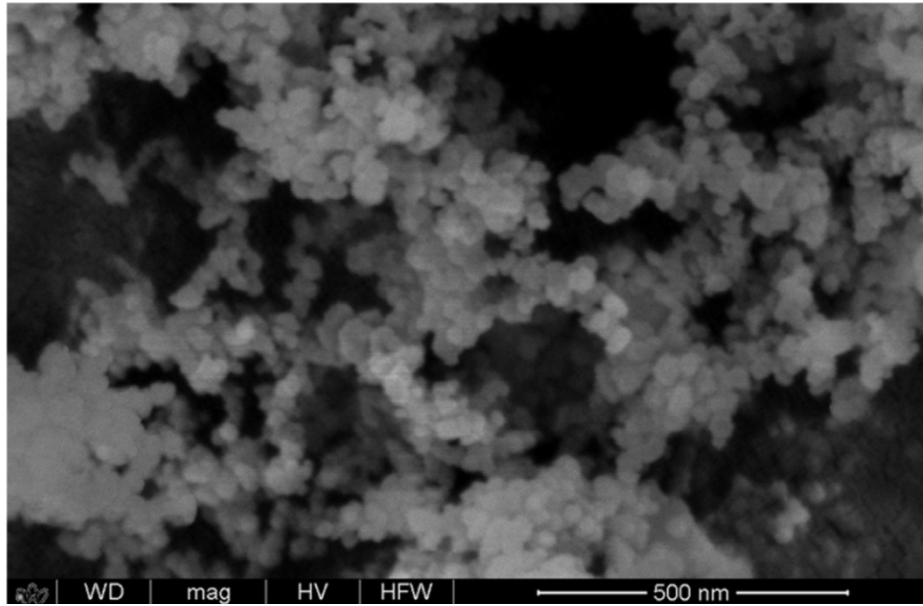


(a)



(b)

Figure 5.7. SEM micrographs of Mg-10 vol%Ti powder mixture after plasma processing. a) A spheroidized Ti particle. b) Mg nanopowders. c) Mg nanopowders synthesized with quenching.



(c)

Figure 5.7. *Continued,*

Crystallite sizes calculated for plasma processed powders are given in Table 5.3. Here the values are relatively large compared to mechanically milled samples. This implies that crystals derived from plasma processing are relatively defect free, i.e. coherently diffracting volumes are larger in size. For instance, Mg-10 vol % Ti with a 2g/min feeding rate yields a crystallite size of 300 nm. This size, however, reduces to 74 nm with the use of quenching gas, as shown in Table 5.3.

It should be pointed out that, where the crystallite size is 74 nm, i.e. with the use of quenching gas, the particle size derived from BET analysis has a value of 80 nm. These values are quite comparable to each other. This is also true for powders obtained without the use of quenching gas. Thus, with plasma processing coherently diffraction domain size is nearly equal to the size of particles themselves.

In conclusion, plasma processing of Mg-10%vol Ti mixture yields Mg powders which are extremely small, i.e. < 100 nm. Ti occur as separate particles with sizes that are comparable to Mg (though some are as coarse as 10 μm). It appears that both in Mg and Ti, coherently diffracting domain sizes are quite large and comparable to the size of individual particles implying that the powders are relatively defect free.

5.4. Discussion

The particulate structures resulting in the one hand from mechanical milling, and in the other, from plasma processing are therefore quite different. The main difference refers to Mg particle size. Mg particles of 95 μm which results from mechanical milling are extremely coarse as compared to plasma processed powders where the size is nearly three orders of magnitude smaller, i.e. 85 nm. Despite the large size of Mg powders, mechanical milling is quite successful in distributing Ti in the form of tiny (approx. 1 μm) particles embedded both to the surface and to the volume of the Mg particles. It is well established that Ti has a catalytic effect in hydrogen sorption i.e. it splits hydrogen molecule into atomic form ready for diffusion into the lattice volume. Thus, the decoration of Mg powders with tiny embedded Ti particles is highly beneficial in improving the hydrogenation characteristics of milled powders.

Hydrogenation behavior of Mg-10 vol % Ti powder mixture milled for 30 hours studied by measurement of PCT curves (not reported here) shows an enthalpy value of 76 kJ/mol. This enthalpy, calculated from Van't Hoff plot, which refers to the dissociation of MgH_2 into Mg and H_2 corresponds to a hydrogen release temperature of 280 $^\circ\text{C}$ (under 1 bar of hydrogen pressure). This value is not far off the lowest desorption temperature reported by Oelerich et al.(2001) for powder processed Mg based alloys.

Powders obtained with plasma processing are extremely fine. How this reduction in size would affect the hydrogenation behavior of Mg powders has not yet been studied. Since the current powders obtained with plasma processing were air exposed, no attempts have been made, in this study, to investigate their hydrogenation behavior. Thin film studies; however, come close to this size, as they cover a variety of film thicknesses ranging from 50-60 nm up to 1 μm . It is known that Mg films (covered with a thin Pd layer) that are less 100 nm in size readily sorbs(absorbs and desorbs) hydrogen near ambient conditions. Thus the reduction in size leads to a reduction in the stability of MgH_2 .

Similar destabilization of MgH_2 may be expected with plasma processing. Powders of 74 nm size are extremely fine and assuming that the substrate plays no role in hydrogenation, they could react with hydrogen in a similar manner as has been the

case with the thin film. The favorable hydrogenation characteristics of powders (as well as thin films) require the presence of a catalytic overlayer. Without the presence of catalytic overlayers, the production of Mg in the form of nanopowders may not be enough to have a sufficiently destabilized MgH_2 .

It appears that processing conditions that would yield Mg nanopowders, of the same size as has been produced in the current work, which are doped or covered with a catalytic layer would be highly desirable for hydrogen storage purposes. This, together with conditions that would allow the incorporation of Ti or other additional elements into the body of nanopowder, would be highly beneficial for designing novel hydrogen storage alloys.

5.5. Conclusions

In this study, Mg-10 vol% Ti powder mixtures were processed for hydrogen storage purposes using two routes: mechanical milling and plasma synthesis. Mechanical milling was carried out with a high speed planetary mill for extended period of time. Plasma processing was carried out with an RF torch of 25-27 kW applied power, the powders being fed axially into the torch. The study has shown the followings;

- i. Mechanical milling of Mg-10 vol% Ti yields large Mg agglomerates, 95-100 μm , with embedded Ti fragments of approximately 1 μm in size uniformly distributed within the agglomerates.
- ii. Mg agglomerates that arise as a result of mechanical milling are made of coherently diffracting volumes of small size. These volumes, determined with X-ray diffraction analysis, can be as small as 26 nm after 30 hours of milling.
- iii. Plasma processing yields Mg powders of extremely small size, <100 nm. Both Mg and Ti occur as separate particles without much sign of dissolution in each other. The powders have coherently diffracting volumes that are comparable to the size of the particles themselves indicating that plasma processing yields relatively defect free crystals.

It appears that the thermal plasma synthesis provides an easy mean for the production of metallic nanopowders, which is expected to yield hydrides of reduced stability. It further appears that conditions that would allow the dissolution of elements in each other or to the formation of covered nanopowders would be highly beneficial for designing novel hydrogen storage alloys.

CHAPTER 6

CONCLUSIONS

In the preceding chapters, Mg-Ti has been processed with a variety of methods, namely; mechanical milling, reactive milling, ECAP and thermal plasma method. In this chapter, we conclude these studies with respect to conditions that would yield Mg-Ti alloy with most favorable hydrogenation properties. As already been mentioned, these properties are altered by the nature of particulate structure that evolves during the processing. Conclusions drawn from each of these processing routes refer to the following parameters; size reduction, the size of coherently diffracting volume, and the distribution of Ti catalyst.

Table 6.1. Structural parameters in Mg-Ti following different processing routes.

| | Mechanical milling | Reactive milling | ECAP | Thermal plasma synthesis |
|--|---------------------------|---------------------------------|------------------|---------------------------------|
| Laser particle size (μm) | 116.4 | | (31)* | |
| Surface area (m^2/g) | 1.76 | 9.86 | | 28.2 |
| Particle size (μm) (BET) | 1.26 | 0.44 | | 0.078 |
| Crystallite size (nm) | 20.78 | 25.09 (20.05) MgH_2 | 69.85 | 74.2 |
| Ti distribution | homogeneous | homogeneous | less homogeneous | irregular |

*ECAP followed by 5 hours of milling

Size reduction;

Particle size values of Mg obtained by different processing routes are collected together in Table 6.1. As seen in the table, the size of Mg particles vary over a wide range; from 116.4 μm to 78 nm. Largest size is obtained with mechanical milling which is even larger than the size of the starting powder (44 μm). This size measured by laser scattering should be treated with care. In fact particle size measured for the same sample converted from BET analysis yield a value which is two orders of magnitude smaller (1.26 μm). This implies that large size Mg agglomerates contain channels or ducts, running through them, formed as a result of cold welding and fracturing process. Thus, in terms of gas-metal reaction, the effective particle diameter in mechanical milling is probably much less than 116.4 μm measured by laser scattering.

ECAP processing is a bulk method and therefore, it cannot yield particulate structures. However, as seen in Table 6.1, ECAP processed material when mechanically milled yields improved size reduction. The particle size obtained in this way has a value of 31 μm which should be compared with 116.4 μm with direct milling. Considering the difficulty of size reduction in ductile powders, this method can provide a new approach for the milling of such powders. The method would involve several passes of ECAP deformation followed by mechanical milling of short duration. Reactive milling and plasma synthesis are clearly more effective processes in terms of size reduction. The particle size resulting from the reactive milling of Mg is in the submicron range, i.e. 0.44 μm .

Of the four processing routes, thermal plasma synthesis result in powders with smallest particle size. This process yields particles spherical in shape with sizes less than 100 nm.

Coherently diffracting volume;

Crystallite size values reported in Table 6.1 are all less than 100 nm. This means that in mechanically milled powders, where the particle size is in the order of 100 μm or so, each particle is made up of a large number of coherently diffracting subvolumes. The number is typically 10^{11} in the case of mechanical milling. This

number reduces to 10^4 in the case of reactive milling, where the subvolumes are typically 20 nm. Plasma processed powders have coherently diffracting volumes that are quite large. It is worth emphasizing that this volume size is quite close to particle size, which implies that plasma processing yields particles which are defect free.

Distribution of Ti catalyst;

As in the size reduction and coherently diffracting volumes, the processing routes also lead to differences in Ti distribution. This additive is homogeneously distributed on and within Mg particles generated by mechanical milling. This is also true for reactive milling where Ti, transforming to TiH_2 and is milled as effectively as MgH_2 . Smallest sized Ti particles have been produced by plasma processing, e.g. 20 nm. The size, however, was not homogeneous. Such fine particles occurred together with particles which were as large as $1\mu m$.

Of the four alternative processing routes, the emphasis may be placed on the route of thermal plasma synthesis. This process produces Mg particles of smallest size and also capable of yielding Ti particles which are at a fraction of Mg particle size. Thus the process seems to be capable of yielding small Mg particles decorated with Ti catalyst.

To employ thermal plasma synthesis, as the main route in the processing of Mg-Ti and the other similar hydrogen storage alloy, it is necessary to improve the process in such a manner that particles have much more homogeneous size distribution. In this respect, significant improvement would be needed with respect to Ti whose size distribution is very important.

REFERENCES

- Aida T., Matsuko K., Horita Z., "Estimating the equivalent strain in equal channel angular pressing", *Scripta Mater*, 44 (2001), P. 575.
- Akiba E., "Hydrogen-absorbing alloys ", *Current opinion in solid state and materials science* 4(1999), P.267.
- Akyıldız H., Öztürk T., "Hydrogen sorption in crystalline and amorphous Mg–Cu thin films", *Journal of Alloys and Compounds*, 492/1-2(2010), P.745.
- Asano K., Enoki H., Akiba E., "Synthesis process of Mg–Ti BCC alloys by means of ball milling", *Journal of Alloys and Compounds*,. 480(2009), P.558.
- Atzmon M., "Formation And Characterization of Amorphous Erbium-based alloys prepared by near-isothermal cold-rolling of elemental composites", *J. Appl. Physics* 58(1985), P.3865.
- Augey-Zinsou K.F., Ares-Fernandes J.R., Klassen T., Bormann R., "Using MgO to improve the (de)hydriding properties of Magnesium" *Mater Res. Bulletin*, 41(2006), P.1118.
- Augey-Zinsou K.F., Ares-Fernández J.R., "Hydrogen in Magnesium:new perspectives toward functional stores", *Energy Environ. Sci.*, 3(2010), P. 526.
- Bai L., Fana J., Hu P., Yuana F., Li J. , Tanga Q., "RF plasma synthesis of Nickel nanopowders via hydrogen reduction of Nickel hydroxide/carbonate", *Journal of Alloys and Compounds* 481(2009) ,P. 563.
- Barhordarian G., Klassen T., Bormann R., "Fast hydrogen sorption kinetics of nanocrystalline Mg using Nb₂O₅ as catalyst" *Scr Mater*, 49(2003),P.213.
- Barkhordarian G., Klassen T., Bormann R., "Effect of Nb₂O₅ Content on Hydrogen Reaction Kinetics of Mg ", *J Journal of Alloys and Compounds*, 364 (2004), P.242.
- Beall R. A., Borg J. O., Gilbert H. L., "Production of Zirconium alloys by consumable electrode arc melting" *J. Electrochem. Soc.*, 102-4(1955), P. 187.
- Benjamin J.S., Volin T.E., "Dispersoids in mechanically alloyed superalloys", *Metall Trans*, 5(1974) ,P. 1929.
- Bobet J L., Evena C., Nakamura Y., Akiba E., B. Darriet, "Study of Mg-M(M=Co, Ni and Fe) mixture elaborated by reactive mechanical alloying–hydrogen sorption properties.", *Journal of Alloys and Compounds*, 298(2000), P. 279.

- Bohmhammel K., Wolf U., Wolf G., Konigsberger E., " Thermodynamic optimization of the system Magnesium–Hydrogen", *Thermochim Acta*, 337(1999), P. 195.
- Bonetti E., Valdre G., Enzo S., Cocco G., Soletta I., " Nanostructured Fe₃Al intermetallic obtained by mechanical alloying and thermal ageing", *Nanostructured Mater*, 2(1993), P.369.
- Bouodina M., Guo Z.X., " Comparative study of mechanical alloying of (Mg+Al) and (Mg+Al+Ni) mixtures for hydrogen storage ", *Journal of Alloys and Compounds*, 336 (2002), P.222.
- Broederz C.P., Germaud R., Dam B., Griessen R., " Highly destabilized Mg-Ti-Ni-H system investigated by density functional theory and hydrogenography", *Phys Rev B*, 77 (2008), P. 24204.
- Bystrzycki J., Czujko T., Varin R.A., Oleszak D., Durejko T., Darlewski W., Bojar Z., Przetakiewicz W., "Nanocrystalline hydrogen absorbing Mg-Ni alloy processed by mechanical (ball) milling", *Rev. Adv. Mater. Sci.*, 5(2003), P.450.
- Bystrzejewski M., Karoly Z., Szepvolgyi J., Kaszuwara W., Huczko A., Lange H., "Continuous synthesis of carbon-encapsulated magnetic nanoparticles with a minimum production of amorphous carbon", *Carbon*, 47(2009), P.2040 .
- Cao P., Lu L., Lai M. O., "Grain growth and kinetics for nanocrystalline magnesium alloy produced by mechanical alloying.", *Materials Research Bulletin*, 36 (2001), P.981.
- Chakkingal U., Suriadi A. B., Thomson. P.F., " Microstructure development during equal channel angular drawing of Al at room temperature", *Scripta Mater*, 39 (1998), P. 677.
- Charbonnier J., De Rango P., Fruchart D., Miraglia S., Pontonnier L., Rivoirard S., Skryabina N., Vulliet P., " Hydrogenation of transition element additives (Ti, V) during ball milling of magnesium hydride ", *J. Alloys Comp.* 383 (2004), P.205.
- Chen C., Wang W., Xu H., Chen Y., *Trans. Nonferrous Met. Soc. China*, 12-3(2002) P. 404.
- Chen J., Dou S. X., Liu H. K., " Research on rapid agile metrology for manufacturing based on real time multi task operating system", *Journal of Alloys and Compounds*, 244(1996), P.184.
- Chen G. Z., Fray D. J., Farthing T. W., "Direct electrochemical reduction of titanium dioxide to titanium in molten calcium chloride", *Nature* 407(2000), P.361.
- Chin Z-H, Perng T-P., "Amorphization of Ni-Si-C Ternary Alloy Powder Mechanical Alloying", *Mater Sci Forum*, 235-238(1997), P.121.

- Choi Y. J., Lua J., Sohn H.Y., Fanga Z. Z., "Hydrogen storage properties of the Mg–Ti–H system prepared by high-energy–high-pressure reactive milling", *Journal of power Sources*, 180/1(2008), P. 491.
- Çakmak G., Károly Z., Mohai I., Öztürk T., Szépvölgyi J., "The processing of Mg-Ti for hydrogen storage; mechanical milling and plasma synthesis", *International Journal of Hydrogen Energy*, 35-19 (2010), P. 10412.
- David E., "An overview of advanced materials for hydrogen storage", *J. Mater Process Technol*, 162-163(2005), P. 169.
- Dinkel M., Pyczak F., May J., Höppel H. W., Göken M., "XRD profile analysis characterization of ultra-fine grained Al-Mg alloys", *Journal of Material Science*, 43/23(2008), P. 7481.
- DOE-2001 <http://www.hydrogen.energy.gov>, accessed 10.01.2010.
- Eckert J., Holzer J.C., Krill III C.E., Johnson W.L., "Investigation of nanometer-sized fcc metals prepared by ball milling", *Mater Sci Forum* 1992;88, P. 505.
- Ershova O. G., Dobrovolsky V. D., Solonin Y. M., Khyzhun O. Y., "Thermal stability and hydrogen sorption properties of the MgH₂ derived by the reactive milling of the Mg+10 wt% Ti mixture" *Carbon nanomaterials in clean energy hydrogen systems*, *Nato Science for Peace and Security Series*(2009), P.473.
- Friedrichs O., Klassen T., Sánchez-López J. C., Bormann R., Fernández A., "Hydrogen sorption improvement of nanocrystalline MgH₂ by Nb₂O₅ nanoparticles", *Scripta Materialia*, 54/7 (2006), P. 1293.
- FACT, Facility for the Analysis of Chemical Thermodynamics, <http://www.crct.polymtl.ca/fact/>, accessed 22.03.2011
- Furukawa M., Iwahashi Y., Horita Z., Nemoto M., Langdon T.G., "The shearing characteristics associated with equal-channel angular pressing", *Mater Sci Eng A*, 257(1998), P.328.
- García-Infanta J. M., Zhilyaev A. P., Cepeda-Jiménez C. M., Ruano O. A., Carreño F. "Effect of the deformation path on the ductility of a hypoeutectic Al–Si casting alloy subjected to equal-channel angular pressing by routes A, BA, BC and C", *Scripta Mater.*, 58 (2008), P. 138.
- Gennari F. C. , Castro F. J., Urretavizcaya G., "Hydrogen desorption behavior from magnesium hydrides synthesized by reactive mechanical alloying", *Journal of Alloys and Compounds*, 321 (2001), P.46.
- Gente C. , Oehring M., Bormann R., "Formation of thermodynamically unstable solid solutions in the Cu-Co system by mechanical alloying" *Phys Rev*, B48 (1993), P. 13244.

- Goswami R., Chattopadhyay K., "Microstructural Developments in Rapidly Solidified Monotectic Alloys", *Mater. Sci. Eng.*, A179/180 (1994), P. 198.
- Greet A. L., "Grain refinement in rapidly solidified alloys", *Mater. Sci. Eng. A*, 133(1991), P.16.
- Gross K. J., Thomas G. J., Jensen C. M., "Catalyzed alanates for hydrogen storage", *J. Alloys and Compounds*, 330-332(2002), P.683.
- Gutfleisch O., Dal Toè S., Herrich M. , Handstein A. , Pratt A. , "Hydrogen sorption properties of Mg-1wt%Ni-0.2wt%Pd prepared by reactive milling", *Journal of Alloys and Compounds*, 404-406 (2005), P. 413.
- Guoxian L., Erde W., Shoushi F., "Hydrogen absorption and desorption characteristics of mechanically milled Mg-35wt %FeTi_{1.2} powders" *J. of Alloys and Compounds* , 223(1995), P. 114.
- Güvendirren M, Baybörü E, Öztürk T. 2004. "Effects of additives on mechanical milling and hydrogenation of magnesium powders", *Int. J of Hydrogen Energy*, 29(2004), P. 491.
- Hanada N., Ichikawa T., Fujii H., "Catalytic effect of nanoparticle 3d-transition metals on hydrogen storage properties in magnesium hydride MgH₂ prepared by mechanical milling", *Journal of Physical Chemistry B*, 109-15(2005), P.7188.
- Haouaoui M., Karaman I., Maier H. J., Hartwig K. T., "Microstructure evolution and mechanical behavior of bulk copper obtained by consolidation of micro and nanopowders using equal-channel angular extrusion", *Metall. and Mat. Trans.*, 35A (2004), P. 2935.
- Higuchi K, Yamamoto K, Kajioka H, Toiyama K, Honda M, Orimo S, Fujii H, "Remarkable hydrogen storage properties in three-layered Pd/Mg/Pd thin films", *Journal of Alloys and Compounds*, 330-332(2002),P.526.
- Hong T. W., Kim S. K., Kim Y. J., "Dehydrogenation properties of nano-/amorphous Mg₂NiH_x by hydrogen induced mechanical alloying", *Journal of Alloys and Compounds*, 312 (2000), P.60.
- Hu P., Yan S., Yuan F., Bai L., Li J., Chen Y., *Plasma Science and Technology*, 9(2007), P. 611.
- Huang J., Wu Y. K., He A. Q., Ye H. Q., "Nanocrystalline Cu-Fe solid solutions prepared by mechanical alloying", *Nanostructured Mater*, 4(1994), P. 293.
- Huang B. L., Perez R. J., Crawford P. J., Nutt S. R., Lavernia E. J., "The synthesis of nanocrystalline Fe₇₈B₁₃Si₉ by cryogenic high-energy ball milling of metglas", *Nanostructured Mater*, 7(1996), P. 57.
- Huot J., Boily S., Akiba E., Schulz R., "Direct synthesis of Mg₂FeH₆ by mechanical alloying", *Journal of Alloys and Compounds* 280 (1998), P.306.

- Huot J., Liang G., Boily S., Van Neste A., Schulz R., "Structural study and hydrogen sorption kinetics of ball-milled magnesium-hydride", *Journal of Alloys and Compounds* 293–295 (1999),P. 495.
- Huot J., Pelletier J. F., Lurio L. B., Sutton M., Schulz R., "Investigation of dehydrogenation mechanism of MgH₂-Nb nanocomposites", *Journal of Alloys and Compounds*, 348 (2003), P.319.
- Ikeda M., Li J. G., Ye R., Kobayashi N., Moriyoshi Y., Ishigaki T., "Size control of TiO₂ nanoparticles through quench gas injections into RF induction thermal plasma" 18th International Symposium on Plasma Chemistry, August 26-31- 2007, Kyoto, Japan.
- Imamura H., Nakatomi S., Hashimoto Y., Kitazawa I., Sakata Y., Mae H., Fujimoto M., "Synthesis and hydrogen storage properties of mechanically ball-milled SiC/MgH₂ nanocomposites", *Journal of Alloys and Compounds* 488-1(2009),P.265.
- Ingason A. S., Olafsson, S., "Thermodynamics of hydrogen uptake in Mg films studied by resistance measurements ", *Journal of Alloys and Compounds*, 404-406(2005), P.469.
- Ingason A. S., Eriksson A.K., Olafsson S., "Hydrogen uptake in Mg:C thin films ", *Journal of Alloys and Compounds*, 446-447(2007), P. 530.
- Ivey D. G., Northwood D. O., "Review, storing energy in metal hydrides: a review of the physical metallurgy", *J. Mater. Sci.*, 18 (1983), P. 321.
- Iwahashi Y., Wang J., Horita Z., Nemoto M., Langdon T. G., "Principle of equal-channel angular pressing for the processing of ultra-fine grained materials", *Scripta Mater*, 35(1996), P.143.
- Iwahashi Y., Horita Z., Nemoto N., Langton T. G., " An investigation of microstructural evolution during equal-channel angular pressing", *Acta Mater.*, 45-11(1997), P.4733.
- Jones H., in "Rapid Solidification of Metals and Alloys," Monograph No. 8. Institute of Metallurgists, London (1982).
- Kavka T.,Gregor, J., Chumak O., M.Hrabovsky, "Study of the Expanding Thermal Plasma Jet by Enthalpy Probe", *Czech. J. Phys.* 54 (2004) P. 753.
- Kawasuso A., Arashima H., Maekawa M., Itoh H., Kabutomori T., "Positron lifetime study on degradation of TiCrV hydrogen storage alloy", *Materials Science Forum*, 607(2009), P. 122.
- Khatamian D., Kazama N. S., Manchester F. D., Weatherly G. C., Alcock C. B., "The effect of the addition of carbon on the hydrogen-absorbing properties of FeTi", *Journal of the Less Common Metals*, 91-2(1983), P. 267.

- Kim W. J., An W., Kim Y. S., "Mechanical properties and microstructures of an AZ61 Mg Alloy produced by equal channel angular pressing", *Scripta Materialia*, 47 (2002), P. 39.
- Kim H. S., Seo M. H., Hong S. I., "Plastic deformation analysis of metals during equal channel angular pressing", *J. Mater Process. Tech.*, 113(2001), P. 622.
- Kim W. J., Chung C. S., Ma D. S., Hong S. I., Kim H. K., "Optimization of strength and ductility of 2024 Al by equal channel angular pressing (ECAP) and post-ECAP aging", *Scripta Materialia*, 49-4(2003), P. 333.
- Kim J. H., Lee H., Hwang K. T., Han J. S., "Hydriding behavior in Zr-based AB₂ alloy by gas atomization process", *International Journal of Hydrogen Energy*, 34 (2009), P.9424.
- Kis-Varga M., Beke D L., "Phase transitions in Cu-Sb systems induced by ball milling" *Mater Sci Forum* 225-227(1996), P.465.
- Klassen T., Friedrichs O., Sanchez-Lopez J. C., Bormann R., Fernandez A., "Hydrogen sorption improvement of nanocrystalline MgH₂ by Nb₂O₅ nanoparticles", *Scripta Materialia* 54 (2006), P. 1293.
- Kobayashi N., Li J. G., Watanabe T., Ishigaki T., 18th International Symposium on Plasma Chemistry, August 26-31, 2007, Kyoto, Japan.
- Komura S., Horita Z., Nemoto M., Langdon T. G., "Influence of stacking fault energy on microstructural development in equal-channel angular pressing", *J. Mat. Res.* 14 (1999), P. 4044.
- Kovářík O., Fan X., Boulos M., "In flight properties of W particles in an Ar-H₂ plasma.", *Journal of Thermal Spray Technology*, 16(2007), P. 229.
- Kumar S., Selvarajan V., "In-flight formation and characterization of nickel aluminide powders in a DC thermal plasma jet", *Chemical Engineering and Processing*, 45 (2006), P.1029.
- Kumara S., Selvarajan V., Padmanabhan P. V., Sreekumar K. P., "Characterization and comparison between APS coatings prepared from ball milled and plasma processed nickel-aluminium powders", *Materials Science and Engineering A*, 486/1-2(2008), P. 287.
- Kyoi D., Sato T., Rönnebro E., Kitamura N., Ueda A., Ito M., Katsuyama S., Hara S. Noreus D., Sakai T., "A new ternary magnesium-titanium hydride Mg₇TiH_x with hydrogen desorption properties better than both binary magnesium and titanium hydrides", *Journal of Alloys and Compounds* 383 (2004), P.205.
- Lai M. O, Lu L. "Mechanical alloying." Boston, MA: Kluwer Academic Publishers, 1998.

- Leiva D. R., Fruchart D., Bacia M., Girard G., Skryabina N., Villela A. C. S., Miraglia S., Santos D. S., "Mg alloy for hydrogen storage processed by SPD", *International Journal of Material Research* 100(2009), P. 1739.
- Liang G. Boily S., Huot J., Neste A. V., Schulz R., "Mechanical alloying and hydrogen absorption properties of the Mg–Ni system", *J. of Alloys and Compounds*, 268(1998), P. 302.
- Liang G., Huot J., Boily S., Van Neste A., Schulz R., "Catalytic effect of transition metals on hydrogen sorption in nanocrystalline ball milled MgH₂–Tm (Tm=Ti, V, Mn, Fe and Ni)", *J. Alloys Comp.*, 292(1999), P.247.
- Liang G., Huot J., Boily S., Schulz R., "Hydrogen desorption kinetics of a mechanically milled MgH₂+5at.%V nanocomposite", *Journal of Alloys and Compounds* 305 (2000), P.239.
- Liang G., Schulz R., "Synthesis of Mg-Ti alloy by mechanical alloying", *Journal of Materials Science* 38(2003), P.1179.
- Liang G., Schulz R., "The reaction of hydrogen with Mg-Cd alloys prepared by mechanical alloying", *Journal of Material Science*, 39, (2004), P. 1557.
- Liebermann H. H., in "Amorphous Metallic Alloys" (E E. Lubrosky, ed.), p. 26. Butterworths, London(1983).
- Liu T., Zhang W., Wu S. D., Jiang C. B., Li S. X., Xu Y. B., "Mechanical properties of a two-phase alloy Mg-8%Li-1%Al processed by equal channel angular pressing", *Materials Science and Engineering A*, 360 (2003) P. 345.
- Løken, S., Solberg, J.K., Maehlen, J.P., Denys, R.V., Lototsky, M. V., Tarasov, B. P., Yartys, V.A., "Nanostructured Mg-Mm-Ni hydrogen storage alloy: structure, properties relationship", *Journal of Alloys and Compounds*, 446-447(2007), P. 114.
- Luo, W., "(LiNH₂–MgH₂): a viable hydrogen storage system ", *Journal of Alloys and Compounds*, 381(2004), P.284.
- Lutterotti L., Matthies S., Wenk H. R., Maud: a friendly java program for materials analysis using diffraction, *Int. U. Crystallogr. Comm. Powder Diffr. Newslett.* 21 (1999) 14.MAUD Version 2.072, 2008, <http://www.ing.unitn.it/luttero/maud>. Accessed at 22.03.2011
- Manchester F.D., San-Martin A., *Phase Diagrams of Binary Magnesium Alloys*, (1988).
- Martin J. N., Doherty R. D., Cantor B., in "Stability of Microstructure in Metallic Systems," Cambridge University Press(1977) P. 84.

- Martin M., Gommel C., Borkhart C., Fromm E., "Absorption and desorption kinetics of hydrogen storage alloys ", *Journal of Alloys and Compounds*, 238 (1996), P.193.
- Mathis K., Gubicza J., Nam N. H., " Microstructure and mechanical behavior of AZ91 Mg alloy processed by equal channel angular pressing", *Journal of Alloys and Compounds*, 394(2005), P. 194.
- Matsuki K., Aida T., Takeuchi T., Kusui J., Yokoe K., "Microstructural characteristics and superplastic-like behavior in aluminum powder alloy consolidated by equal-channel angular pressing", *Acta Mater.*, 48 (2000), P. 2625.
- Mckenzie P. W. J., Lapovok R., Estrin Y., " Influence of back pressure on ECAP processed AA 6016: modeling and experiment", *Acta Mater.* 55 (2007), P.2985.
- Mingfen W., Chongli S., Lian C., Yuchun Z., "Study on the structure and electrochemical properties of melt spun $Zr_{0.9}Ti_{0.1}(Ni,Co,Mn,V)_{2.1}$ alloys", *Journal of Material Chemistry*, 12 (2002), P. 2543.
- Mohai I., Szépvölgyi J., "Treatment of particulate metallurgical wastes in thermal plasmas", *Chemical Engineering and Processing*, 44(2005), P.225.
- Moss M, Lapovok R, Bettles C. J., "The ECAP of magnesium and magnesium alloy Powders", *JOM* 59(2007), P. 54.
- Muñoz-Morris M. A., Garcia Oca C, Gonzalez Doncel G., Morris, D. G. "Microstructural evolution of dilute Al-Mg alloys during processing by equal channel angular pressing and during subsequent annealing", *Materials Science and Engineering A*, 375-377(2004), P. 853.
- Nayeb-Hashemi A. A., Clark J. B., editors, *Phase diagrams of binary magnesium alloys*, ASM International, Metals Park, OH, (1998), 324-327.
- NESSHY-2006 <http://www.nesshy.net>, accessed 10.01.2010.
- Oelerich W., Klassen T., Bormann R., "Metal oxides as catalysts for improved hydrogen sorption in nanocrystalline Mg-based materials ", *Journal of Alloys and Compounds*, 315 (2001),P.237.
- Oelerich W., Klassen T, Bormann R, "Comparison of the catalytic effects of V, V_2O_5 , N, and VC on the hydrogen sorption of nanocrystalline Mg", *Journal of Alloys and Compounds*, 322 (2001), P.1
- Okuyama H., Uda M., Uchikoshi T., Suzuki T. S., Sakka Y.," Hydrogen storage properties of Nb-Zr-Fe alloys disintegrated by Hydrogen gas", *Materials Science Forum*, 534-536 (2007), P. 73.
- Oleszak D, Burzynska-Szyszkó M, Matyja H., "Structural changes during mechanical alloying of elemental Al-Ti, Al-Nb and Ti-Si powders", *J Mater Sci Lett* 12(1993),P. 3.

- Orimo S., Fujii H., "Materials science of Mg-Ni-based new hydrides", *Applied Physics* 72(2001), P.167.
- Örs T., Tan S., Öztürk T., Karakaya İ., "Synthesis of Fe-4.6 wt% B alloy via electro-deoxidation of mixed oxides.", *Journal of Materials Science*, 44 , (2009), p.3514.
- Öztürk T., Mirmesdagh J., Ediz T., "Strain partitioning and plastic flow in some metal/metal laminates", *Mater Sci Eng A*, 175(1994), P.125.
- Padella F., Paradiso E., Burgio N., Magini M., Martelli S., Guo W., Iasonna A., "Mechanical alloying of the Pd-Si system in controlled conditions of energy transfer", *J Less-Common Metals*, 175(1991),P. 79.
- Pedneault S., Huot J., Roue L., "Nanostructured Mg₂Ni materials prepared by cold rolling and used as negative electrode for Ni-MH batteries", *Journal of Power Sources*, 185/1(2008), P. 566.
- Pedersen A. S., Kjoller J., Larsen B., Vigeholm B., "Magnesium for hydrogen storage", *International Journal of hydrogen Energy*, 8(1983), P. 205.
- Pei P., Song X. P., Liu J, Chen G. L., Qin X. B., Wang B. Y., "The effect of rapid solidification on the microstructure and hydrogen storage properties of V₃₅Ti₂₅Cr₄₀ hydrogen storage alloy", *International Journal of Hydrogen Energy* , 34(2009), P.8094.
- Pushin V. G., Stolyarov V. V., Valiev R. Z., Kourov N. I., Kuranova N. N., Prokofiev E. A., Yurchenko L. I., "Features of structure and phase transformations in shape memory TiNi-based alloys after severe plastic deformation", *Annales de Chimie Science des Matériaux*, 27 (2002), P. 77.
- Quang P., Jeong Y. G., Yoon S. C., Hong S. H., Kim H. S., "Consolidation of 1vol.% carbon nanotube reinforced metal matrix nanocomposites via equal channel angular pressing", *J Mater Proc Tech*, 187–188(2007), P.318.
- Raab G. I., "Plastic flow at equal channel angular pressing" *Mater. Sci. Eng. A* ,410-411(2005), P. 230.
- Reilly J., Wiswall R., "Reaction of hydrogen with alloys of magnesium and nickel and the formation of Mg₂NiH₄", *Inorganic Chemistry*, 7(1968), P. 2254.
- Remhof A., Borgschulte A., "Thin-film metal hydrides" *Chem Phys Chem*, 9(2008), P. 2440.
- Reule H., Hirscher M., Weibhardt A., Kronmüller H., "Hydrogen desorption properties of mechanically alloyed MgH₂ composite materials ", *Journal of Alloys and Compounds* 305 (2000), P. 246.
- Riktor M. D., Deledda S., Herrich M., Gutfleisch O., Fjelvag H., Hauback B. C., "hydride formation in ball-milled and cyromilled Mg-Fe powder mixtures", *Materials Science and Engineering B*,158 (2009), P. 19.

- Rönnebro E., Kyoï D., Kitano A., Kitano Y., Sakai T., "Hydrogen sites analysed by X-ray synchrotron diffraction in Mg₇TiH₁₃₋₁₆ made at gigapascal high-pressures", *Journal of Alloys and Compounds*, 404–406 (2005), P. 68.
- Rochman N. T., Kawamoto K., Sueyoshi H., Nakamura Y., Nishida T., "Effect of milling temperature and additive elements on an Fe-C system alloy prepared by mechanical alloying", *Journal of Materials Processing Technology*, 89-90 (1999), P. 367.
- Ryu T., Sohn H.Y., Hwana K. S., Fang Z. Z., "Chemical vapor synthesis (CVS) of Tungsten nanopowder in a Thermal Plasma Reactor", *International Journal of Refractory Metals and Hard Materials* 27 (2009), P. 149.
- Sakintuna B., Lamari-Darkrim F., Hirscher M., "Metal hydride materials for solid hydrogen storage: a review", *International Journal of Hydrogen Energy* 32(2007) , P. 1121.
- Sandrock G., A Panoramic overview of hydrogen storage alloys from gas reaction point of view, *J. Alloys Comp.*, 293-295(1999), P.877.
- Schlapbach L., Zuttel A., Hydrogen storage materials for mobile applications, *Nature* 414(2001), P.353.
- Schulz R., Liang G., and Huot J., "Hydrogen sorption in mechanically alloyed nanocrystalline and disordered materials", *Proceedings of the 22nd Riso International Symposium on Materials Science* (2001) Denmark.
- Schulz R., Huot J., Liang G., Boily S., Lalande G., Dennis M. C., Dodolet J. P., "Recent developments in the applications of nanocrystalline materials to hydrogen technologies", *Materials Science and Engineering*, 267 (1999) p. 240.
- Segal V. M., "Equal Channel Angular Extrusion: From macromechanics to structure formation", *Mater. Sci. and Eng. A*, 271 (1999), P. 322.
- Selvam P., Wiswanata B., Swamy C. S., Srinivasan V., 1988," XPS and XAES studies on hydrogen storage magnesium-based alloys ", *Int Journal of Hydrogen Energy*, 13 (1988), P.87.
- Senkov O. N., Senkova S. V., Scott J. M., Miracle D. B. "Compaction of amorphous aluminum alloy powder by direct extrusion and equal channel angular extrusion." *Mater Sci Eng A* (2005), 393, P. 12.
- Shanmugavelayutham G., Selvarajan V. ,"Plasma spheroidization of Nickel powders in a plasma reactor", *Bull. Mater. Sci.*,27(2004), P.453.
- Shanmugavelayutham G., Selvarajan V., Padmanabhan P. V. A., Sreekumar K. P., Joshi N. K., "Effect of powder loading on the excitation temperature of a plasma jet in DC thermal plasma spray torch ", *Current Applied Physics*, 7(2007), P. 186.

- Shao H., Xu H., Wang Y., Li X., "Preparation and hydrogen storage properties of Mg₂Ni intermetallic nanoparticles", *Nanotechnology* 15 (2004), P. 269.
- Shin D. H., Kim B.C., Kim Y.S., Kim K.T., "Microstructural evolution in a commercial low carbon steel by equal channel angular pressing", *Acta Mater*(2000) 48, P. 2247.
- Shingu P.H., Ishihara K.N., Otsuki A., Daigo I., "Nano-scaled multi-layered bulk materials manufactured by repeated pressing and rolling in the Cu-Fe system", *Mater Sci Eng A* 304-306(2001), P.399.
- Skripnyuk V., Buchman E., Rabkin E. Estrin Y., Popov M., Jorgensen S., "The effect of equal channel angular pressing on hydrogen storage properties of a eutectic Mg-Ni alloy, *Journal of Alloys and Compounds*", *Journal of Alloys and Compounds*, 436(2007), P.99.
- Skripnyuk V. M., Rabkin E., Estrin Y., Lapovok R., "Improving hydrogen storage properties of magnesium based alloys by equal channel angular pressing", *International Journal of Hydrogen Energy*, 34(2009) ,P.6320.
- Song D., Wang Y., Wang Y., Jiao L., Yuan H., "Electrochemical hydrogen storage performance of AB₅-CoB composites synthesized by a simple mixing method", *Rare Metals*, 28-6(2009), P. 629.
- Srivastava S., Srivastava O. N., "Investigations on synthesis, characterization and hydrogenation behaviour of the spin- and thermal-melted versions of LaNi_{5-x}Si_x (x=0.1, 0.3, 0.5) hydrogen storage materials", *Journal of Alloys and Compounds*, 267/1-2(1998), P. 240.
- Stanley R. W., Berube M, Celik C., Oosaka Y., Pearcy J., Avedesian M, *Proceedings of the International Magnesium association 54: Magnesium trends, Toronto Canada*(1997), P.58.
- Stolyarov V. V., Zhu Y. T., Alexandrov I. V., Lowe T. C., Valiev R. Z., "Influence of ECAp routes on the microstructure and properties of pure Ti ", *Materials Science and Engineering A*, 299(2001), P.59.
- Suresh K, Selvarajan V, Mohai I., "Synthesis and characterization of iron aluminide nanoparticles by DC thermal plasma jet", *Vacuum*, 82(2008), P.482.
- Suryanarayana C., Chen G.H., Froes F.H., "Structural evolution of mechanically alloyed Ti-Al alloys", *Scripta Metall Mater*, 26(1992), P.1727.
- Suryanarayana C., "Mechanical alloying and milling", *Progress in Materials Science*, 46 (2001), P. 1.
- Szépvolgyi J., Gál L., Mohai I., Mészáros I., Gubicza J., "Synthesis of Spinel ferrites in rapid frequency thermal plasma reactor" 18th International Symposium on Plasma Chemistry, August 26-31 2007, Kyoto, Japan. P.538.

- Szépvolgyi J., Mohai I., Károly Z., "Synthesis of nanosized ceramic powders in a radio frequency thermal plasma reactor", *Journal of the European Ceramic Society*, 28(2008), P. 895.
- Szepvolgyi J, Mohai I, Baksa G, "Formation of nanosize particles in an RF thermal plasma torch" *Nanoparticles in solids and Solutions*, Nato Advanced Science Institute Series, Sub-series 3: High Technology, 18(1996): P. 543.
- Tan S., Örs T., Aydinol M. K., Öztürk T., Karakaya I., "Synthesis of FeTi from mixed oxide precursors", *Journal of Alloys and Compounds* 475 /1-2(2009), P. 368.
- Tan S., Aydinol K., Öztürk T., Karakaya I, "Direct synthesis of Mg-Ni compounds from their oxide" *Journal of Alloys and Compounds* 504 (2010) , P. 134.
- Tendero C., Tixier C., Tristant P., Desmaison J., Leprince P., "Atmospheric pressure plasmas: A review", *Spectrochimica Acta Part B*, 61(2006), P. 2.
- Terashita N., Kobayashi K., Sasai T., Akiba E., "Structural and hydriding properties of $(\text{Mg}_{1-x}\text{Ca}_x)\text{Ni}_2$ Laves phase alloys", *Journal of Alloys and Compounds* 327 (2001), P. 275.
- Tessier P., Enoki H., Bououdina M., Akiba E., "Ball milling of Mg_2Ni under hydrogen", *J. of Alloys and Compounds*, 268(1998), P.285.
- Tessier P., Akiba E. , "Catalyzed reactive milling", *Journal of Alloys and Compounds*, 293-295 (1999), P.400.
- Thompson J. R. and Politis C., "Formation of amorphous Ti-Pd alloys by mechanical alloying methods", 1987 *Europhys. Lett.* 3, P.199.
- Tsushio Y., Tessier P., Enoki H., Akiba E., "Hydrogen desorption properties of the quaternary alloy system $\text{Mg}_{2-x}\text{M}_{1-x}\text{Ni}_{1-y}\text{M}_{2-y}$ " *Journal of Alloys and Compounds* 280 (1998) P.262.
- Uesaka G., Han H., Takashima S., Xue S. Jurewicz J. M., Boulos,, "Induction plasma spheroidization of molybdenum powder" 18th International Symposium on Plasma Chemistry, August 26-31, 2007, Kyoto, Japan, P.541.
- Urgnani J., Chio M Di, Palumbo M., Feuerbacher M., Fernandez J. F., Leardini F., Baricco M., "Hydrogen absorption and desorption in rapidly solidified Mg- Al alloys", *J. Phys.: Conf. Ser.*, 144 (2009), P.012016.
- Valiev R. Langdon T. G., "Principles of equal-channel angular pressing as a processing tool for grain refinement," *Progress in Materials Science*, 51 (2006), P. 881.
- Varin R. A., Li S., Calka A., "Environmental degradation by hydrolysis of nanostructured MgH_2 synthesized by controlled reactive mechanical milling (CRMM) of Mg", *Journal of Alloys and Compounds* 376 (2004), P. 222.

- Vermeulen P., Niessen R. A. H., Notten P. H. L., "Hydrogen storage in metastable $Mg_yTi_{(1-y)}$ thin films" *Electrochemistry Communications*, (2006), P. 27.
- Von Zeppelin F., Reule H., Hirsher M., "Hydrogen desorption kinetics of nanostructured MgH_2 composite materials", *Journal of Alloys and Compounds* 330-332 (2002), P.723.
- Wang J. Y., "Comparison of hydrogen storage properties of $Ti_{0.37}V_{0.38}Mn_{0.25}$ alloys prepared by mechanical alloying and vacuum arc melting", *International Journal of Hydrogen Energy*, 34/9 (2009), P. 3771.
- Warren B. E. and Bischof J., "Fourier analysis of x-ray patterns of soda-silica glass", *J Am Ceram Soc*, 21 (1938), P. 49.
- WENET-1993, http://www.ena.or.jp/WE-NET/contents_e.html, accessed at 10.01.2010.
- Wu Z., Huang T., Cheng J., Xia B., Xu, N., "Effect of surface oxide layer on activation performance of hydrogen storage alloy $TiMn_{1.25}Cr_{0.25}$ " *International Journal of Hydrogen Energy* 29 (2004), P.81.
- Wu H. M., Hung S. S., Lee P. Y., "Characterization of $Ni_{57}Zr_{20}Ti_{20}Sn_3$ amorphous powders obtained by mechanical alloying ", *J Alloy Compd* 434-435(2007), P. 386.
- Xia K., Wu X., "Back pressure equal channel angular consolidation of pure Al particles", *Scr Mater*, 53 (2005), P.1225.
- Yamada K., Koch C. C., "Nonomaterial: Synthesis, properties and applications" *J Mater Res*, 8(1993), P. 1317.
- Yamashita A., Horita Z., Langdon T. G., "Improving the mechanical properties of magnesium and a magnesium alloy through severe plastic deformation" *Materials Science and Engineering A300* (2001), P.142.
- Yermakov A Y, Mushnikov N V, Uimin M A, "Hydrogen reaction kinetics of Mg-based alloys synthesized by mechanical milling." *J Alloys Compd*425(2006),, P.367.
- Yonkeu A. L., Swainson I. P., Dufour J., Huot J., "Kinetic investigation of the catalytic effect of a body centered cubic-alloy $TiV_{1.1}Mn_{0.9}$ (BCC) on hydriding/dehydriding properties of magnesium", *Journal of Alloys and Compounds*, 460 (2008), P.559.
- Yu X. B., Wu Z., Xia B. J., Xu N. X., "Enhancement of hydrogen storage capacity of Ti-V-Cr-Mn BCC phase alloys", *Journal of Alloys and Compounds*, 372/1-2(2004), P. 272.
- Yugeswaran S., Selvarajan V., "Electron number density measurement on a DC argon plasma jet by stark broadening of Ar I spectral line", *Vacuum* 83(2009), P. 841.

Zaluski L., Zaluska A., Ström-Olsen J. O., "Nanocrystalline metal hydrides", Journal of Alloys and Compounds 253-254 (1997), P.70.

Zaluska A., Zaluski L., Ström-Olsen J. O., "Nanocrystalline magnesium for hydrogen storage", Journal of Alloys and Compounds 288 (1999), P. 217.

Zehetbauer M., Grössinger R., Krenn H., Krystian M., Pippan R., Rogl P., Waitz T., Würschum R., "Nanostructured functional materials by severe plastic deformation", Adv Eng. Mater, 12(2010), P. 692.

Züttel A., "Hydrogen storage methods" Naturwissenschaften, 91(2004), P. 157.

CURRICULUM VITAE

PERSONAL INFORMATION

Last Name, Name :Çakmak, Gülhan
Nationality :Turkish(T.C.)
Date and Place of birth :12 June 1979, Ankara
Marital Status :Single
Voice :533-5579459
E-mail :glhnckmk@hotmail.com



EDUCATION

| Degree | Instution | Year of Graduation |
|-------------|---|--------------------|
| B.S. | Anadolu University, Ceramic Engineering | 2002 |
| High school | Yunus Emre High School | 1997 |

WORK EXPERIENCE

| Year | Place | Enrollment |
|-----------------------|---|----------------------------|
| 2002-present | METU, Metallurgical and Materials Eng. | Research Assistant |
| January-April 2010 | Institute of Material and Environmental Chemistry, HAS | Visiting Researcher |
| March-May 2007 | Institut de Chimie de la Matière Condensée de Bordeaux, ICMCB-CNRS | Visiting Researcher |
| 2000 August | Eczacıbaşı A.Ş. | Intern engineering student |
| 2001 August | Toprak A.Ş | Intern engineering student |

PUBLICATIONS

- **Çakmak G.**, Károly Z., Mohai I., Öztürk T., Szépvölgyi J., "[The processing of Mg-Ti for hydrogen storage; mechanical milling and plasma synthesis](#)", International Journal of Hydrogen Energy, Vol. 35, Issue 19, October 2010, P.10412
- Ölmez R., **Çakmak G.**, Öztürk T., "[Combinatorial search for hydrogen storage alloys: Mg-Ni and Mg-Ni-Ti](#)" , International Journal of Hydrogen Energy, Available on line 16 september 2010
- **Çakmak G.**, Öztürk T., "[Effects of Equal Channel Angular Pressing on Microstructural Refinement in Mg and Mg-Ti Powders](#)", Journal of Material Science, in press
- Akyıldız H, **Çakmak G**, Tan S, Öztürk T, " [A Screening Method for Hydrogen Storage Alloys](#)", Turkish J. Eng. Env. Sci. 31 (2007) , 289 – 295.
- **Çakmak G**, Bobet J-L, Ölmez R, Öztürk T., "[Hydrogen Storage in Mg-Ti using Powder Processing and Severe Plastic Deformation](#), A Comparative Study", Proceedings International Hydrogen Energy Congress and Exhibition IHEC 2007 Istanbul, Turkey, 13-15 July 2007
- Akyıldız H, **Çakmak G**, Tan S, Öztürk T., "[A Rapid Method to Assess Hydrogen Storage Potentials in Binary or Multi-Component Systems](#)", International Symposium on Metal-Hydrogen Systems Fundamentals & Applications , Cracow, Poland, 1, (2004), p.49